Retinal Structure and Function in Typical Children and Young Adults

by

Hussain Albuhayzah

A thesis
presented to the University of Waterloo
in fulfillment of the
thesis requirement for the degree of
Master of Science
in
Vision Science

Waterloo, Ontario, Canada, 2021

AUTHOR'S DECLARATION

I hereby declare that I am the sole author of this thesis. This is a true copy of the thesis, including any required final revisions, as accepted by my examiners.

I understand that my thesis may be made electronically available to the public

Abstract

Purpose. Children with visual impairment may be referred for ERG and OCT testing to aid in diagnosis and monitoring, particularly those with suspected retinal diseases. To establish if a result is abnormal, knowledge of typical development of retinal structure and function is essential to detect, monitor, and understand pathological processes that may affect the pediatric retina. The purpose of the first study was to investigate the development of the ERG waveforms from childhood until adulthood in healthy children of European descent to better understand how retinal function changes with age. Additionally, the study aimed to provide a pediatric normative dataset for the standard ERGs to be used for clinical interpretations for children with suspected retinal diseases. The purpose of the second study was to investigate the maturation of the retinal structure from childhood until adulthood. Also, the study aimed to provide a pediatric normative dataset of retinal layer thickness maps measurements for each of the seven layers that were automatically generated by SD-OCT in the retinal regions defined by the Early Treatment of Diabetic Retinopathy Study (EDTRS) (Heidelberg Spectralis) in the same population (children of European descent). The additional purpose was to provide reference values for each sector of the peripapillary RNFL thickness. Adults were included in both studies for comparison.

Methods. For the first cross–sectional study (ERG study), thirty-two participants of European descent with normal ocular and general health were recruited. The sample included 12 children between 7 and 11 years, 10 older children and adolescents between 12 and 15 years and 10 adults between 20 and 33 years. Full-field ERGs were recorded simultaneously in each eye from thread electrodes (DTL® fiber) using the Espion E3 system with fully dilated pupils (0.5% tropicamide). Stimuli were ISCEV standard dark-adapted ERGs (DA 0.01, DA 3, DA 10) as well

as a light-adapted ERG series with flash strengths of 0.3, 1.0, 3.0, 10 & 24 cd.s.m2 (which includes the standard LA 3.0). We measured a- and b-wave amplitudes and implicit times using the average of the right and left eye values to compare age groups.

For the cross–sectional second study (OCT study), thirty-six participants of European descent with normal ocular and general health were recruited. The sample included 6 children between 4 and 7 years, 9 children between 8 and 11 years and 10 adolescents between 12 and 15 years and 11 adults between 20 and 33 years. SD-OCT scans centered on the fovea were acquired with fully dilated pupils (0.5% tropicamide). Retinal thickness values were measured for the ETDRS regions for each of the seven layers that were automatically generated by SD-OCT (Heidelberg Spectralis, Eye Explorer software version 1.9.10.0). The peripapillary RNFL thickness measurements were calculated using the Spectralis OCT device. The influence of age on the foveal subfield, inner ring and outer ring of the ETDRS maps, as well as on the peripapillary RNFL thickness was determined using parametric or ranked correlations. Adjusted Bonferroni correction was applied to correct for multiple comparisons.

Results. For the first study, both DA a- and- b-wave implicit times were significantly positively correlated with age for all stimuli except for the b-wave of the DA 3.0 ERG i.e., implicit times were shorter for children compared to adults. Rank correlations of a-wave with age were $r=0.573$, $p = 0.001$ for the DA 3.0 ERG, $r = 0.570$, and $p < 0.001$ for the DA 10 ERG. DA b-wave implicit times were correlated with age for the weak and strong flash stimuli but not for the LA standard 3.0 ERG (DA 0.01 ERG [$r = 0.596$, $p< 0.001$] or DA 10 ERG [$r = 0.434$, $p< 0.013$]). With respect to the LA ERGs, a-wave implicit times did not correlate with age except

for the LA 0.3 ERG ($r = 0.548$, $p = 0.001$). LA b-wave implicit times did not correlate with age except for the LA 1.0 ERG time age ($r = 0.363$, $p= 0.041$). In contrast, none of the ERG DA and LA amplitudes for both a- and b-waves were significantly correlated with age.

For the second study, average global peripapillary RNFL thickness was $104.86 \pm 9.43\mu m$. The peripapillary RNFL thickness was not significantly correlated with age except for the nasal superior sector where it thinned with age ($r = -0.379$, $p = 0.023$). Regarding the ETDRS regions, the total retinal thickness was positively correlated with age in the foveal subfield ($r = 0.487$, $p = 0.003$) but not in the other ETDRS rings. All the individual inner retinal layers thickened with age in some regions, except for the ganglion cell layer. While the retinal nerve fiber layer was significantly positively correlated with age in the fovea ($r = 0.557$, $p<0.001$) and parafovea (0.474, $p = 0.004$), the inner plexiform layer was only influenced by age in the parafoveal area (0.495, $p= 0.002$). In contrast, the inner nuclear layer was positively influenced by age only at the fovea ($r = 0.452$, $p= 0.006$). The individual outer retinal layers were associated with age in some regions except for the outer nuclear layer. While the outer plexiform layer thinned significantly with age in the parafoveal area ($r = -0.394$, $p = 0.017$), the retinal pigment epithelium thickened with age ($r = 0.387$, $p = 0.020$) in the foveal area.

In Chapter 5 examples of OCTs and ERGs from children with retinopathy due to HARS syndrome are compared qualitatively with the present results.

Conclusion. The present study provides evidence that the functional and morphological development of the retina may not be mature for children aged from 4 to 15 years. So that, the implicit times of both DA a- and b-waves and some of the LA ERGs (0.3[a-wave], 1.0 [b-wave]) increase with age to approach the adult values. Similarly, the OCT findings of the present study indicate that both the inner and outer retinal layers were influenced by age except for the ganglion cells and outer nuclear layers. Nevertheless, the peripapillary RNFL thickness measurements were not affected by age except for the nasal superior sector such that the thickness values decrease with age. In this study, we were able to obtain OCT scans using standard instruments for children as young as 4 years, and as young as 7 years for ERG. For the quantitative measurements from these techniques to be most beneficial in detecting and monitoring retinal disorders in pediatric patients, they have to be compared to an age-matched database. Age-norms and ranges were therefore calculated for those measures that were correlated with age, and overall means/medians and 95% ranges for those that were not correlated with age. These normative values can be used as a reference against which to compare for children with suspected retinal diseases.

Acknowledgements

I would like to express my deepest appreciation to my supervisors Drs. Daphne McCulloch and Susan Leat for providing their invaluable guidance, and gracious support throughout the course of the project. This project could not have been accomplished without their inspiration, constant critical reviews and suggestions.

I would like to express my sincere gratitude to Drs. Zay Khan and Natalie Hutchings for sharing their knowledge and expertise in the project.

I would like to thank my sponsor Saudi Arabian Cultural Bureau in Canada for their financial support.

I would like to thank all the study participants for making this happen.

Dedication

To my beloved parents, brothers and sisters, your love and support are the reasons behind my success.

Table of Contents

List of Figures

List of Tables

Chapter 1 Introduction and Literature Review

1.1 General retinal development

The retina develops over a considerably long period of time starting from early gestation through early adulthood. Despite its importance, there are surprisingly few studies that have documented the morphological changes of the human fovea from gestation until it becomes truly adult-like.[1–4] This is likely due to the difficulty of obtaining normal well-preserved human eyes at prenatal, neonatal and childhood ages. Therefore, most of our knowledge regarding the maturation of the human fovea has relied heavily on histologic studies of simian retina[5,6]. Additionally, existing studies vary in their conclusions: Earlier studies reported that foveal development is complete between 11 months and 5 years of age[1–3,7], but more recent studies indicated that it continues even after 12 years of age[4,8]. The light micrograph is considered the gold standard for studying the development retinal morphology allowing for high-resolution images of the retinal cells. However, the technique has several limitations such as shrinking of the tissue and artifacts which may adversely affect the apparent maturation of the retina[8]. Thus, histological studies may not always determine with certainty the developmental patterns as well as time course for each retinal layer.

1.1.1 Histological maturation of the retina from mid-gestation to adulthood

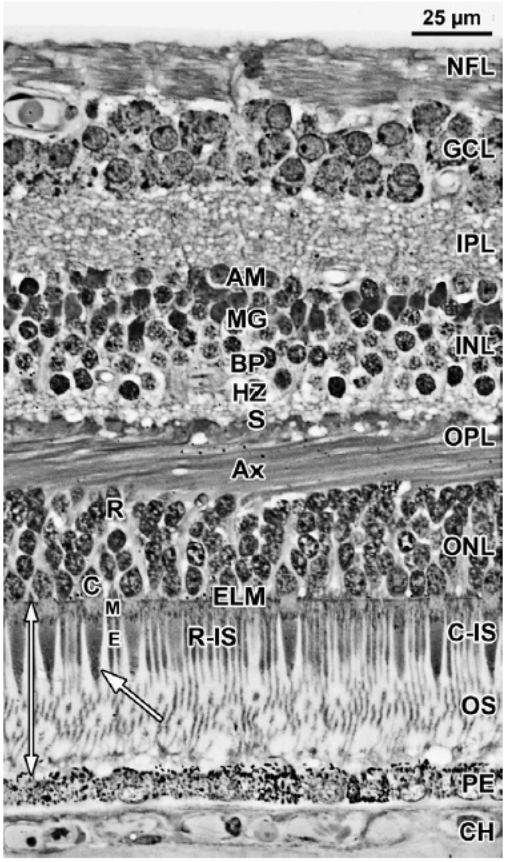

Figure 1-1: A histological cross-section of retinal layers of normal adult human retina (2 mm nasal from the foveal center). Choroid (CH); retinal pigment epithelium (PE); outer nuclear layer (ONL) which is separated into photoreceptor inner (IS) and outer (OS) segment layers that includes a single layer of cone (C) nuclei and multitudinal rows of rod (R) nuclei. The rod's inner segments are thin (R-IS) whereas the thickness of the rod OS are approximately half of those R-IS. The shorter cone OS has a larger tapered cone IS (C-IS). The distal edge of the retina is marked by the external limiting membrane (ELM). The outer plexiform layer (OPL) comprises photoreceptor axons (AX), also known as fibers of Henle and synaptic terminals, including cone pedicles and rod spherules. The inner nuclear layer includes horizontal cells (HZ), bipolar cells (BP) cell bodies as well as Muller glia (MG) and amacrine cells (AM). The inner plexiform layer (IPL), ganglion cell (GCL), and nerve fiber layer (NFL). *Retrieved from Hendrickson et al[9], used with permission.*

Time courses of the morphological development of retinal layers are shown in (Table 1-1).

Table1-1: Morphological changes of the retinal layers in utero and after birth[2–4].

Age	Development of retinal layers
22 fetal weeks	• At this stage of the immature eye, there is no evidence of foveal depression. Instead, the macular zone appears elevated owing to the presence of a thick ganglion cell layer (GCL) which is 5 to 7 cells deep. • Vitreal to the GCL, the nerve fiber layer (NFL) can be recognized as a thin layer which is surrounded by a delicate inner limiting membrane (ILM). • The IPL layer is well developed and is nearly as thick as that in adults. • INL is considerably thick and each cell type is divided into sublayers marking the regions of the future horizontal, Muller, and bipolar cells. The transient layer of Chievitz (TC) is not evident at this stage. • The outer plexiform layer (OPL) is well recognized but is still somewhat thinner than in older fetuses. • The outer nuclear layer (ONL) comprises a single row of cones that do not appear to develop either IS or OS, forming a regular columnar epithelium. These cells are located directly opposed to the thin pigment epithelium (PE) which lacks apical processes.
24-27 fetal weeks	• The inner retinal layers are displaced peripherally to develop a slight foveal depression. • The GCL is nearly 6 cells deep around the fovea and 3-4 cells deep in the center. • The RNFL is considerably thicker than the previous stage. • The IPL is relatively thick and has a vertical and horizontal fiber pattern with the vertical fibers being Müller fibers. • In contrast to the earlier stage, the INL becomes more complex as the presence of TC is evident separating the innermost cells from the remainder of the INL. Additionally, the layer is reduced to 4 to 5 cells deep centrally and 8 to 10 nuclei deep on the slope. • The outer limiting membrane appears as a thin and darkly stained band. • Over the central 1500–1800μm, the rods are absent, forming an area known as rod-free zone. Central cones have a large thick nucleus with a short axon that ends in a synaptic terminal. IS and OS are evident at this stage but are extremely immature. Even though cones are immature at this stage, they have many of the essential molecules. • The rods are more prominent outside the area of pure cones so that the ONL contains a single row of cone cell bodies and 3-4 layers of rod nuclei. Both rod and cone IS are longer at 2mm away from the fovea compared to the foveal centre.

28 to 37 weeks	• The foveal pit is prominent and clearly formed and appears wider and shallower than earlier stages as both INL and GCL are reduced to 3-4 cells deep at the foveal centre. • Until birth, the ONL is formed by a single layer cone nuclei under the developing foveal pit, whereas a double cell layer of nuclei is being formed on the slope which appears more mature than foveal cones. In contrast, the rods develop 2-6 deeper layers of rod cell bodies peripheral to the foveal center. • Both IS and OS are clearly identified and have elongated photoreceptor axons (AX) that end in the synaptic pedicle. • The rod-free zone is narrowed with the rods being present at 600µm away from the foveal depression, suggesting that the process of the cone packing density has begun despite the fact that the foveal center is still overlaid by a single row of cone inner segments. • The PE layer has fine apical process interdigitating with the OS.
Post-natal 1 day - 6 weeks	• The foveal pit continues to increase in-depth due to the marked outward displacement of the GCL and INL away from the fovea. • The GCL is no more than 1-2 cells deep with wide spaces between the cells and the INL is reduced to less than 3 cells deep in the foveal pit. • The TC is prominent and extends for around 1100µm on the nasal edge and 1000µm on the temporal edge. • After birth, the OPL undergoes a profound change in and around the fovea as elongated cone axons are evidence in the foveal center making the OPL considerably thicker layer than the previous stages. • ONL in the foveal pit is still formed of a single layer of cone cell bodies, but the IS and OS appear tapered and elongated while the slope cones are packed into 2-3 cells deep and are thinner and longer than foveal cones.
Post-natal 9 to 15 months	• At the foveal centre, GCL, IPL, and INL have fused into a single thin layer making the foveal depression shallower and wider. • TC is still present, but it is reduced in size on both sides of the fovea. • Foveal cones continue to narrow and elongate the IS/OS and are packed into 2-3 cells deep and 3-4 nuclei deep in the slope. Central cone axons elongate further due to the process of the cone packing density, making OPL a thick layer of axons and cone synaptic pedicles. In addition, OPL around the foveal center is much thicker than in the slope which primarily includes synaptic terminals. • Foveal and peripheral IS and OS are almost identical in length with foveal IS/OS being approximately 46µm compared to 36µm long for the peripheral cones.

Post-natal 28 months to 13 years	• By 3.8 years old, the foveal depression becomes wider and deeper than earlier stages and appears similar to those of adults. • Central cones have narrower IS and longer OS than peripheral cones. • The 3.8 years old fovea appears morphologically similar to mature fovea except the process of cone packing density is not complete at this stage. • There is no evidence of TC at this stage. • The fovea is mature by most criteria by 13 years of age: (1) the foveal pit is wide and shallow; (2) the foveal cones are packed into 12 cells deep; (3) the foveal cones IS/OS are thin and elongated; (4) the TC has disappeared.

Generally, there are several developmental indicators that mark the maturation of the human retina. These include the curvature of the foveal depression, the elongation of cones' inner and outer segments, the presence of a prominent acellular zone in the inner nuclear layer (INL) known as the transient layer of Chievitz (TC), and the cone packing density[2–4].

The earliest sign of the developing macula is the appearance of a central elevated zone in the future site of the foveal pit due to the presence of a prominent thick ganglion cell layer (GCL). Hendrickson et al.[2] traced the morphological changes of human fovea from 22-week gestation to 45 months, and the study documented that at 22 weeks gestation, the future site of the foveal pit is not evident owing to the thickened GCL. This changes considerably in the 24-26 fetal weeks as a slight foveal depression begins to form indicated by the thinning of both GCL and INL. The formation of the foveal depression includes two neural displacements that occur in opposite directions: the outward migration of the inner retinal layers away from the fovea and the central ward migration of the cone photoreceptors toward the fovea. Consequently, the peripheral displacement of the GCL and INL leads to a steady thinning of the central fovea forming the

foveal depression. The foveal depression continues to widen and deepen progressively with time reaching dimensions within the adult range by around 45 months after birth (Figures 1-2 and 1-3) or possibly later.

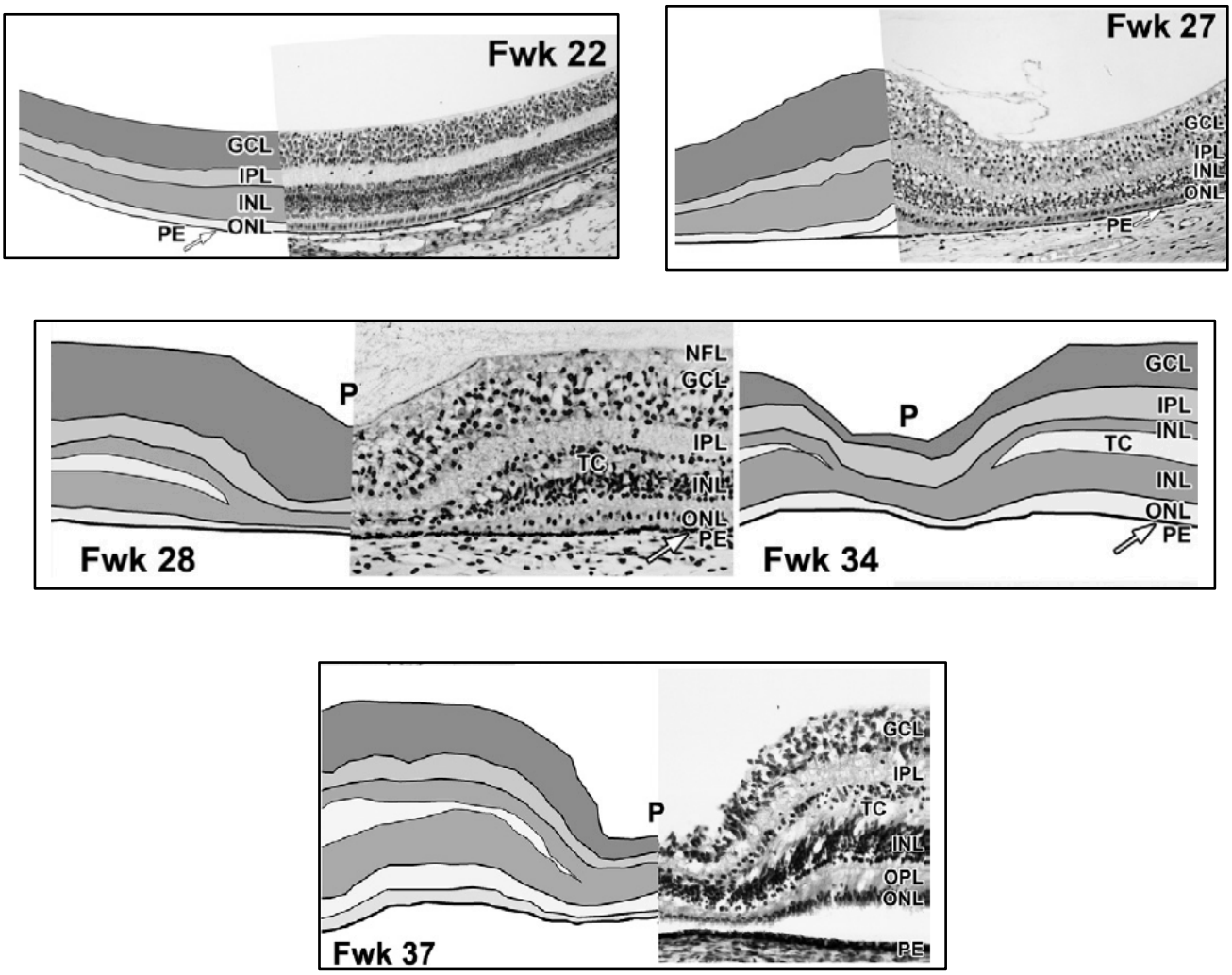

Figure 1-2: Histological development of retinal layers in utero. At 22 fetal weeks, the foveal area is identified as an elliptical zone approximately 1.5mm in diameter characterized by the presence of a thickened GCL as well as the ONL that is made up of a single row of cell bodies. At 25-27 fetal weeks, the formation of a slight foveal depression is evident marked by the peripheral migration of inner retinal layers away from the fovea. At 28-37 fetal week, the foveal depression is prominent and well-developed owing to the pronounced thinning of both GCL and INL at the foveal center compared to the layers surrounding the pit (foveal slope). The INL becomes more complex than the previous stage owing to the presence of the transient layer of Chievitz (TC). The ONL is still formed from a single layer of cell bodies. *Retrieved from Hendrickson et al[9], used with permission.*

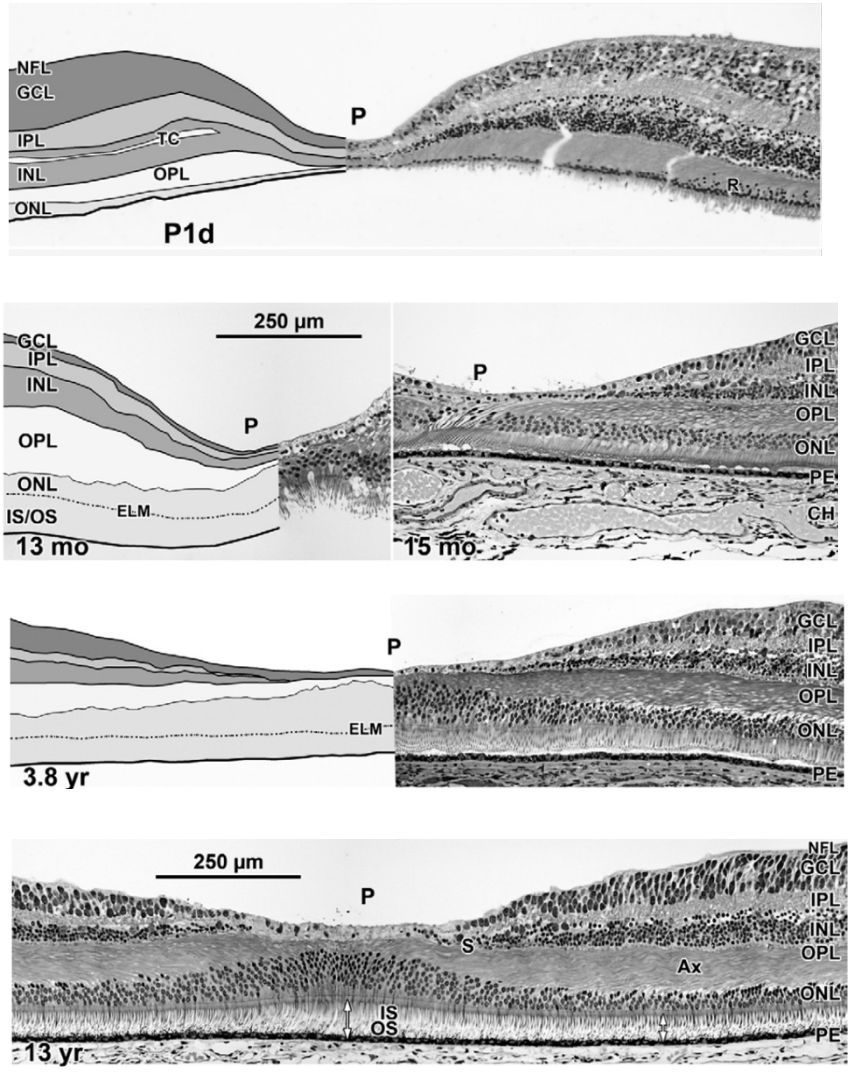

Figure 1-3: Post-natal histological development of the retinal layers. After birth, the foveal depression appears thicker and shallower than pre-natal fovea, has extended close to cone synapses, and most of the inner retinal layers have been displaced peripherally. The TC is still present in the INL at this stage. The cones are approximately 2-3 nuclei deep and have elongated axons on the pit slope, but the foveal center is still formed of a single layer of cones. Over the first 15 months of life, the foveal pit is wide and shallow, with virtually no neurons over the foveal pit excluding the cone nuclei within the ONL. The OPL layer has increased in thickness primarily owing to the increased number and elongation of the cone axons. The ONL in the foveal pit is approximately 2-3 cone cell bodies indicating the process of postnatal cone packing density. Between 3.8 to 13 years, the foveal pit appears wide and deep. The center of the fovea contains narrow and elongated cone's IS/OS and is nearly 8-12 cell bodies deep. Note that the fovea at 3.8 years old is morphologically similar to that at 13 years save for the cone packing density, which is approximately half of the 13 years old fovea. *Retrieved from Hendrickson et al, used with permission.*

Concurrently, the cone photoreceptors migrate centrally towards the foveola leading to a decrease in the diameter of the rod free zone area and an increase in the cone packing density. Yuodelis et al.[3] reported that at 22 weeks gestation, the diameter of the rod free zone is around 1600μm wide, and the area becomes narrower with time until the diameter of the pure cone nuclei zone reaches the adult range (750-700μm) between 15 to 45 months after birth. It should be noted that this process is asymmetrical as the distance from the central foveal pit to the first rod nuclei is always greater in the nasal edge compared to the temporal side. With regards to the cone packing density, it has been previously reported that the cone density increases from 13 cones/100μm at 22 fetal weeks to 18 cones /100μm at birth when the pit is narrowed. After birth, the cone density in the foveola slightly increases from 22 cones/100μm at 15 months to 31cones /100 μm at 45 months, and doubles from the density at birth to 42 cones /100μm by 37 years with a gradual decline to 32 cones/100μm by 72 years[3]. A similar pattern was found 250μm away from the foveola[3]. The fact that the cone density at 45 months is approximately half that at 37 years old (based on one human child's eye) reflects the long sequence of post-natal foveal development even though the foveal dimensions may be within the adult range by 45 months of age. The main issue in existing histologic studies is the small sample size that has been

documented. For instance, Yuodelis et al.[3] reported the number of cones within the foveal area to vary between 49 and 76 per 100µm (based on two adult eyes). Both these numbers are significantly higher than the 34 per 100µm reported by Polyak et al.[10] which was based on one adult human eye. Therefore, the variation between individuals of the same age is still not well understood.

The retinal development can be marked by the changes in the structure of the cones inner and outer segments within the foveal region. The cone photoreceptors undergo a profound thinning and elongation, allowing them to be tightly packed into the fovea (Figure1-4). By 25 fetal weeks, the inner segment (IS) is identified as a short thick extension of the cone cytoplasm, but it is prominent at birth being approximately 6µm wide by 9µm long. Within the first 15 months of life, the diameter of the inner segment narrows to 2.5µm and more than doubles in length. By 45 months, the inner segment reaches the adult size being approximately 2µm wide and 25-30µm long[3,4]. The outer segments (OS) have a similar maturation pattern, but over a longer period of time. Yuodelis et al.[3] indicated that the outer segment is first observed by light microscopy prenatally at 36 weeks gestational age; however, immunolabeling analysis demonstrated that the central cone outer segments are present between 24-26 weeks but are extremely immature[9]. At birth, the outer segments are still short and rudimentary being only 3µm long, but they increase 7 times within the first 15 months of life to be approximately 22µm. The outer segment continues to elongate further, reaching 30µm long by 45 months, and doubles to 60 µm long in the adult fovea[3,9].

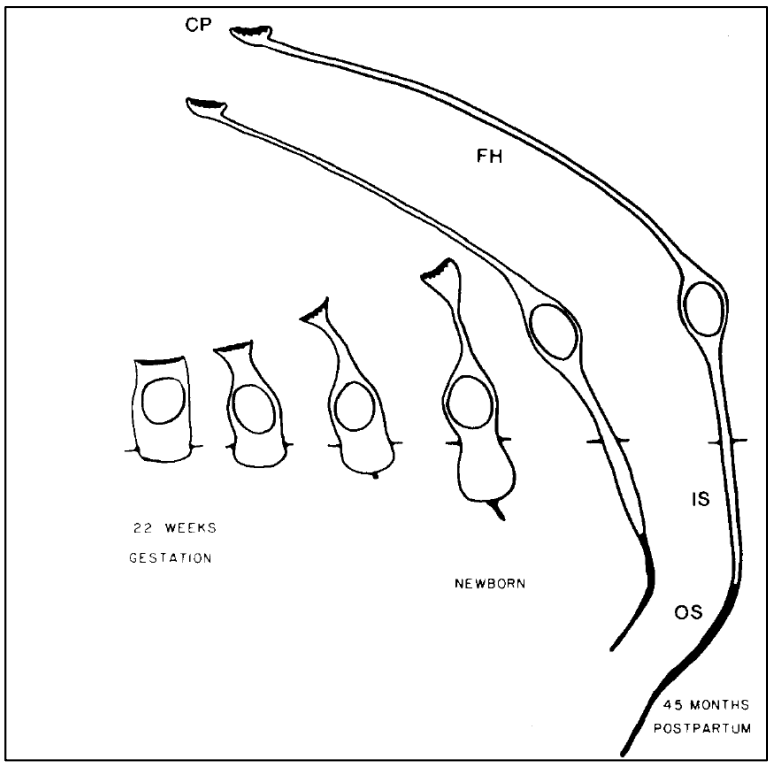

Figure 1-4: A schematic drawing representing the maturation of cone inner and outer segments from 22 weeks gestation to 45 months after birth. *Retrieved from Hendrickson et al.[2] used with permission.*

The transient layer of Chievitz (TC) is a unique characteristic of primate retinae[2,11] and is composed of pale fibers that separate the innermost row of nuclei from the reminder of the INL. Immunocytochemical analysis has demonstrated that the TC fibers are primarily Muller cells processes[9] (Figure 1-2). The TC layer within the INL is not present at 22 weeks and becomes almost visible at 24-26 fetal weeks. Subsequently, the layer continues to increase in thickness with time, reaching a maximum thickness in the newborn retina. By 15 months of age, the layer is still identifiable, but it is significantly thinner than the previous stage, before it disappears by 45 months old[2].

According to Hendrickson et al.[9] the fovea is completely developed in all aspects by 13 years of age. By this age, the foveal depression appears wide and shallow and the base of the depression includes Muller cytoplasm and cone axons. The layer of cone nuclei within the ONL are up to 12 cone nuclei deep compared to a single layer of cones at birth. The cone IS and OS within the fovea are narrow, elongated and densely packed so that it is difficult to distinguish individual IS and OS (Figure 1-3).

1.2 Full-field electroretinogram (ERG)

Electroretinography (ERG) is a non-invasive clinical procedure that records electrical potentials generated in the retina in response to light stimulation.[12] By manipulating the stimulation and adaptation conditions, ERG recordings can selectively evaluate the rod- or cone-generated responses as well as be critical in diagnosing several retinal diseases such as cone-rod dystrophy, rod monochromatism, Leber congenital amaurosis and other genetic disorders that affect the retina. Full-field flash ERGs do not provide topographical information regarding localized lesions and isolated retinal defects abnormalities. Hence, clinically, they should be performed in addition to other ocular testing such as visual field and fundus examinations and/or additional electrophysiologic testing such as pattern or multifocal ERGs[13].

The full-field ERG was discovered in the middle of 1800s in excised animal eyes and the clinical application of the procedure in humans started in the 1940s[13,14]. However, a wide range of techniques were used under various conditions such as varieties of recording equipment with different amplifiers, different period of dark adaptation, several electrical filtration techniques, and numerous colors of lights. Consequently, the testing variability led to difficulty in

interpreting and comparing both the ERG literature and clinical reports[14]. Hence, the International Society for Clinical Electrophysiology of Vision (ISCEV) established standardized the procedures for recording and reporting clinical ERGs based on a consensus of best clinical practice. The procedure is updated periodically and the most recent revision of the ISCEV Standard for clinical full field electroretinography was published in 2015[15]. Regardless, it is critical to understand and recognize the power and limitations of the standard protocols. The standard includes protocols that facilitate consistent clinical diagnosis and monitoring that can be compared between laboratories. Therefore, the standard protocols should be used as part of the electrophysiological examination, but not to the exclusion of other specialised protocols that might be included in the ERG tests either routinely or for certain clinical situations. For instance, ERGs recorded to chromatic stimuli can be used in addition to the standard protocols to improve the differentiation of rod- and cone-generated ERG waveforms. In other words, clinical testing should include, but not necessarily be limited by, the standard protocols.

1.2.1 Retinal responses to the light

The full field ERG is initiated by the photoreceptors which are the light detecting cells that convert the light signals into electrical signals in the outer portion of the retina. Generally, there are two types of photoreceptors known as rods and cones. The rods include a visual pigment known as rhodopsin that has a peak spectral absorption for light with a wavelength of 496nm. In contrast, there are three classes of cone color sensitive pigments that peak at 558 nm for L-cone (long-wavelength), 531nm for M-cone (mid-wavelength), and 419nm for S-cone (short-wavelength).

The retina has 4-5 million cones and 80-120 million rods. The maximal density of cones is located within the foveal region approaching around 140 cones per 100µm[13]. The density of cones decreases considerably outside the foveal zone, particularly beyond 10° from the fovea reaching a cone density around 1 per 100µm. The maximum density of both L-cones and M-cones is at the foveal center whereas S-cones, which account for only 9% of all cones, have their highest density within 1-2° around the center of the fovea. On the other hand, rods are found throughout the retina but are absent at the center of the fovea with a maximum density being located between 15° to 40° from the fovea reaching around 10 per 100µm[13,16].

The ERG is generated by light-stimulated movements of extracellular retinal ions. In non-invasive clinical testing, the electric field potentials generated are recorded indirectly at the corneal surface with special types of electrodes. The extracellular flow of primarily positive potassium (K+) and sodium (Na+) ions are due to depolarization (opening) and hyperpolarization (closure) of cellular membrane channels. In the darkness, the channels of the photoreceptor outer segments for the sodium (Na+) and calcium (Ca^{2+}) ions are opened to enable them to enter the cells. The exchange of the NA^{+}/Ca^{2+} and K^{+} amplifies at the cellular membrane of the outer segment. In addition, the intracellular and extracellular cation concentration is maintained by a compensatory extrusion of K^{+} within the rod inner segment. Consequently, there is a circulation of an extracellular current (the dark current) maintaining the photoreceptors in a depolarized state, which results in a release of a neurotransmitter known as glutamate at a high rate. In the presence of light stimulation, the phototransduction process leads to the closure of the Na+ and Ca^{2+} channels of the outer segment and blocks the release of glutamate. Phototransduction is initiated when, light-activated rhodopsin activates the enzyme transducin

which in turn activates phosphodiesterase (PDE) leading to hydrolyzation of cyclic guanosine monophosphate (cGMP). The process is amplified resulting in the activation of up to 100,000 cGMP by a single rhodopsin molecule. The reduction of intracellular cGMP results in the closure of Na+ and Ca^2 cellular membrane channels. Thus, the photoreceptors become hypolarized causing a rise in the extracellular of Na+ and Ca^{2+} leading to stopping the dark current and a relative increase in the positivity of the outer retina. This can be indirectly recorded at the corneal surface as the initial negative portion of the ERG (a-wave)[13,16].

The retinal function can be studied by the same stimulus to obtain ERG recordings under photopic or scotopic conditions. For instance, the developmental rate of both a- and b-waves under the scotopic condition can be used as an index of retinal function. The sensitivity of the rods and cones changes to adapt to a variety of light levels. In fact, the dark adaptation rate of the cones is noticeably faster compared to the rods reaching maximum light sensitivity after approximately 10 to 12 minutes. Although the dark adaptation period of the rods is significantly longer than the cones, they reach a considerably lower final light threshold after around 30 to 40 minutes. The dark adapted (scotopic) condition of the ERG can be approximated after a period of 20 minutes of dark adaptation. However, a period of 30 to 40 minutes of dark adaptation is recommended for completely activating the rod photoreceptors. Under photopic conditions, the sensitivity of the photoreceptors decreases markedly reaching maximum light adaptation after approximately 15 minutes of light exposure. Thus, the light adapted (photopic) ERG condition can be measured after approximately 10 minutes of light adaptation by either exposing the individual to the light room or by using the photopic background of the full field dome[13,17] .

1.2.2 Physiological origin of the standard ERG waveforms

The ERG waveform demonstrates a summation of the electrical changes of all retinal cells based on several factors including the adaptive state of the retina (dark adapted (DA) vs. light adapted (LA)), the intensity and duration of the stimulus (flash vs. long duration), the type of the stimulus (flash vs. flicker), and the color of the stimulus (white vs. chromatic). Our understanding of the physiological origin of ERGs was mainly driven from animal studies using intraretinal microelectrode analyses and ERG changes from using chemical substances with known retinal effects[18].

1.2.2.1 Origin of DA 0.01 ERG

Following 20 minutes of dark adaptation, the dark-adapted weak flash ERG has a prominent b-wave but almost no or very small a-wave. This is because the electrical activity generated by the rods in response to dim light stimulus is too small to be identified as an a-wave. However, the rod signal is greatly amplified by the depolarizing ON bipolar neural pathway in the inner retina (b-wave)[19]. In addition, the extracellular current of the b-wave includes activity of the Muller cells which is more extensive (stronger and longer duration) than the rod photoreceptors current (a-wave)[13,20].

1.2.2.2 Origin of DA 3.0 ERG

This is the dark-adapted standard flash ERG, and it has prominent a- and b-waves. The descending portion of the a-wave reflects the activity of the photoreceptors (rods and cones)[21,22]. Computational models demonstrated that the leading edge of the a-wave is directly associated with the phototransduction cascade of the photoreceptors which produces electrical activity[21,23].

Thus, the first 14-20ms of the activity is primarily due to the photoreceptors' response with no influence from the inner neural retina[24]. The morphology of the b-wave is defined by the interaction between the photoreceptor activity and inner retinal activity. Accordingly, the origin of the b-wave is mainly owing to depolarizing ON rod bipolar cell responses that generate the extraretinal light current[13,25–28].

1.2.2.3 Origin of LA 3.0 ERG

The Light-adapted standard ERG has distinct a- and b-waves. Computational models showed that the initial phase of the a-wave likely reflects the electrical response produced by the phototransduction cascade of the cone[29–32]. Nevertheless, Bush et al.[33] documented that the photopic a-wave is considerably influenced by the inner retinal activity postsynaptic to the cones specifically for standard ERG stimuli. Therefore, the trough of the a-wave receives a considerable contribution from the inner retinal activity including hyperpolarizing OFF bipolar neurons in addition to the cone photoreceptors contributions. With regards to the light adapted b-wave, it is not only formed by the depolarizing ON bipolar cell activities and/or Muller cells, but is also influenced by the electrical activities of horizontal cells and hyperpolarizing OFF bipolar cells[34]. This process is known as a push pull model where the ascending portion of the b-wave is pulled up by the activities of depolarizing ON bipolar cells and the amplitude of the b-wave is being pushed toward the baseline due to the activity of hyperpolarizing OFF bipolar cells.

1.2.2.4 Origin of LA 30 Hz flicker ERG

The human photopic flicker ERG (30-Hz) was initially thought to be primarily due to photoreceptors activity. Evidence for the photoreceptors theory is supported by the analysis of intraretinal recordings in monkey, which concluded that isolating the cone responses using NA^+ aspartate did not influence the phase of the flicker ERG suggesting that the photoceptors make the major contribution to the ERG independently from the inner retinal activities[35,36]. However, pharmacological dissection studies were conducted to selectively remove the post-receptoral inner retinal activities and revealed that the flicker ERG reflects the activity of post-receptoral cells, primarily those of the inner nuclear layer in response to cone activity and that the direct contribution from cones is minimal[37,38]. Therefore, the steady-state waveform of the flicker ERG is due to the ON and OFF pathways with large phase differences between the pathways, so that they partly cancel each other.

1.2.2.5 Origin of DA 3.0 oscillatory potentials ERG

The oscillatory potentials (OPs) consist of a series of high frequency and low amplitude wavelets, approximately 4-6 wavelets, during the ascending phase of the b-wave and can be recorded under both light-adapted and dark-adapted conditions with input from both rod and cone photoreceptors[39]. The OPs have a different physiologic origin than a- and b-waves. It has been previously proposed the OPs are likely due to inhibitory feedback activities associated with circuits in the inner plexiform, but not all OPs have the same origin[40,41]. Wachmeister et al.[42] documented that the earlier OPs are depressed by using GABA and dopamine antagonists while later OPs are reduced by using glycine antagonists and ethanol, indicating that not all OPs arise from the same cells. Therefore, OPs likely reflect the electrical activity of amacrine and bipolar

cells. The earlier wavelets (cone mediated) are likely due to the ON neural pathway where the later wavelets (rods mediated) are associated with the OFF pathways[13,42].

1.2.3 ISCEV standard protocols

The standard full-field ERG includes 6 protocols which are named based on the luminance emitted from the surface of the ganzfeld dome and the frequency of the brief flash stimuli (the units for the time-integrated luminance of brief flashes are candelas seconds per square meter, [cd.s.m^{-2}]). The responses to the six standard ERG protocols are shown schematically in Figure 1-5 and will be described below in turn. Evaluating and measuring ERGs is described in Chapter 3.

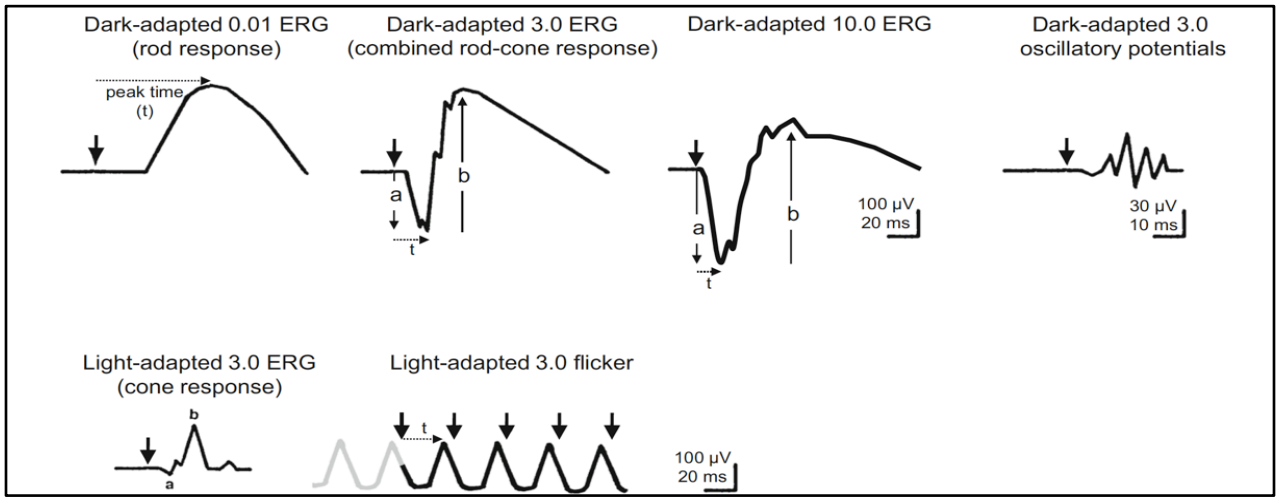

Figure 1-5: Schematic illustration of six ISCEV Standard ERGs waveforms. Bold arrows show the timing of the stimulus flash, solid arrows illustrate a -wave and b- wave amplitudes and dotted arrows demonstrate how time to peak is measured. *Retrieved from McCulloch et al*[15]*., republished with permission.*

1.2.3.1 Dark-adapted 0.01 ERG (Rod ERG)

The dark adapted 0.01 ERG (weak flash) is typically recorded first after at least 20 minutes of dark adaptation. The stimulus is weak, 0.01 cd.s.m^{-2} to elicit the rod response. This is 2.5 log units below the standard flash and below the cone threshold to allow the rod-generated response to be isolated and quantified. The DA 0.01 ERG waveform is simple and has a small or non-detectable a-wave even in individuals with normal vision. It is usually less than 5uv in adults with a peak time of nearly 40ms. With regards to the b-wave, it is typically slow and smooth and peaks in healthy adults at around 85ms after the flash[15,43].

1.2.3.2 Dark-adapted 3.0 ERG (Combined rod-cone response)

The dark adapted 3.0 ERG (standard flash) is normally measured immediately after the DA 0.01 ERG to stimulate both rod and cone functions. The minimum recommended time interval between flash stimuli should be at least 10s to allow retinal recovery and prevent light adaptation. The morphology of the response is biphasic and includes both rod and cone activity in individuals with normal vision[15,43].

1.2.3.3 Dark-adapted 3.0 oscillatory potentials

Oscillatory potentials are elicited from the dark-adapted eye with the same standard flash as the DA 3.0 ERG by using a high-pass analogue or digital filter to eliminate low frequencies (75Hz and lower). Alternatively, several forms of digital filtration settings can be used after the testing is complete. The technical instructions for using and selecting the filters are indicated in ISCEV technical guidelines[15,43,44]. The oscillatory potentials can be optimized by using a “conditioning flash” nearly 15-30s before data acquisition. Generally, the oscillatory potential includes at least

two peaks named sequentially as OP1 and OP2 etc. The summed activity of the amplitude components ("caliper-square" method or "oscillatory index") is usually used as an index to reflect the function of the middle and inner retinal cells. OPs are generally reduced in diseases associated with retinal ischemia, for instance sickle cell retinopathy and diabetic retinopathy. Nevertheless, OPs will also be affected by the disorders of the outer retina that decrease input to the OPs.

1.2.3.4 Dark-adapted 10 ERG (standard strong flash ERG)

The dark-adapted 10 ERG (standard strong flash ERG) is typically recorded immediately after the standard flash (DA 3.0 ERG), and because the flash is very strong, a minimum period of at least 20s seconds between the stimuli is necessary to allow retinal recovery. The standard strong flash stimulus is a brief flash of 10 $cd.s.m^{-2}$. This ERG waveform is characterized by having a larger a-wave with better defined implicit time (the time from the mid-point of the flash stimulus to peak of the wave) compared to the standard flash and it will assist in identification of the a-wave, particularly when the a-wave has a low amplitude compared with the DA Standard 3.0 ERG. For example in certain conditions such as opaque media or immature retina[15,43].

1.2.3.5 Light-adapted 3.0 ERG

The LA 3.0 ERG is primarily generated by the cone system as both the light adaptation and a rod- suppressing white light background luminance of 30 $cd.m^{-2}$ are used to reduce input from the rod system. The subject should be light adapted for 10 minutes prior recording and the ERG is elicited by using the standard flash (3 flash). The LA ERG waveform has a prominent a- and

b-wave with typical implicit times of approximately 15ms and 30ms respectively for adults with normal vision. The interval between flashes for the LA 3.0 ERG can be as short as 500 ms[15].

1.2.3.6 Light-Adapted 30 Hz flicker ERG

The flicker response is also obtained in the presence of the standard 30 cd/m^2 rod-suppressing background immediately after recording single-flash cone response. The response is elicited by the standard flash (3.0 flash) flickering at a rate of approximately 30 Hz. It should be noted that a flickering rate exactly at 30 Hz will cause electrical activity of the same frequency to be included in the averaged ERG, in particular electrical noise due to the power supply and computer processing frequencies. Thus, the flickering rate should be close to, but not exactly, 30 Hz (for example, 30.3). Usually, the initial responses are larger than the subsequent responses, hence the measurement should begin when the stable-state response is reached[15,43].

1.2.4 Development of the ERG components from infancy to adulthood

1.2.4.1 The ERG in pre-term infants

The retina is not completely mature at birth and undergoes several structural and functional changes including the development of photopic and scotopic functions obtained by the ERG. Several studies have documented that ERGs are detectable for both term and preterm infants as early as 30 weeks post conception[45–48], but infants have smaller amplitudes and longer implicit times. Thus, the Standard stimulus for the rod response is too low to reliably detect abnormality at birth (Figure 1-6). Fulton et al.[48] reported that 25% of infants who were 5 weeks and younger had no detectable ERG for the Standard dark-adapted ERG, and the lower limits of typical b-wave amplitudes for the dark-adapted 0.01 ERG, the dark-adapted 3.0 ERG and the light adapted

3.0 ERGs include zero until later in infancy (15 weeks/3.5 months of age). Therefore for dark-adapted ERGs, stronger stimuli than the standard flashes (typically up to 2.0 log units stronger) are necessary to generate a reliable dark-adapted ERG waveforms in infants after birth[48,49]. A summary of previous studies on preterm infants are shown in Table 1-1.

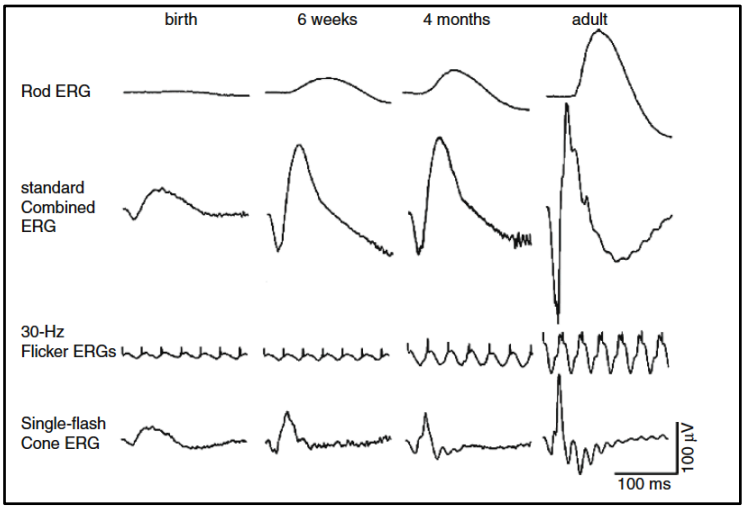

Figure 1-6: Representation of ISCEV parameters for typically developing infants at different ages. *Retrieved from Birch et al.,*[49] *republished with permission.*

Berezovsky et a.l[50] investigated the development of standard ERGs for healthy preterm infants at 3 (-3.1 to +3.6) or 8 weeks (+5.3 to +10.9) after term age. They documented a small developmental change in ERG components between the two infant age groups, such that an increase in the amplitude and a decrease in implicit time was evident for LA 3.0 and LA 30 Hz flicker ERG, but not for all ERG waveforms. This is consistent with the study of Birch et al.[49] in which the ERGs were obtained from full-term newborn infants and at 17 weeks post-term age in infants born prematurely. Therefore, large cone response amplitudes in older infants may indicate a developmental change of cone mediated responses from 8 (Berezovsky et al.[50]) to 17 (Birch et al.[49]) weeks old. On the other hand, rod mediated activity at 8 weeks and 17 weeks

were similar in both studies suggesting that rod responses might mature at a faster rate or earlier compared to cone responses during the period of birth to 17 weeks.

It is described above how the a-wave reflects photoreceptor activity while the b-wave is due to inner retinal responses. Using the ratio of b-wave to a-wave amplitude as an index to reflect the maturation of retinal inner and outer elements, Berezovsky et al.[50] reported that the ratio of b/a amplitude in preterm infants was considerably larger than that documented for adults suggesting that inner nuclear layer (Muller/bipolar cells) matures earlier than the outer photoreceptor layer. This is in a good agreement with Mets et al.[51] who reported a definitive b-wave and no detectable a-wave in first month of life, a pronounced light-adapted b-wave and the emergence of a dark-adapted a-wave for strong flashes by 3 months, and more distinct dark-adapted a-wave by 6 months of age.

Table 1-2: Previous ERG reports in preterm infants.

Study	**Sample**	**Age**	**Findings**
Birch et al[45]. (1992)	81	36 weeks and 57 weeks post-conception	An increase of rod amplitude by a factor of 10 between the 36 and 57-week-old
Mets et al.[51] (1995)	26	First 16 months of life	Systematic increase in amplitude and decrease in latency with time (a- and b-waves)
Leaf et al.[52] (1996)	16	40 weeks post conception (term age) 23-51 days post-natal)	There is an association with birth weight and a small effect of dietary intervention
Berezovsky et al.[50] (2003)	17	3 weeks and 8 weeks post term	Larger amplitude and shorter peak time of cone responses for the older group. Also, shorter peak times for rod generated ERGs.

1.2.4.2 DA 0.01 ERG (Rod responses)

Previous reports revealed that, despite the faster development between 8-17 weeks, rod mediated ERG waveforms were slower to reach maturity compared to other ERG parameters. Normative values are shown in Table 1-2. Birch et al.[49] studied the development of the ERG waveforms from infancy including DA and LA ERGs. They reported that the DA ERGs to a very weak flash (0.004 $cd.s.m^{-2}$) are extremely immature at birth with mean amplitudes and implicit times of 2.7μv and 117.2ms respectively. This changes progressively in the following years approaching the adult values by 5-15 years old with b-wave amplitudes of 145μv and implicit times approaching 79.4ms. Using a logistic growth curve to describe the developmental changes of the ERG components, Westall et al.[53] documented that DA ERG amplitudes reach half of the adult values by 19 months of age and approach the adult data by 7 years of age with an estimated developmental growth rate slope of 0.62 (age exponent of the logistic curve in months). Fulton et al.[48] undertook the largest child study which includes 400 participants with the aim of providing provisional normal ranges for the standard ERGs. However, the data were collected from two labs and each lab used a different technique to obtain ERGs (white flashes for the first lab, blue and red flashes for the second lab). They concluded that the median amplitude of the 0.01 ERG b-wave at birth (1-5 weeks) is approximately 15% of the median for adults and the rod responses fall within the lower limit of the adult values by 1-10 years of age. With regards to the implicit time of the light-adapted 0.01 ERG b-wave, Fulton et al.[48] reported that it varies little between 1-5 weeks to 20 years old as well.

To conclude, previous studies suggested that the b-wave amplitude of the rod response is adult-like between 5-15 years of age. The data were grouped, however, such that any differences

between younger and older children could not be identified. Nevertheless, Westall et al. included younger children in their study, and they reported that the amplitude of the b-wave reaches maturity by 7 years of age. On the other hand, existing studies varied in their conclusions in terms of maturation of b-wave implicit times. While Fulton et al.[48] reported that light-adapted b-waves were prolonged up to 15 weeks of age and overlapped with adult values in older infants. Similarly, Birch et al.[49] documented that the implicit times are considerably longer in infancy (birth and 17-week-old age groups) and were mature in children tested between 5-15 years of age. This variability of findings between studies is likely due to the different techniques were used to obtain ERG recordings.

Table 1-3: Normative values reported by previous studies for ERG rod response.

Dark Adapted weak flash ERG: b-wave				
Birch et al[49] (0.0004 cd.s.m^{-2})				
Age	Mean b-wave implicit time (ms)	Upper limit (95% CI in ms)	Mean b-wave amplitude (μv)	Lower limit (95% CI in μv)
Birth	117.2	144.6	2.7	0
4 months	94.2	107.9	45	22
5-15 years	81.3	91.1	145	99
15-24 years	79.4	89.0	145	92
25-34 years	81.3	91.1	138	88
35-44 years	81.3	91.1	135	92

Fulton et al[48] 0.01 cd.s.m^{-2}		
Age	Median b-wave implicit time (ms)	Median b-wave amplitudes (μv)
1-5 weeks	105	42
5-10 weeks	104	63
10-15 weeks	98	80
15-25 weeks	119	192
1-10 years	116	161
10-20 years	110	235
>20	110	244

1.2.4.3 DA 3.0 ERG (Combined rod-cone response)

Available evidence seems to suggest that combined rod-cone responses mature more rapidly than the rod response, reaching maturity during the first 3-5 years of life. Table 1-4 summarizes the results provided by previous studies for combined rod-cone response. Birch et al.[49] concluded that rapid development of the combined response is evident during the first four months of life, so that the b-wave amplitude reaches half of the adult values and the implicit time is within 12 months of the adults range by that age. The response enters the range of the normal adult values for both implicit time (28 months) and amplitude (372μv) during 5-15 years of age. However, Westall et al.[53] reported that the amplitude of dark-adapted 3.0 b-wave is about half of adult values by only 1.2 months (5 weeks) of age and approaches the adult range by 3 years of age. Similarly, Fulton et al.[48] documented that the median amplitude of the b-wave is approximately 32% of adult values during the first two months of life and it continues to grow gradually

reaching the adult values between 1-10 years old. The implicit time decreases with age from 65ms during infancy to 47months by 1-10 years.

To sum up, there is little available evidence of when the b-wave amplitude is mature, as it is reported as sometime between 1 and 15 years. There is similar uncertainty about when the implicit time is adult like, also reaching maturity between 1 and 15 years. This is largely because available data are sparse, so that determining the exact age of maturity has not been possible. Only one study included younger children aged 3-5 years in their report and concluded that the amplitude of the b-wave is adult-like by 3 years of age.

Table 1-4: Normative values reported by previous studies for ERG combined rod-cone response.

Dark adapted standard ERG				
Birch et al.[49](2 cd.s.m^{-2})				
Age	Mean b-wave implicit time(ms)	Upper limit of 95% CI (ms)	b-wave amplitude mean (μv)	Lower limit of 95% CI (μv)
Birth	62.8	70.9	33.1	11
4 months	48.9	54.9	170	92
5-15 years	38	44.3	372	354
15-24 years	35	36.9	363	248
25-34 years	38	44.3	355	225

35-44 years	37.2	40.1	331	235
b-wave amplitude	584.3	1.2	0.58	37
a-wave amplitude	345.4	16	0.51	68
Fulton et al.[48] (2.25 cd.s.m^{-2} Boston group, 2 cd.s.m^{-2} Toronto group)				
Age	Median b-wave implicit time (ms)	Median b-wave amplitudes (μv)	Median a-wave implicit time (ms)	Median a-wave amplitudes (μv)
1-5 weeks	65	137	23	39
5-10 weeks	61	253	21	63
10-15 weeks	55	271	22	75
15-25 weeks	53	452	21	145
1-10 years	47	473	21	190
10-20 years	46	538	20	264
>20	45	517	20	266

1.2.4.4 DA 3.0 ERG Oscillatory potentials

Dark adapted oscillatory potentials (OPs) are the most immature ERG waveforms during infancy and are slower to begin their development compared to other dark-adapted ERG components.

Westall et al.[53] found that OPs in infants (< 4 months) are not recordable above noise and the individual OPs develop over different time scales so that the amplitude of the later OPs (OP3, OP4) reach 50% of the adult amplitude by 12 months whereas the OP2 has reached this point by 4.7 months. After this initial delay, they develop rapidly reaching maturity before any other components of the ERG, at around 2 years of age. Accordingly, 95% of infant OP amplitudes fall within the normal ranges for adult data by 9 months for OP2, 18 months for OP3 and 21 months for OP4. The implicit times have been shown to be within the normal limits of adult values by 16 months for OP2, 17 months OP3 and 34 months for OP4. Moskowitz et al[54] studied the developmental changes of photopic and scotopic OPs between infants at 10-weeks of age and adults. They reported that infants' scotopic OPs are about 19% of adult values compared to approximately 50% for photopic OPs indicating that scotopic OPs are less mature than photopic OPs.

In conclusion, only one study has reported the development of standard OPs from infancy until adulthood and they found that OPs are extremely immature or non-recordable very early in infancy and approach maturity in the first two years of life. Also, OP2, OP3 and OP4 mature over different time scales indicating not all OPs have the same physiologic origin.

1.2.4.5 LA 3.0 ERG (Single-flash cone dominated ERG)

Single-flash light-adapted ERG amplitudes develop over a similar period of time as dark-adapted ERGs, but they have a less dramatic growth. Table 1-5 summarizes the results of normal limits for light-adapted ERGs. Fulton et al[48] found that the amplitudes of the b-wave increase systematically with age until they fall within the lower limits of normal adult data by 15-52

weeks of age with an amplitude of128μv. Westall et al.[53] documented that b-wave amplitudes are about half of the mean adult amplitude during the first two years of life with 95% overlap of the adult data by 5 years of age with an estimated maximum growth rate of 0.44. This is consistent with Birch et al.[49] who found that the amplitudes of 4 month old infants are less than half the adults' amplitude, reaching maturity by 5-15 years.

To conclude, there is a wide range of age (1-15 years) over which previous studies have reported that the b-wave amplitude is considered adult-like and during which time there is considerable overlap with adult values. However, the data in the majority of studies are grouped such that the exact age of maturation cannot be determined. Using a criterion of 95% overlap with the adult range helps to narrow the maturation estimates for specific ERG waveforms. The implicit time across LA 3.0 ERG waveforms has been shown to vary little between 4 months and 15 years of age with considerable overlap with the adult ranges from early childhood.

Table 1-5: Normative data previously reported for ERG cone response.

Light adapted ERGs				
Birch et al[49] (0.4 cd.s.m^{-2})				
Age	Mean b-wave implicit time (ms)	Upper limit of normative data (ms)	Mean b-wave amplitudes(μv)	Lower limit of normative data (μv)

Birth	42.1	48.5	16.2	5.2
4 months	34.6	37.4	76	43
5-15 years	28.8	31.1	115	76
15-24 years	28.8	31.1	107	73
25-34 years	28.2	31.6	98	60
35-44 years	28.8	32.3	91	60

Fulton et al (2.25 cd.s.m^{-2} Boston group, 2 cd.s.m^{-2} Toronto group)				
Age	Median b-wave implicit time (ms)	Median b-wave amplitudes (μv)	Median a-wave implicit time (ms)	Median a-wave amplitudes (μv)
1-5 weeks	36	60	19	30
5-10 weeks	36	102	18	43
10-15 weeks	35	92	16	43
15-25 weeks	30	128	15	27
1-10 years	29	128	15	34
10-20 years	28	155	14	43
>20	28	160	14	42

1.2.4.6 LA 3.0 Flicker ERG

The flicker ERGs show considerable immaturity at birth, both in terms of amplitudes which are smaller by a factor of 15-fold compared with adult normative data and implicit time to the first positive peak which is 8ms slower than adult values[49]. Table 1-6 summarizes the normative data for flicker ERG waveforms. During the first four months of life, the flicker ERG amplitude matures rapidly and reaches half of the adult mean value by the end of that time. The implicit times decrease more gradually to be approximately 6ms longer than adult mean values by 4 months. By 5-15 years, the flicker ERG waveforms have matured sufficiently to be considered adult-like, both in terms of amplitudes and implicit times[49]. This is consistent with Westall et al.[53] who reported that flicker responses are about 50% of the adult value by 5 months of age and fall within the range of adult data by 5 years of age.

Table 1-6: Normative data previously reported for ERG Flicker response.

LA 30 Hz flicker ERG				
Birch et al[49] **(0.4 cd.s.m^{-2})**				
Age	Mean b-wave implicit time (ms)	Upper limit of normative data (ms)	Mean b-wave amplitudes (μv)	Lower limit of normative data (μv)

Birth	41.8	46.5	4.7	1.2
4 months	36.1	41.3	32	9
5-15 years	28.8	31.1	68	41
15-24 years	28.8	31.1	69	44
25-34 years	28.8	31.1	65	38
35-44 years	29.5	31.8	63	42

1.2.4.7 Summary of the developmental changes of the ERG waveforms

The studies reviewed above used contact lens electrodes to obtain ERG waveforms, and they show general agreement in terms of maturation of standard ERGs. Generally, a number of studies have agreed that infants have smaller amplitudes and longer implicit times in response to full-field standard flashes in light- and dark-adapted conditions. ERGs are detectable as early as 30 weeks gestational age in preterm infants. During the first 4 months of life, there is a rapid development of the amplitudes and implicit times of the a-wave and b-wave, and development is slower thereafter. Both a- and b-wave amplitudes and implicit times mature sufficiently to be considered adult-like somewhere between 1-15 years. Oscillatory potentials are considerably immature in early infancy, as they are undetectable above noise before one month of age. After this initial delay, they develop rapidly reaching maturity before any other components of ERG around 2 years of age. It should be noted that, existing studies obtained ERG recordings using a variety of techniques. For instance, Birch et al. and Westall et al. used a dimmer flash for the DA

3.0 ERG known previously as maximal response (2.0 cd.s.m^{-2}). Similarly, the luminance intensity used for the weak flash varies substantially between studies. While Birch et al used 0.0004 cd.s.m^{-2}, Berezovsky et a.l[50] used 0.00981 cd.s.m^{-2} to obtain rod responses. Additionally, Fulton et al. used both white and chromatic stimuli to investigate the developmental changes of ERG waveforms. Therefore, when interpreting ERG normative data, the technique used to acquire ERGs should be considered as the results may vary depending on several factors including technique and protocol.

1.2.5 Examples of clinical applications of full-field ERG

1.2.5.1 Retinitis Pigmentosa

Retinitis Pigmentosa (RP) is defined as a large family of inherited heterogeneous disorders that involve dysfunction of metabolic retinal processes, usually leading to progressive loss of photoreceptors. The disease affects roughly 1 in 3000-4500 individuals of the population. The clinical findings associated with RP vary even within families with the same genotype. The ocular symptoms include night vision loss, peripheral visual field loss and photophobia which typically manifest gradually between the second and fifth decades of life. Visual acuity and macular function typically show relative sparing until the late stages of the disorders. Advances in genetics have made it possible to identify biochemical defects as well as the hereditary pattern of many variants of RP. There are several modes of inheritance including autosomal recessive and dominant as well as X-linked. Nearly half of affected individuals have no family history of RP and have sporadic RP[13,43].

Full-field ERGs play a key role in diagnosing and following the progression of RP even when clinical findings are mild. In the early stages of the disorder all ERG waveforms are markedly depressed and prolonged while in some cases ERGs associated with the cone pathways show relative sparing. With further progression, both rod and cone responses become diminished, prolonged and non-detectable[13]. In a longitudinal study (4 years) that involved 67 RP patients, Birch et al.[55] reported that an average annual reduction of the amplitude of 64% and 60% for dark-adapted and light-adapted ERGs, respectively. The mean annual increase in the rod and cone thresholds was 28% and 13%, respectively. In addition, the average annual decline in the flicker ERG amplitude was approximately 13%. This is consistent with previous longitudinal studies by Berson et al.[56] which included 94 RP patients who may or may not have had detectable rod ERGs. They found that the average annual loss of the flicker ERG amplitude was 16-18.5% for RP patients.

1.2.5.2 Leber Congenital Amaurosis

Leber congenital amaurosis (LCA) is a genetically heterogenous autosomal recessive group of retinal degeneration diseases characterized by visual impairment normally noted soon after birth and frequently accompanied by infantile nystagmus. Other ocular signs associated with LCA include cataracts, hyperopia and keratoconus. Mutations in several genes have been reported to be associated with LCA. RPE65 is a specific protein in retinal pigment epithelium that plays an essential role in the visual cycle[57]. Other genes that have been identified include retinal guanylate cyclase (GUCY2D)[58] and photoreceptor-specific homeo box gene (CRX)[13,43].

Full-field ERG is a critical test in diagnosing LCA and identifying related retinal dysfunction. Several reports have indicated that full field ERGs are undetectable in most patients with LCA even in the early stages of the disease. A few patients have detectable ERG waveforms, but they are markedly depressed and prolonged.

1.2.5.3 Usher syndrome

Usher syndrome is a complex genetic disorder that is primarily a heterogeneous group of autosomal recessive defects with several genetic subtypes characterized by hearing loss and progressive pigmentary retinopathy (syndromatic RP). Generally, there are three types of Usher syndrome which are classified based on the reduction of ERGs and the onset of retinal degeneration. Type I Usher syndrome is characterized by severe hearing loss and vestibular dysfunction. Individuals with type II Usher syndrome have mild congenital deafness and typical vestibular function, and individuals with type III Usher syndrome have almost normal hearing with progressive deafness. Thus, hearing examination with audiometry is critical in determining the type of Usher syndrome[13,59].

A previous report suggested that type I Usher syndrome is associated with at least 5 inherited loci found on chromosomes 14q (type IA), 11q (type IB), 11p (type IC), 10q (type ID). Almost 75% of patients with type I Usher syndrome have type IB which is due to mutations of the gene that causes abnormal myosin VIIA[60]. Type II Usher syndrome is associated with at least 3 genes found on chromosomes 1q (type IIA), 3q (type IIB) and 5q (type IIC). Nearly 90 % of patients with type II Usher syndrome have type IIA which is likely owing to mutations of the gene encoding usherin[13,61].

Ocular findings and degree of vision loss vary even with patients within the same family. The ocular signs of Usher syndrome are comparable to those of RP (severe, early onset) which include night vision loss, peripheral vision impairment and light sensitivity. In the early stage of the disorder, visual acuity and macular function are relatively preserved. Additionally, retinal atrophy with pigmentary clumping and vascular attenuation develop with progressive optic nerve atrophy[13,62].

Full-field ERGs in Usher syndrome are markedly depressed even in the early stage of the disease and the impairment of rod function is typically greater compared to cone function, but ERGs become non-detectable early in these conditions. The type I of the syndrome has an earlier onset and greater severity of progressive pigmentary retinopathy than type II. Similarly, visual acuity and visual field are likely to be more affected in type I compared to type II[60,63]. Nevertheless, there is a noticeable overlap of these clinical components in terms of the degree of the impairment that occurs between Type I and type II, so that differentiating the types of Usher syndrome is complex and challenging. Bharadwaj et al.[64] reported that ERGs, visual field, and visual acuity of type IB and other types of I Usher syndrome patients do not differ significantly. Likewise, Seeliger et al.[65] documented a reduction of multifocal ERG amplitude in individuals with type I Usher syndrome, RP and Usher type II. However, patients with type I had a slightly prolonged implicit times in the peripheral region (30° tested area) compared to individuals with type II RP who showed considerably prolonged implicit times.

1.3 Optical coherence tomography (OCT)

Optical coherence tomography (OCT) is an imaging modality that has increasingly become the indispensable cornerstone of managing various ocular pathologies over the past few decades. The fundamental aspects of the OCT evolved from the previously designed imaging system known as low coherence reflectometry which was based on a broadband light source and a Michelson interferometer. In 1991, the application of transverse scanning (B-scan) enabled two-dimensional scanning of the retinal tissue and this unprecedented technique was named as OCT by James Fujimoto. The OCT provides non-invasive applicability, high-resolution scans and cross-section topographical images of the retina with a short acquisition time, allowing detailed examination of the retina without the need for sedation or anesthesia. Since its introduction in 1991, our understanding of the retina has been enhanced, enabling *in vivo* assessment that corresponds with histopathology. Accordingly, the OCT has facilitated our understanding of retinal development including the crucial correlation between the foveal maturation and visual potential from infancy until adulthood[66–69].

1.3.1 OCT-scanning principle

Optical coherence tomography is an advanced diagnostic imaging procedure that enables capturing a micron resolution three-dimensional scan. The technique uses the principle of optical refractometry, which includes measuring the backscattering light from a tissue of interest or the time that emitted light takes to travel between biological tissue and return to the lens, generating an echo time delay with quantifiable signal intensity. The image is formed by measuring the intensity and the echo time delay of the scattered light from the tissue. Subsequently, the light from a broadband light source is divided into two arms known as a reference arm and a sample

arm that is reflected back from the retinal structures at different depths. Generally, there are two techniques used to capture the backscattered light, which are Time-domain (TD) detection and Fourier domain (FD) detection, which is subdivided into the Spectral Domain (SD) and Swept-source (SS) (Figure 1-7)[67,70].

1.3.1.1 Time-domain optical coherence tomography (TD-OCT)

In this technology, the light returning from the sample and the reference arms are recombined, such that interference is used to produce an A-scan (depth-resolved the retinal image at a particular point). Moving the reference and the sample arms with respect to each other produces several A-scans that are merged into a cross-sectional scan known as the B-scan (line scan). Generally, the imaging speeds of time domain OCTs are relatively slow, with approximately 400 A-scans per second. The commercially available TD-OCT instrument is the Stratus OCT™ (Carl Zeiss Meditech)[67,71,72].

1.3.1.2 Spectral domain optical coherence tomography (SD-OCT)

In spectral-domain OCT, the spectral interference pattern of the sample arm and the reference arm is diffused using a spectrometer and assembled concurrently with an array detector. This simultaneous collection enables much faster image acquisition than the time-domain system (TD-OCT), in which the data are collected over time by the interferometer. Subsequently, A-scans are produced by inverse Fourier transforms on the concurrently collected data. The imaging speed of such technology typically ranges between 18,000 and 70,000 A-scans per second. Therefore, this faster acquisition time provided by the SD-OCT minimizes the effect of eye movements during the imaging, particularly in individuals with poor fixation. In addition,

higher scanning speed allows denser sampling of the macula, minimizing the chances of missing pathology and better visualization of the retinal structure[67,72].

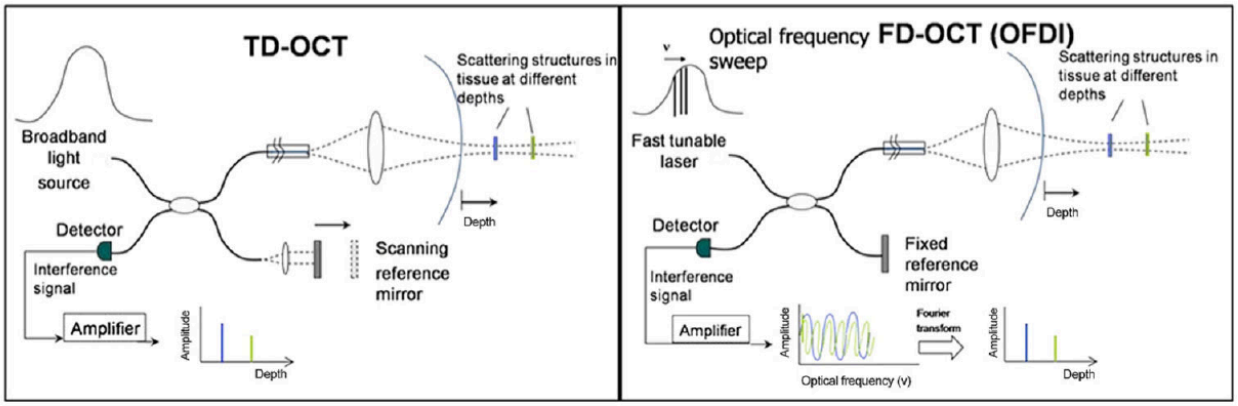

Figure 1-7: A schematic drawing representing the time-domain optical coherence tomography (TD-OCT) and a subtype of spectral-domain optical coherence tomography (FD-OCT), knowing as optical frequency domain imaging (OFDI OCT). In both imaging technologies, an interferometer and a reference arm are used to detect the echo time delay of backscattered light. The interferometer has a beam-splitter, separating the light into a reference arm and a sample arm. In TD-OCT, the reference arm is scanned through a moving mirror to generate a time-varying time delay. In the FD-OCT, the light source is frequently swept, so that the interference of the light beams returning from both reference and sample arms oscillates with respect to the frequency difference. Additionally, all echo delays in FD-OCT are collected simultaneously, allowing for a considerable increase in image acquisition speed. *Retrieved from Bezerra et al.[67], republished with permission.*

1.3.2 Macular scanning protocols

Generally, the widely used protocols for macular scanning are macular cube scan, raster scan, and radial scan (Figure 1-8). Macular cubes are three dimensions scans comparable to computed tomography scans that obtain volumetric cubes of data. Spectral-domain OCT instruments obtain a series of rapid B-scans in a 6 mm x 6mm square centered on the fovea. The resolution of the scans is minimized to reduce the acquisition time of scanning. Therefore, when evaluating a single line scan (B-scans) from a cube scan, some details are likely to be lost. The cube scan is centered at the fovea by default. Nevertheless, other retinal regions can be captured by manually

adjusting the scan position in the area of interest. For instance, optic nerve scans are cube scans positioned at the center of the nerve. Raster scanning is an approach used to acquire macular cube scans, which includes a systematic pattern of scans recorded over a rectangular area through tightly spaced parallel lines resulting in a consistent sampling density over the entire scanned area. Radial scanning includes six to twelve high-resolution B-scans (line scans) obtained at radial orientations, so that all scans pass through the fovea. The limitation of this technique is that interpolation is used between the scans when producing macular thickness maps. This may be ideal at the foveal region where the lines are closely spaced; however, lesions can be missed in the macular area where the lines are not tightly spaced. Consequently, macular maps are directly driven from the cube scan or radial scans depending on the instrument and contain numeric values indicating the retinal thickness over the scanned area and color-coded illustrations showing the age-matched normative data set (Figure 1-8)[72,73].

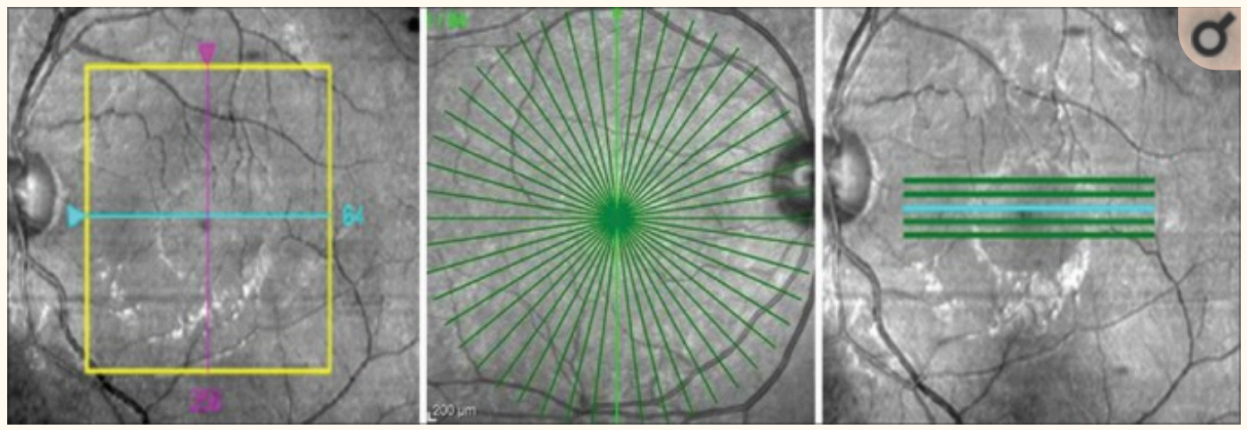

Figure 1-8: Commonly used macular scanning protocols for SD-OCT. Macular cube (left), radial scan (centre), and raster scan (right). *Retrieved from Bhende et al,[73] used with permission.*

1.3.2.1 Interpretation of OCT scans

Interpretation of OCT scans includes both qualitative and quantitative assessments, and both are essential to evaluate an OCT image thoroughly. In qualitative evaluation, individual B-scans (line-scans) of the targeted area in the retina are qualitatively reviewed to assess the presence or absence of retinal pathology based on the knowledge of typical OCT anatomy (Figure 1-9). Line scans can be displayed in a color-coded or a gray-scale image indicating the reflectivity of different retinal layers. Retinal pathologies and their response to treatment can be evaluated by comparing B-scans performed over time[72].

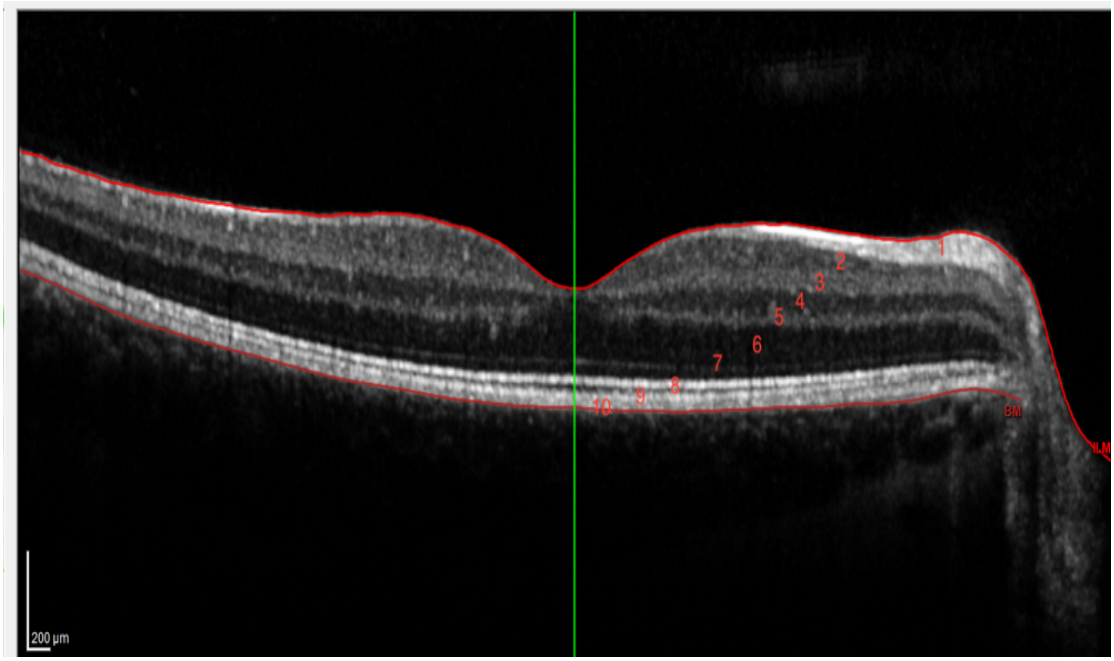

Figure 1-9: An example of an OCT scan with segmentation showing normal OCT anatomy. 1= nerve fiber layer; 2= ganglion cell layer; 3= inner plexiform layer; 4= inner nuclear layer; 5= outer plexiform layer; 6= outer nuclear layer; 7 external limiting membrane; 8= ellipsoid zone; 9= interdigitation zone; 10= retinal pigment epithelium**.** *Scan by Hussain Albuhayzah.*

Qualitatively, the areas of the B-scans are described as hyper-reflective or hypo-reflective and indicate shadowing or reverse shadowing. Hyper-reflective zones have higher light reflectivity than typical for a specific zone and appear whiter than nearby areas on a gray-scale image (e.g., hard exudates and epiretinal membranes). Hypo-reflective zones have lower light reflectivity than the nearby regions. An example is regions with more fluid content (e.g., intraretinal cysts). Shadowing refers to an increase in light absorption in a given area compared to the area underneath leading to optical shadowing and reduced visualization of outer retinal layers. Examples include hard exudates, clear debris and larger retinal vessels. In contrast, reverse shadowing characterized by atrophy of retinal pigment epithelium layer results in transmission of excessive light through outer retinal tissues[72,74].

It is essential to be aware of several issues associated with qualitative interpretation, such as registration, sampling error, and subjective evaluation. First of all, registration refers to the registration of future B-scans to previous scans. In other words, the clinician must ensure the exact retinal region is scanned similarly in subsequent tests. Secondly, sampling error means that the presence of pathology may be misdiagnosed if only a single or several line scans are evaluated. Therefore, it is critical to examine multiple B-scans through the macula when performing a qualitative assessment. Finally, qualitative assessment is subjective and means that the interpretation of the B-scans will be individualized owing to the lack of numeric values. Also, it is challenging to assess the progression of a disorder that improves in a specific area of the macula and deteriorates in other areas[72,74].

On the other hand, quantitative evaluation of OCT scans depends on the OCT software's capability to accurately segment retinal layers - the ability of the software to identify sub-retinal layers and precisely calculate retinal thickness. Accordingly, the acquired retinal thickness is then compared to an age-matched database to assess for normalcy and to monitor the pathology's progression over time. Quantitative measures are often displayed as color-coded maps or as grids established for use as in the Early Treatment of Diabetic Retinopathy Study (ETDRS)[75]. It should be noted that the numeric values obtained by different OCT equipment are not directly comparable across all OCT instruments as different OCT instruments use different algorithms to obtain retinal thickness values. Also, some OCT instruments include ETDRS maps to calculate retinal thickness measurements while others (hand-held OCTs) are not provided with such maps (retinal thickness typically being calculated using a custom software). Nevertheless, the main disadvantage of the quantitative interpretation is that even in the most advanced OCT instruments, the generated numeric values are subject to artifacts. For instance, the software may fail to determine the inner and outer retinal margins accurately; hence, the obtained retinal thickness is inaccurate[72,74].

1.3.2.2 The maturation of the retinal layers *in vivo*

The development of OCT technology has made it possible to image different retinal layers *in vivo* depending on the retinal layers' intrinsic reflectance or the interference between adjacent tissues. Therefore, the reflective difference between alternating layers of highly reflective axons, dendrites, melanosomes, and low reflective cell bodies enables easy differentiation of retinal layers[76]. Accordingly, it is essential to be familiar with some definitions used to define retinal sublayers and areas before understanding the retinal development from infancy until adulthood.

Figure 1-10 shows the layers of a newborn baby as visualised by OCT. The central foveal thickness (CFT) indicates the thickness of the whole retina from the inner border of the inner limiting membrane to the inner aspect of the RPE at the center of the fovea. The inner retinal layers (IRLs) extend from the inner border of the inner limiting membrane to the outer aspect of the inner nuclear layer (INL). The outer retinal layers (ORLs) include all the retinal tissue from the inner border of the outer plexiform layer (OPL) to the inner aspect of the RPE. The photoreceptor layer comprises the entire area from the outer aspect of the OPL to the RPE's inner aspect. The foveae of premature babies have several characteristic features compared to adult foveae, which include (1) a noticeably shallower foveal depression, (2) the appearance of persisting inner retinal tissues at the foveal center including the IPL and INL, (3) overall thinner retinal layers, (4) the absence of photoreceptor sublayers[8,69,77,78] .

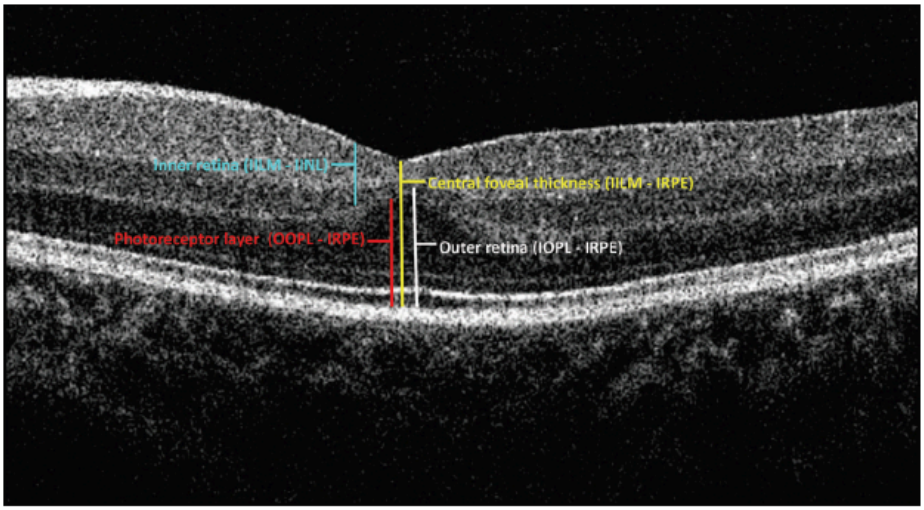

Figure 1-10: The areas and layers identified on an SD-OCT scan of a newborn infant. *Retrieved from Mangaleshl et al.*[69]*, used with permission.*

1.3.2.2.1 The maturation of the inner retinal layers

During infancy, the inner retinal layers (IRLs) at the foveal center are characterized by the appearance of GCL, IPL and INL as distinct measurable bands before they are condensed into a single hyper-reflective layer in children and adults. This is because of the outward migration of the inner retinal layers away from the fovea. The number and thickness of the inner retinal layers at the center of the fovea reduce with time as the premature fovea matures. Previous studies reported that most of the outward migration of IRLs occurs between 31 and 42 weeks[8,69,78]. Lee et al.[77] documented that the centrifugal displacement of the retinal layers is complete by 17.5 months. The outward displacement of the GCL from the fovea reaches 95% of normal adult values by 10.6 months, whereas the IPL and INL reduce significantly in thickness before reaching mature thickness levels by 18.7 and 17.6 months, respectively. However, at the parafovea and perifovea, the development is greater than at the foveal center. The RNFL and IPL undergo a significant reduction in thickness until 31.4 and 39 months, respectively. The GCL and INL are initially reduced in thickness compared to adults until approximately 17 months, followed by a subsequent increase in thickness until 65.5 months and 41.5 months, respectively. This developmental trajectory may indicate the displacement processes of IRLs away from the fovea and their thickening over time. The time courses of these dual processes are unique for each inner retinal layer. The mean thickness estimates for the inner retinal layers reported by previous studies are indicated in Table 1-7.

Table 1-7*:* Review of normative data reported for the inner retinal layer thicknesses. RNFL = retinal nerve fiber layer; GCL = ganglion cell layer; IPL = inner plexiform layer; INL = inner nuclear layer; OPL = outer plexiform layer; ONL = outer nuclear layer; IS = inner segment of the photoreceptor; OS = outer segment of the photoreceptor; RPE = retinal pigment epithelium; m = age in months; SD = standard deviation. NR = not reported in these studies.

Maldonado et al[78]

Inner retinal layer thicknesses at the foveal area (μm) measured by SD-OCT

Sample	Age range	Total IRLs	RNFL (μm)	GCL (μm)	IPL (μm)	INL (μm)
13	24-29 weeks	78	NR	3	26	55
4	1-9 months	10	NR	2	10	11
5	2-15 years	23	NR	0	0	8
9	20-49 years	7	NR	0	0	7

Lee et al[77].

Age at which inner retinal layers approaches adult values at the foveal area

Retinal layers	Age (months)	Mean thickness (μm)	Std. Deviation	95% confidence interval	
				Lower	Upper
RNFL	NR	NR	NR	NR	NR
GCL	10.6	NR	NR	NR	NR
IPL	18.7	2.81	4.07	0.00	10.96

INL	17.6	1.87	2.92	0.00	7.70

Age at which inner retinal layers approach adult values in the parafoveal areas

Nasal parafovea						Temporal parafovea				
Retinal layers	Age (mo)	Mean (μm)	SD	95% CI		Age(m)	Mean (μm)	SD	95% CI	
				Lower	Upper				Lower	Upper
RNFL	16.8	12.61	3.94	4.74	20.49	17.4	8.76	4.77	0.00	18.30
GCL	61.9	48.55	10.47	27.62	69.49	55.3	46.72	7.39	31.95	61.49
IPL	39.1	42.81	7.83	27.16	58.46	15.1	47.14	9.79	27.56	66.72
INL	13.1	54.53	10.30	33.92	75.14	22.5	48.09	7.57	32.95	63.23

Age at which inner retinal layers approach adult values at the perifoveal area

Nasal perifovea						Temporal perifovea				
Retinal layers	Age (m)	Mean (μm)	SD	95% CI		Age(m)	Mean (μm)	SD	95% CI	
				Lower	Upper				Lower	Upper
RNFL	31.4	36.43	4.97	26.50	46.37	12	12.05	3.34	5.36	18.74
GCL	53.5	29.26	7.65	13.96	44.56	65.5	26.96	7.98	11	42.92
IPL	13.4	45.84	5.65	34.54	57.13	22.1	45.81	4.51	36.78	54.84
INL	41.5	36.64	5.98	24.69	48.59	34.8	35.13	5.60	23.93	46.33

1.3.2.2.2 The outer retinal layers

The development of the photoreceptor layers has been well understood since SD-OCT enabled better understanding of the development patterns *in vivo*. In contrast to the IRLs, the photoreceptor layer's thickness increases significantly from infancy to adulthood, which occurs rapidly after 38 weeks gestation in all areas, particularly in the cone-dense region[8,77,78]. A previous study reported that the photoreceptor layer at the fovea increase significantly by 185% from a mean thickness of 67.03 to 194.07μm from birth to approximately 47 months before it reaches maturity (196.14μm) by 75 months. The thickness of the ONL, IS and OS at the fovea increases with age between birth and 3.8, 2.2 and 2.7 years respectively, so that the average thickness at birth of 34.37μm increases to 95.57 for the ONL, 20.44 to 32.43μm for the IS, and 3.06 to 30.79μm for the OS. Similarly, the ONL, IS and OS thickness at the parafovea undergo an initial logarithmic increase, followed by a more gradual increase, reaching maturity by 10.6, 2.4 and 12 years, respectively[77]. The data for the outer retinal layers reported by previous studies are summarized in Table 1-8.

Table 1-8: Review of normative data reported for the outer retinal layer thicknesses. RNFL = retinal nerve fiber layer; GCL = ganglion cell layer; IPL = inner plexiform layer; INL = inner nuclear layer; OPL = outer plexiform layer; ONL = outer nuclear layer; IS = inner segment of the photoreceptor; OS = outer segment of the photoreceptor; RPE = retinal pigment epithelium; mo = age in months; SD = standard deviation. NR = not reported in these studies. NP = no evidence of a plateau in the development of the retinal layer.

Maldonado et al[78].				
Outer retinal layers thickness at the foveal area (μm) using SD-OCT				
Sample	Age range	Total ORLs	OPL (μm)	PRL (μm)

13 4 5 9	Preterm (24-29 wk) 1-9 months 2-15 years 20-49 years	39 111 156 173	10 8 3 7	29 103 153 150

Lee et al[77].

Age at which outer retinal layers approaches adult values at the foveal area

Retinal layers	Age (months)	Mean thickness (μm)	SD	95% confidence interval	
				Lower	Upper
OPL	17.8	4.99	6.02	0.00	17.02
ONL	45.3	99.88	14.21	71.46	128.30
IS	26.9	31.93	4.01	23.92	39.94
OS	32.4	30.81	7.92	14.97	46.65
RPE	54.4	16.44	3.29	9.87	23.09

Age at which outer retinal layers approaches adult values at the parafoveal area

Nasal parafovea	Temporal parafovea

Retinal layers	Ag (mo)	Mean (um)	SD	95% CI		Age (mo)	Mean (μm)	SD	95% CI	
				Lower	Upper				Lower	Upper
OPL	11.6	27.17	11.41	4.34	49.99	N.P	NR	NR	NR	NR
ONL	19.4	59.52	19.56	20.40	98.64	92.9	71.28	12.4	45.41	97.15
IS	18.6	25.41	2.67	20.06	20.75	17.9	27.63	3.63	20.37	34.90
OS	23	14.18	5.69	2.81	25.55	31	13.51	5.75	2.01	25.02
RPE	27	17.34	3.32	10.70	23.99	41	17.76	3.44	10.88	24.64

Age at which outer retinal layers approaches adult values at the perifoveal area

Nasal perifovea						Temporal perifovea				
Retinal layers	Age (mo)	Mean (μm)	SD	95% CI		Age (mo)	Mean (μm)	SD	95% CI	
				Lower	Upper				Lower	Upper
OPL	10	26.93	10.65	5.64	48. 23	11.5	23.42	5.91	11.61	35.23
ONL	42.7	57.80	12.64	32.51	83.09	128.4	63.52	8.94	45.64	81.39
IS	29.8	26.48	3.76	18.95	34	19.7	25.70	2.24	21.23	30.18
OS	68.5	8.49	3.41	1.68	15.30	146	11.02	5.81	0.00	22.65
RPE	N.P	NR	NR	NR	NR	17.3	15.81	3.61	8.58	23.03

Photoreceptor sublayers that can be imaged with the current SD-OCT instruments include the external limiting membrane (ELM), the IS/OS junctions (also known as the ellipsoid zone [EZ]),

and photoreceptor OS to RPE layer (interdigitation zone). The time courses when these bands can be imaged vary considerably and are likely a function of the image quality of the currently available instruments. For instance, Maldonado et al.[78] reported that the ELM could not be imaged until 42 weeks postmenstrual age (PMA), while Vinekar et al.[79] found that it can be observed as early 40 to 41 weeks PMA in babies with heavier bodyweight. During infancy, the photoreceptor layer is thinner in the foveal center compared to the adult retinae, and it undergoes a progressive centripetal development that extends into the center of the fovea, including the ELM, EZ and OS-RPE. The EZ zone is characterized by having a low reflective band slightly elevated from the RPE peripheral to the foveal area observed as early as 33 weeks gestation, which shrinks over time and moves towards the foveal center. It should be noted that this band cannot always be imaged in the foveal center before the age of 46 weeks. This is likely due to the fact that the IS/OSs are extremely immature and short and so do not show as a distinct band in OCT[69,77,78,80].

To conclude, recent studies used the hand-held OCT to investigate foveal developmental trajectories from infancy until adulthood and found that the fovea continues to develop until approximately 12 years of age. However, a direct comparison between these studies is limited by the variation in age subgroups used to calculate the mean thickness of the retinal layers. For instance, Maldonado et al. documented that the infants aged between 1 to 9 months have a mean thickness of 10um for the inner retinal layers. In contrast, Lee et al. subdivided this age group into four age groups and reported a mean IRLs thickness of 37.85um (1-6 weeks), 22.93 (27-52 weeks), 17.88um (12-14 months) and 13.92 um (15-17 months). Also, the diameter of the foveal, parafoveal and perifoveal areas varies between studies. While Lee et al. defined the parafoveal

area as 2mm in diameter, it was 4mm in diameter in the study conducted by Yanni et al. Another difference reported in the previous studies includes the description of which layers can be considered as part of inner and outer retinal layers. For example, the OPL was included as part of the IRLs in Lee et al. study while in the study by Maldonado et al. it was considered as part of the outer retinal layers. Therefore, it is critical to have a standard description for retinal layers, age groups and foveal areas when documenting pediatric reference data using OCT to ensure that all values are comparable across laboratories.

1.3.3 Retinal Nerve Fiber Layer (RNFL)

OCT instruments measure the retinal nerve fiber layer (RNFL) thickness around the optic nerve as the distance between the inner limiting membrane and the outer boundary of the nerve fiber layer (Figure 1-11). Most OCT instruments are provided with a reference point, a circle of predefined diameter (often around 3.4 mm) within the center of the optic nerve head to acquire RNFL thickness. This is owing to variation in the distance from the center of the optic nerve. Therefore, RNFL thickness values obtained by different OCT machines are not interchangeable as each instrument is provided with a circle of different diameters within the center of the optic nerve head. Accordingly, the acquired RNFL thickness is then compared to age-matched normative data sets. The outputs are presented in different formats including a pseudo-color scale where the green indicates typical RNFL thickness, yellow indicates borderline (a probability of less than 5% of being typical), and red indicates outside the normal range of RNFL thickness (a probability of less than 1% of being in the typical range, Figure 1-11). The sinusoidal profile analysis is considered the most useful RNFL display in the clinic, which describes the profile of the RNFL thickness in a circle (360 degrees) around the optic nerve displayed with the typical

thickness ranges, starting from the temporal area and proceeding through the superior, inferior, nasal and returning to the temporal region. It typically shows a double hump pattern with thicker superior and inferior quadrants[72,74].

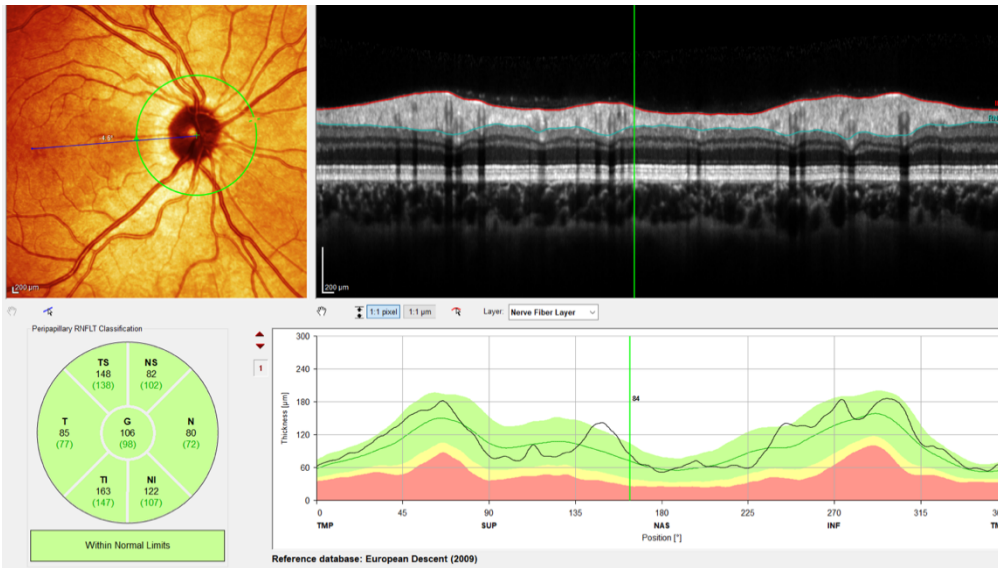

Figure 1-11: RNFL thickness acquired by SD-OCT. The red and green lines in the upper image indicate the distance between ILM and the outer aspect of RNFL measured at the macular area. In the lower left figure, bold numbers under each sector indicate the average RNFL thickness. Numbers in parentheses are the adult's normative database provided by the Spectralis SD-OCT. The green area in the lower right image indicates typical RNFL thickness, the yellow area indicates borderline, and the red area indicates outside the normal range. *Scan by Hussain Albuhayzah*.

1.3.3.1 Development of the peripapillary RNFL

The vast majority of studies on peripapillary RNFL thickness with OCT have been performed in the adult populations and only a few studies have been reported on children[81,82]. Therefore, some degree of uncertainty exists as to when peripapillary RNFL thickness is considered adult-like. Table 1-9 summarizes the results of previously reported studies on child RNFL thickness. This uncertainty is likely due to the variations in methods and distribution of the samples that have

influenced the studies' outcomes. For instance, a variety of OCT techniques (TD-OCT vs. SD-OCT) were used, and some used the standard protocol[83,84] while others used the fast scan protocol[85,86]. Knight et al.[87] reported that RNFL thickness measurements acquired by TD-OCT yields relatively thicker values compared to SD-OCT, and a difference may also occur between different versions of SD-OCT instruments[88]. Thus, thickness values may vary depending on the OCT model used.

Additionally, the majority of studies were hospital-based[83,84,86,89–93]. Huynh et al.[85] documented the largest population-based study in six year old Australian children of mixed ethnicity using TD-OCT, and they found marked differences in RNFL thickness between White and Asian children. In addition, Kim et al.[94] reported that Asians may have a thicker RNFL in the non-nasal areas compared to individuals of white and Hispanic backgrounds. Using TD-OCT Racette et al. found the average RNFL thickness to be greater in black adults compared to white adults. Thus, available evidence seems to suggest that RNFL thickness varies in different ethnicities and such factors should be considered when interpreting children's normative data in clinical practice.

The effect of the refractive error state on RNFL analysis is still controversial. Some authors reported that as myopia increases, the RNFL thickness decreases, and as hyperopia increases, the RNFL thickness increases[82,95,96], while others reported no significant correlation between myopia and RNFL thickness[117–119]. This variation is presumably attributed to the distribution of the refractive error in study samples and using different versions of OCT software.

Both adult and child studies find that the RNFL is thicker in the superior and inferior quadrants and thinner in the temporal and nasal quadrants[101,120–123]. This is likely due to a larger number of nerve fibers converged into the superior and inferior arcuate bundles of the optic nerve compared to the nasal and temporal retina. Therefore, the typical neural rim usually is the thickest in the inferior quadrant followed by the superior and nasal quadrants and is the thinnest in the temporal quadrants. This pattern is known as "ISNT" rule[83,104,105]. Nevertheless, there are several studies in this regard that report different variations[83,85,103,106]. Contrary to the ISNT rule, Leung et al.[107] documented that RNFL thickness decreases from the superior to inferior to temporal to the nasal rim while Turk et al.[99] found that the sequence of average RNFL thickness was inferior, superior, temporal and nasal (ISTN).

Age is considered a significant factor influencing RNFL thickness, with most previous findings indicating that RNFL thickness decreases with age in adult populations[100,101,108], whereas children's studies varied in their conclusions. Some publications reported a significant positive correlation with age during childhood[82,83], while others reported no significant correlation with age[85,103,107]. Nevertheless, the reported r values in the studies that found a significant correlation with age during childhood were relatively small, suggesting that age has a limited effect in the pediatric population. From Table 1-9 we can conclude that the average global RNFL using SD-OCT for white children aged between 5-16 years ranges between 100 and 107um. But the available evidence should be interpreted with caution as the results may vary depending on ethnicity, refractive error, type of OCT and scanning protocol.

Table 1-9: The average RNFL thickness for each sector provided by previous studies for both TD-OCT and SD-OCT. NS= nasal superior, TS = temporal superior, NI = nasal inferior, TI = temporal inferior.

Study	Sample n	Age, (Years)	Technique	Ethnicity	RNFL global (μm)	RNFL superior (μm)	RNFL inferior (μm)	RNFL temporal (μm)	RNFL Nasal (μm)
Ahn et al[89]. (2005)	72	9-18	TD-OCT	Asian	107	133	133	85	76
Altinas et al[90]. (2005)	14	5-18	TD-OCT	Mixed	104	129	122	74	86
Yoon et al[92]. (2005)	31	5-12	TD-OCT	Asian	107	NA	NA	NA	NA
Huynh et al[85]. (2006)	1369	6	TD-OCT	Mixed	104	130	128	76	82
Kee et al[93]. (2006)	42	4-17	TD-OCT	Asian	109	135	137	83	78
Repka et al[84]. (2009)	17	7-17	TD-OCT	Mixed	109	131	140	73	92
Salchow et al[83]. (2006)	92	4-17	TD-OCT	Hispanic	107	135	137	72	83
El-Dairi et al[86]. (2007)	36	5-14	TD-OCT	White	106	139	120	75	88
Leung et al[107]. (2010)	97	6-17	TD-OCT	Asian	113.5	146	142	87	78
Qain et al[82]. (2011)	199	5-18	TD-OCT	Asian	112.36	148.73	142.08	83.82	74

Larsoon et al[81]. (2011)	56	5-15	TD-OCT	White	98	123	125	70	77
Park et al.[109] (215)	58	4-14	SD-OCT	Asian	101.63	108	122	80	69
						NS / TS	NI / TI		
Turk et al[99]. (2012)	107	6-16	SD-OCT	White	106.4	102 / 138	106 / 144	74	71
Yanni et al[103]. (2013)	83	5-15	SD-OCT	Mixed race	107.6	116.2 / 145	125 / 147	76	84.5
Wang et al[110]. (2018)	1440	6-21	SD-OCT	Asian	101.3	106 / 143	109 / 157	85	61

1.4 HARS syndrome

HARS syndrome is a complex genetic disorder that takes an autosomal recessive form and is associated with homozygosity mutation in histidyl tRNA synthetase (HARS c.1361A>C,Y454S). This rare syndrome was initially observed in several individuals of Old Order Amish in Pennsylvania and classified as Usher syndrome type IIIB with clinical findings including progressive hearing loss, ataxia, visual hallucinations and vision loss with febrile episodes[111]. Subsequently, a retrospective clinical study in 18 molecularly confirmed patients of an extended Old Order Amish kindred of Southwestern Ontario documented a partial recovery of vision in addition to other clinical findings beyond the vision and hearing loss[112,113]. These findings

indicate that Usher syndrome may not be an ideal classification of the syndrome. Additionally, the studies reported that many affected patients had experienced febrile episodes with life-threatening clinical deteriorations such as Acute Respiratory Distress Syndrome (ARDS), hypotension, and encephalopathy.

Aminoacyl-tRNA (ARS) synthetases are a group of enzymes that play a vital role in protein translation by connecting tRNAs with their cognate amino acids. It has been reported that 17 of the ARS genes act uniquely in the cytoplasm, 17 function solely in the mitochondria, and three are characterized by having bifunctional features[114]. All identified genes of ARS have been reported to be associated with inherited disorders in humans[113,115]. The phenotypes related to autosomal recessive forms of ARSopathies have been shown to cause a wide range of neurological clinical defects and are likely to affect newborns and children. The autosomal recessive mutations in HARS2 have been reported to cause sensorineural hearing loss and gonadal anomalies in the female population[116], while the autosomal recessive mutations in HARS have been shown to cause a variety of peripheral neuropathy[113,117].

A retrospective clinical review was undertaken to investigate the retinal structure, function, and pathological processes associated with the mutation of histidyl t-RNA synthetase gene (HARS). Clinical information was collected from 14 patients including 3 patients who have died[112,118]. The study revealed that most affected patients experienced some degree of visual defects and abnormal fundus findings. Visual impairment was evident in all patients who were three years or older, at least monocularly, with some meeting the definition of legal blindness. During febrile episodes, several patients experienced severe vision loss, which is usually reported to be

followed by partial recovery. There is documented evidence of visual recovery in two patients. Patients who have a history of acute fever had poorer vision compared to those who have not experienced severe fever illnesses[113].

The fundus examination revealed a lack of foveal reflex and granular appearance of the macula in most affected patients. Several individuals presented with a distinct lesion with a "beaten-metal" appearance, and some patients showed optic disc pallor and vascular attenuation (Figure 1-12). Several patients showed a rod-cone dystrophy in the peripheral retina after six years of age.

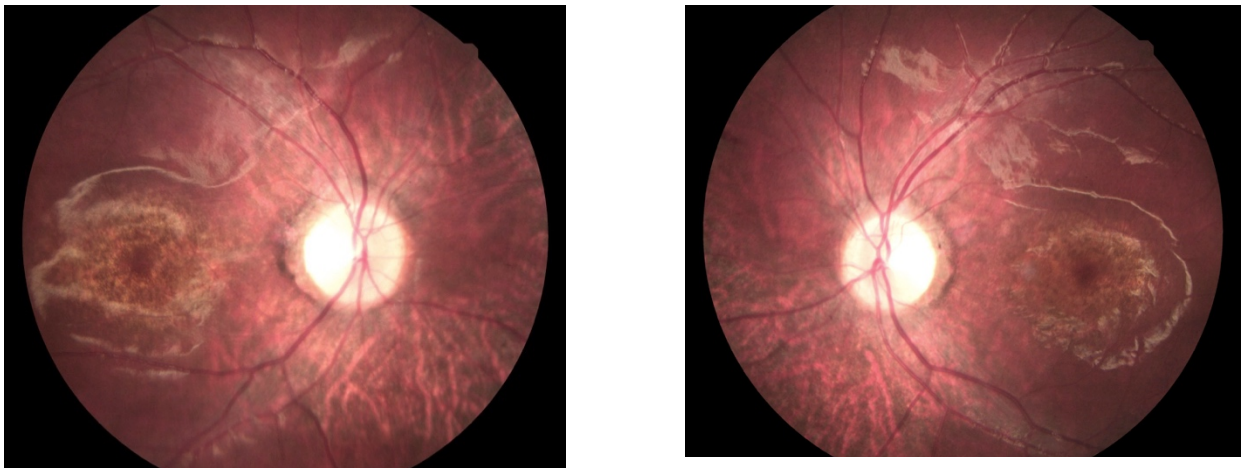

Figure 1-12: Fundus photographs of a patient with HARS-associated retinopathy showing: pale optic nerves, attenuated retinal vessels, bilateral macular lesions that have a beaten-metal appearance. *Courtesy Natalie Hutchings[118], used with permission.*

Refractive errors such as astigmatism, hyperopia, and myopia were frequently reported. Four children experienced poor night vision, and two patients had photophobia. The majority of the patients who performed color vision testing showed color vision defects, including red-green and

blue-yellow deficits. Strabismus was reported in four children, whereas nystagmus was observed in three patients[113].

Full-field ERG recordings revealed significant abnormal findings in all ISCEV standard conditions, including undetectable ERGs above noise in some patients. Affected patients with detectable ERGs showed an inconsistent depression of LA-ERGs as well as DA b-waves and OPs, suggesting that cone functions are likely to be affected more than rod function (Figure 1-13). OCT examination revealed disruption of the outer retinal layers, including non-detectable photoreceptor subcellular layers, as well as overall foveal thinning (Figure 1-14).

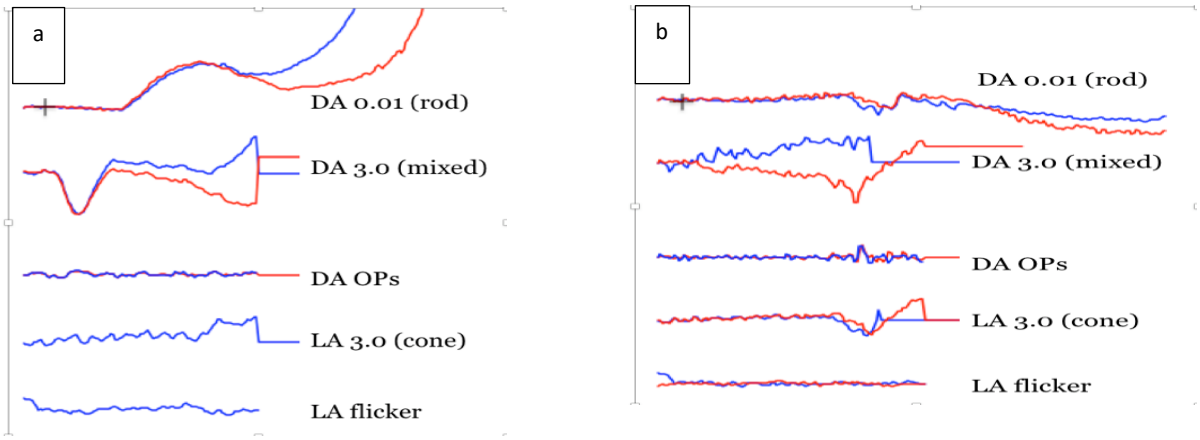

Figure 1-13*:* (a) A representative example of ERGs showing that OPs and cone related ERGs are undetectable, and dark-adapted ERGs are relatively preserved. (b) A representative example of an ERG undetectable above noise. *Courtesy Daphne McCulloch, used with permission*[112,118].

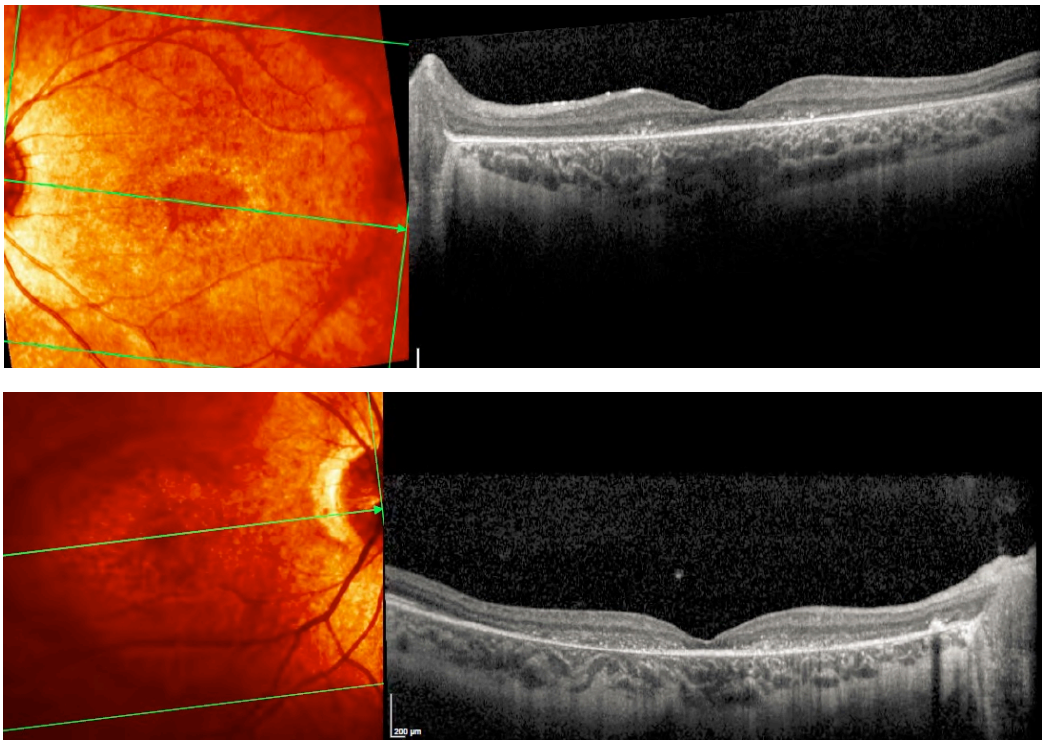

Figure 1-14: B-scan OCT images in a patient with HARS-associated retinopathy showing a perimacular disruption of the outer retinal layers and relative thinning of overall retinal thickness. *Courtesy Natalie Hutchings*[118]*, used with permission.*

Chapter 2: Purpose and Hypotheses

2.1 Purpose

The ultimate purpose of this cross-sectional study was to establish normative data for retinal structure and function in children aged between 4-15 years old using OCT and ERG. This is important data in itself for diagnosis of children with potential suspected conditions. This was particularly relevant at the time of the study, as we were concurrently studying children with HARS syndrome, which results in a retinal dystrophy and has been described in Chapter 1. The protocol of each clinical technique (ERG and OCT) was designed based on standard protocols and an in-depth review of previous literature.

Even though it is widely accepted that the human retina has an immature appearance at birth, the structural development of the retina *in vivo* has not previously received adequate attention to be fully understood or described. Few published *in vivo* studies have investigated the maturation of retinal layers from infancy until they become truly adult-like[8,77,78]. This is likely because of the difficulty of obtaining data in young participants. Until recently, most of our knowledge of the retinal development is based on histological studies, which may not always determine with certainty the developmental patterns as well as time course for each retinal layer. This is due to the fact that samples could be affected by shrinking of the tissue and artifacts such as retinal detachment[5,6] The *in vivo* studies that do exist used the hand-held OCT to study the developmental patterns of the retinal layers but showed general disagreement in terms of identifying which layers should be considered as part of the inner and outer retinal layers[77,78]. Additionally, a direct comparison between studies is limited by differences in the age groups

used to obtain the values of the retinal layer thicknesses. Additionally, retinal thickness values are not consistent across different OCT instruments, as different OCT equipment use different algorithms to obtain numeric values[72]. Also, it has been previously reported that there is a considerable amount of variation between individuals within the same age range making the comparison between studies more challenging[77,78,80,103]. To our knowledge, none of the studies have investigated the development of each retinal layer from childhood until maturity using the Spectralis-OCT (tabletop OCT) with the automatic segmentation software provided by the manufacturing company. The present study adopts this approach.

Similarly, there has been little research published that has documented the maturation of the ERG waveforms from childhood until maturity[49,50,53]. Existing studies used contact lens electrodes to obtain ERG responses, and they show general agreement in terms of the maturation of standard ERG components. In two reports, the data were grouped such that any variations between younger children (3-5 years) and older children cannot be determined[48,49]. When comparing the ERG data between previous studies, the type of electrode and techniques used to obtain ERGs should be considered. To our knowledge, none of the existing studies used the DTL-electrode to obtain normative values in the six conditions specified by ISCEV standards. This study attempts to fill this gap in data.

Knowledge of the time course for normal development of the retina using these clinical techniques is essential to detect, monitor, and understand pathological processes that affect the pediatric retina.

OCT and ERG measures taken under similar protocols for children with HARS will be compared against the normal data, to demonstrate the importance of having normal data sets.

2.2 Objectives

The objectives of the study are:-

1- Measure the development of ERG and OCT components in children ranging from 4-15 years old and compare with adult data.
2- Investigate whether the results agree with previously published data.
3- Publish data age-norms for OCT and ERG components.
4- If possible, compare the normal data sets with children with HARS syndrome as a demonstration of the utility of the normal data sets.

2.3 Hypotheses

The hypotheses are:

- The development of the retina is likely to continue during childhood and not become adult-like until late childhood[4,8,77].
- The ERG and OCT diagnostic techniques can be used effectively to detect and monitor various diseases of the pediatric retina such as HARS syndrome.

2.4 Experiment design

Two cross-sectional studies were undertaken to investigate the development of 1. Retinal function and 2. Retinal structure. Retinal function was investigated in children aged 7-15 using the full-field ERG procedure and is described in Chapter 3. Retinal morphology was investigated using Spectralis OCT in children aged between 4-15 years old and is described in Chapter 4. These two studies were designed to provide pediatric normative data for OCT and ERG to be used for clinical interpretations.

Chapter 3: Dark and Light-Adapted Electroretinograms (ERGs) in 7-15-year-Old Children and Adults

3.1 Introduction

Morphologically, it has been shown that the retina is not completely mature at birth, and it undergoes several post-natal structural changes, including the elongation of the outer photoreceptor segment and an increase in cone packing density[2,3]. The functional changes of an immature retina can be assessed with the full-field electroretinogram (ERG), which is a non-invasive clinical procedure that records the electric field potentials generated in the retina in response to a light stimulus. Standard clinical testing protocols record ERGs from remote electrodes in contact with the cornea or on the skin near the anterior eye with stimuli delivered in a full field dome[49]. Typical ERG waveforms to brief flashes include an initial corneal negative component (a-wave) and a slower positive component (b-wave) [119]. It is known that the a-wave reflects the photoreceptor activity, and the b-wave is elicited within the inner nuclear layer and indirectly reflects bipolar cell function. Retinal function can be studied by using the same stimulus between participants to obtain ERG recordings under photopic or scotopic conditions. For instance, the developmental rate of both a- and b-waves can be used as an index of retinal function. Such developmental changes are likely to reflect the activities of the inner and outer retinal layers.

The full-field ERG plays a decisive diagnostic role in modern ophthalmic practice and is routinely used as an initial diagnostic indicator of several inherited retinal disorders such as retinitis pigmentosa. While progressive retinal degeneration often results in prolonged implicit

time of the b-wave, a wide range of ocular diseases can result in reduction in the amplitude[43]. Implicit time of DA 0.01 b-wave is often longer in individuals with all inheritance patterns (dominant, recessive and X-linked)[43] of retinitis pigmentosa. The technique is also useful in following the progression of retinal disorders.

Pediatric retinal diseases can present a diagnostic challenge because of the inability of young children to undertake such testing, and there are also limitations of psychophysical testing in the pediatric population[120].Thus, ERG testing may have additional value in this patient group. The diagnosis may require ERG procedures, particularly when the fundus appears normal, but there is reduced visual function in an infant or young child[120,121]. For instance, in the early stages of the enhanced blue cone syndrome (a rare genetic disorder) fundus examination typically appears normal in infants, while ERGs often show abnormalities[13].Thus, the ERG is often an essential component of diagnosis in early or late stages of disease and documenting progression. Procedures for identifying inputs of the cone and rod generated ERGs and of their pathways have been incorporated into a standard protocol specified by the International Society for Clinical Electrophysiology of Vision (ISCEV)[15]. Accordingly, the technique has a promising clinical application in the pediatric population, but its utilization has been limited by the obstacles inherent in acquiring ERG recordings from young infants and children who cannot participate as adults do. Unlike contact lens electrodes, the DTL conductive fiber electrodes[122] are less invasive and allow the acquisition of ERGs in younger children more easily than previously with contact lens electrodes, making ERG a more accessible technique for both clinical and research purposes. Additionally, they enable recording larger amplitudes than those acquired using skin electrodes on the eyelids.

Despite the inherent difficulties, the full-field ERG has been used previously to understand the maturational changes of the retinal functions in depth from infancy until adulthood. Several studies reported that infants have smaller amplitudes and longer implicit times in response to full-field light- and dark-adapted stimuli. Birch et al.[49] found that there is a rapid development of the amplitudes and implicit times of the b-wave for both LA and DA ERGs during the first four months of life, with slower development thereafter. Westall et al.[53] documented that the a- and b-wave amplitudes mature sufficiently to be considered adult-like during 3 and 5 years for both LA and DA ERGs. Oscillatory potentials are considered immature in early infancy, as they are undetectable above noise under one month of age. After this initial delay, OPs develop rapidly, reaching maturity before any other ERG waveforms at around two years of age[53,54]. These studies[48,49,53] used Burian-Allen bipolar contact-lens electrodes to record ERG waveforms, and the author is not aware of any report that has used DTL electrodes to acquire ERG normative data with the ISCEV standard protocol.

Using contact lens electrodes, ERGs have been obtained from preterm infants as early as 30 weeks post-conception after developing effective ERG procedures in neonates[123,124], to assess the effect of nutritional factors in retinal maturation[45,52,125], to evaluate the typical development of the retinal functions[51], and to understand more deeply the influence of retinopathy of prematurity on development of retinal functions[51,123,124]. Reference data with the ISCEV standard protocol have been acquired for preterm infants both with and without ROP and for post-term infants[49,50].

The purpose of this study was to determine the developmental change of ERG waveforms from childhood until adulthood using the ISCEV standard protocols and an additional light-adapted

luminance series using DTL electrodes. The light adapted ERG series with flash strengths were included in the protocol to investigate whether the ON and OFF pathways mature at different times. These results will inform our understanding of retinal maturation during childhood and provide reference data for future clinical interpretation of retinal function in suspected retinal disease in children.

3.2 Methods

3.2.1 Study participants

In this cross-sectional study, thirty-two participants of European descent with normal ocular and general health were recruited. The sample was a purposeful sample to include children evenly spread within the ages of 4-15 years. The final numbers were 12 participants between 7 and 11 years, 10 between 12 and 15 years and 10 adults between 20 and 33 years.

An electronic search was conducted of pediatric records at the School of Optometry and Vision Science at the University of Waterloo to find potentially eligible participants whose parents or guardians had given consent to be contacted about research studies. For those who were eligible (e.g., had normal vision according to the clinical record), the parent or guardian was contacted and given a description of the project and asked if they were willing for their child to participate. If so, they were first asked a few questions to determine that the child met the general inclusion criteria (normal development, full term birth, good general health and no known ocular disorders). If these criteria were met, an appointment was made for the first visit.

Also, potential participants were recruited through the email list of School of Optometry and Vision Science staff, faculty and grad students as well as through the University of Waterloo Graduate Studies office, and the Graduate Student Association. For children contacted by email lists, the participant's parents or guardians were asked to reply to the researcher either by email or phone. The researcher then proceeded as above i.e., checking that the child met the broad inclusion criteria and making the appointment. Potential adult participants were recruited in a similar fashion. Emails were also sent out to the Centre for Ocular Research & Education (CORE) database. Snowball recruiting was also used, whereby one parent was asked if they knew of other parents who might be willing for their child to take part. If so, they were given the letter of information to give to that person, who may then choose to contact us if they were interested in their child participating. Recruitment was also from among the unaffected siblings of children in an ongoing study of HARS syndrome.

Inclusion criteria included: (1) either gender, (2) age range between 4 to 15 years of age for children and 20 to 40 years of age for adults (3) healthy participants with no known significant medical or ocular history and no medications affecting the nervous system (4) no strabismus (5) visual acuity within the normal range for age (6/9 or better in each eye) (6) refractive error within the following ranges; hyperopia not greater than +3D, myopia not greater than -5D, astigmatism $\leq$2D at any axis and anisometropia not greater than 1.5D in any meridian, (7) European descent. For child participants, criteria also included (8) normal developmental milestones being met (9) and not born prematurely (i.e., $\geq$ 37 weeks gestational age).

3.2.2 Study protocol

3.2.2.1 Screening tests for eligibility

All adults and parents or guardians of child participants gave consent prior to the participation in this study. Assent was obtained from child participants who were 7 years or older. All participants underwent the following screening tests prior to being admitted to the study:

1. Case history which included previous medical and ocular history, general development as well as current medications.
2. Refraction was measured using standard clinical methods as appropriate for age, to ensure it was within the inclusion criteria listed above. This included retinoscopy for child participants who were younger than 8 years old, during which they were asked to wear fogging glasses (+2D) to relax their accommodation and the child's attention was attracted to a movie at 6 m. For adult participants, refractive error was measured using autorefraction (Topcon, KR.1). For participants who already had a refractive correction, the prescription was measured using lensometry.
3. The unilateral cover test was used to assess for the presence of strabismus.
4. Best corrected visual acuity was measured monocularly with the participants' current prescription or uncorrected vision (for those who did not wear glasses and had low refractive errors) using digital HOTV charts with three lines of the same acuity to maintain equal crowding for all the letters. Older children and adults were asked to read the letter chart while younger children were asked to match the letters on a key card.

3.2.2.2 Screening test for dilation

1. A dilating agent (tropicamide 1%) was instilled topically in both eyes for participants who met the eligibility criteria described below in order to obtain good quality OCT scans and ERGs.
2. No allergy to tropicamide and/or proparacaine or related drugs was confirmed.
3. Female participants were asked if they were pregnant, lactating or planning a pregnancy (by self-report) at the time of enrollment, in which case they were excluded from the study.
4. Intraocular pressure (IOP) using non-contact tonometry was recorded pre- and post- the study procedure for all adult participants who had not had a topical dilating agent within the last two years. For child participants, tonometry was not undertaken, as there is a very low risk of elevated intraocular pressure. However, anyone with a history of elevated IOP following dilation (a rare complication) was excluded from the study.
5 The presence of an adequate anterior chamber angle and the clarity of the cornea were determined using the slit lamp (Van Herrick technique was used to estimate the angle).

3.3 Full-field clinical electroretinography (ERG) Measures

3.3.1 Equipment

Full field electroretinograms (ERGs) were measured using a clinical visual electrophysiology stimulation and recording system (Espion E3 Visual Electrophysiology System) available at the School of Optometry and Vision Science (Optometry Clinic). Reference electrodes, either silver-silver chloride cup electrodes with conductive paste (WEAVER, Ten20 conductive) or disposable adhesive gel EEG electrodes (Ambu. Neuroline 710) were placed on the participants'

skin near the outer canthus of the eye after cleaning the skin using NuPrep Skin Prep Gel to improve conductivity and reduce impedance. DTL (Diagnosis LLC, DTL plus Electrode) active electrodes were approved for use and placed in contact with the conjunctiva (Figure 3.1) on the front surface of the eye after instilling topical anesthetic eye drops (Alcaine 0.5%) in both eyes to reduce sensitivity and increase the participant's comfort during the test (Figure 3-1). A ground electrode was placed on the wrist. Active electrodes were connected to the positive input of the recording system, reference electrodes were connected to the negative input of the recording system, and a ground electrode was attached to the common input of the recording system.

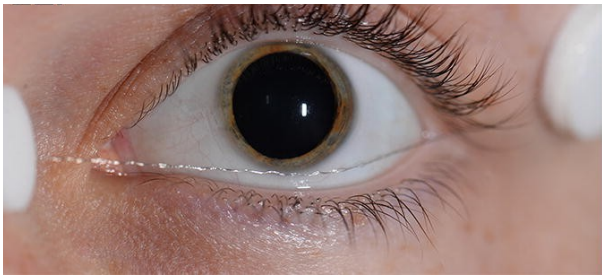

Figure 3-1: Typical position of the DTL electrode. *Retrieved from Brouwer et al, used with permission.*

3.3.2 Stimuli

Light stimuli were presented as brief (4ms) white flashes in a full field dome stimulator (Colordome® Diagnosis UK) to achieve uniform luminance over the entire visual field. White was defined as the combination of long, medium and short wavelength LEDs that gave an equivalent color temperature of 6500K. The stimulus strength, duration of the stimulus and recording bandpass were set according to the ISCEV standards for full-field clinical electroretinography[15], see Table 3-1.

Table 3-1: ERG Stimulation and recording parameters.

ERG protocols				
Stimulus name	Adaptation time	Number of sweeps	Inter-stimulus time	Filter (Hz)
DA 0.01 ERG	DA 20 min	20	2.0 s	0.312 - 300
DA 3.0 ERG	DA 20 min	20	10 s	0.312 - 300
DA 10 ERG	DA 20 min	20	20 s	0.312 - 300
DA OPs	DA 20 min	20	10 s	75 - 300
LA 0.3 ERG†	LA 10 min	20	0.5 s	0.312 - 300
LA 1.0 ERG †	LA 10 min*	20	0.5 s	0.312 - 300
LA 3.0 ERG	LA > 10 min*	20	0.5 s	0.312 - 300
LA 10 ERG†	LA > 10 min*	20	0.5 s	0.312 - 300
LA 24 ERG†	LA > 10 min*	20	0.5 s	0.312 - 300

* Light adaptation continued for the duration of the ERG recordings and thus was greater than the initial 10-minute adaptation period

† Stimuli added to the standard protocols to expand the LA series.

3.3.3 Clinical Protocol:

Participants were asked to sit in front of the dome stimulator and rest their head in a chin and head rest to keep it steady. Younger children were seated on their parent's lap. Participants were directed to look at the fixation target incorporated in the stimulus dome, which was adjusted, so as not to interfere with dark adaptation. A red fixation target was also visible during photopic

conditions. Those who could not see the fixation point were directed to look straight ahead and keep their eyes stationary. All participants were instructed to minimize blinking and eye movements to avoid producing electrical artifacts or altering the position of the electrode on the eye. In addition, the study participants were monitored during the test using a small infra-red camera provided by the instrument to assess their compliance as well as any other issues with fixation such as difficulty in maintaining eye-opening.

The ERG was observed in real time to determine repeatability at the time of the study and a minimum of 20 responses at each luminance intensity was acquired. Thus, when the data had to be eliminated because of electrical noise, blinking or eye movements, we had adequate data to have at least three valid responses for each participant. Subsequently, we determined a- and b-wave amplitudes and implicit times using the average of the right and left eye values to compare age groups. This is justified as we did not obtain observations for the left and right eye for all participants.

The order of recording is as described below.

3.3.4 Light-adapted ERG

Light-adapted ERGs were recorded under normal room illumination, after ensuring that the pupil of both eyes was maximally dilated. Participants either sat in a light room or were exposed to the photopic background of the full field dome (10 min @ 30 cd.m^{-2} with uniform illumination). This was to ensure that the visual system was light adapted in order to increase the response of cone photoreceptors and decrease the input of rod photoreceptors. Participants were presented

with stimulus flashes on the same light-adapting background with 0.5s interval between the stimuli.

3.3.5 Dark-adapted ERG

The procedure was conducted in a completely dark room. Participants were asked to sit in a dark room for at least 20 minutes to maximally activate the rod system. Following dark adaptation, the participants were presented with weaker flashes before stronger stimuli to avoid the effects of partial light adaptation caused by the exposure to the flash stimuli during the test. Therefore, dark-adapted 0.01 ERG was recorded first followed by dark-adapted 3 ERG and dark-adapted 10 ERG. Oscillatory potentials were acquired simultaneously to the DA 3.0 ERG recording using a high pass filter (75 Hz to 300 Hz) to isolate them from the main ERG waveforms.

3.3.6 ERG recording

Single-flash ERGs

The amplitude and implicit times of a-wave and b-wave ERGs were recorded for all single flash ERGs. The a-wave amplitude was measured from the average of the 50 ms pre-stimulus baseline to the trough of the a-wave and the b-wave amplitude was measured from the a-wave trough to the b-wave peak. The peak times of a-wave and b-wave were recorded from the time of the flash to the peak of the wave.

Oscillatory potentials

A total index of oscillatory potential amplitude was calculated as the sum of amplitude measurements of three to five main peaks, which were measured from the base of the adjacent

preceding trough. Although the OPs were automatically recorded, the analysis was not included in this thesis.

3.4 Statistical analysis

Statistical analysis was conducted using SPSS or Excel. The Shapiro-Wilk test was used to test the distribution of the data for normality. Age was transformed into a log10 scale which spread the age range more evenly and resulted in a normal distribution for age. Depending on whether the data were distributed normally or not, Pearson's correlation coefficient or Spearman's rank correlation respectively was used to test the correlation between age and the a- and b-wave amplitudes and implicit times for each stimulus. P values <0.05 were considered to be statistically significant and the adjusted Bonferroni correction[126] was applied to correct for multiple comparisons. For the data that were not significantly correlated with age after the adjusted Bonferroni, and which were normally distributed, the 95-confidence interval was calculated (mean ±1.96xSD). For those data that were not normally distributed, the 2.5th, 50th and 97.5th percentiles were calculated. For the data that were significantly correlated with age, scatterplots were created, and mean/median and reference ranges were calculated for each age group.

3.5 Results

3.5.1 Population Demographic

A total of 32 participants were included in the study. The sample included 10 adult participants (median age = 23.12 ranging from 20 to 33.42 years), 10 older children (median age = 13.5 ranging from 12 to15.33), and 12 young children (median age = 10.29 ranging from 7.17 to

11.75 years). All participants met the eligibility criteria and successfully completed the study's procedure.

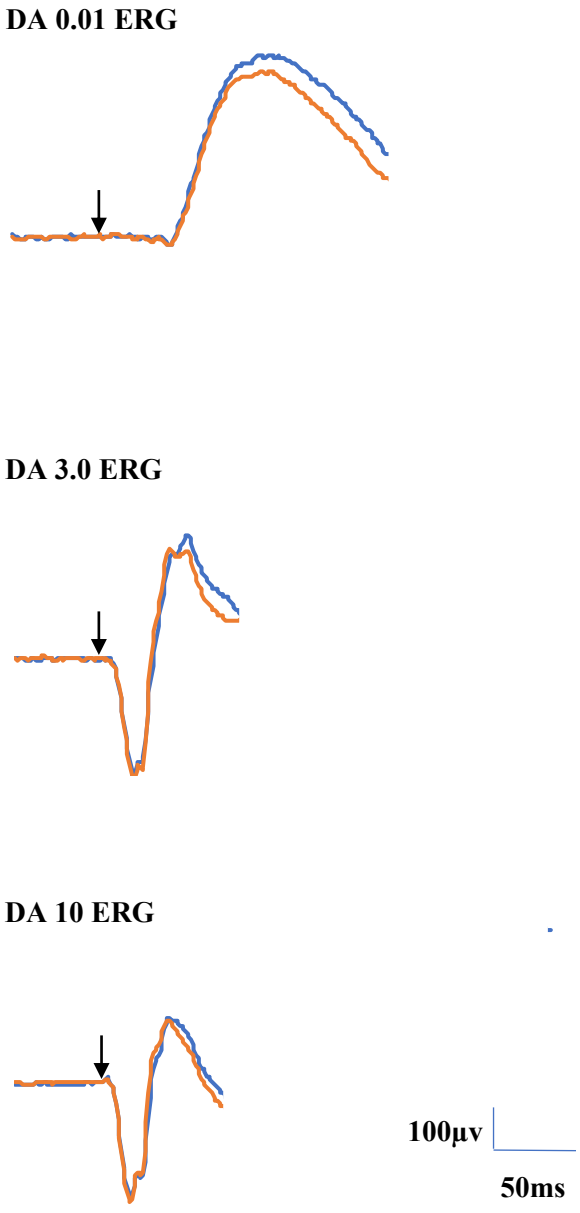

Figure 3-2: Representative DA standard ERG waveforms including 0.01, 3.0, and 10 ERGs for a 13-year-old female participant. Blue = right eye. Red = left eye.

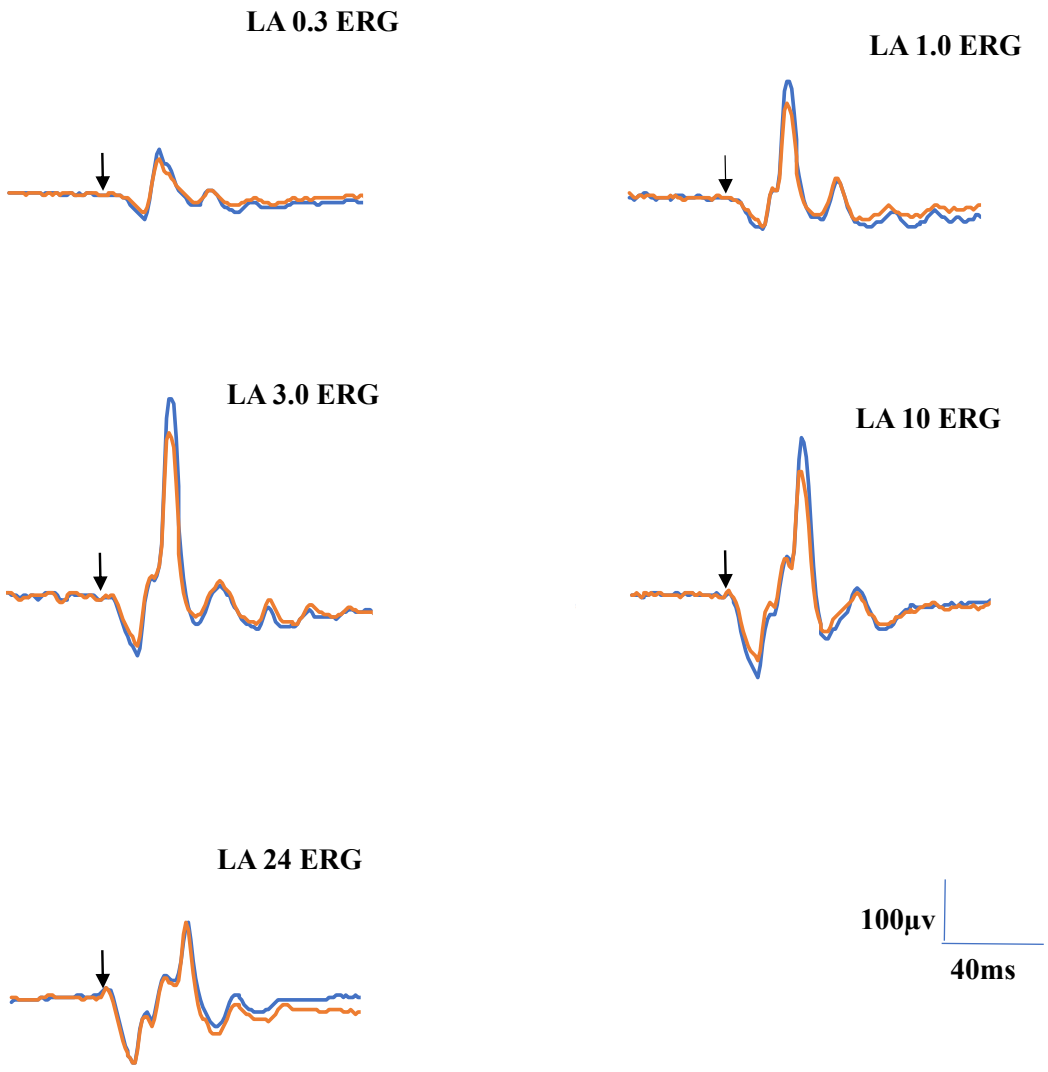

Figure 3-3: Representative LA ERG series in response to flash stimuli including 3.0, 1.0, 3.0, 10, and 24 ERGs for a 13-year-old female participant. Blue = right eye. Red = left eye.

3.5.2 Light adapted (LA) a-wave

The Shapiro-Wilk test showed that the light adapted a-wave amplitudes were normally distributed for all stimuli. Therefore, Pearson's correlation coefficient was used to analyze the data. However, the implicit times were not normally distributed for all stimuli. Therefore, Spearman's rank correlation was used to analyze the data. The correlation coefficients with age are shown in Table 3.2 and 3.3.

Table 3-2: Pearson correlation coefficient for the LA a-wave amplitudes with Log age.

Stimulus	r value	p value
LA 0.3 a-wave amplitudes	- 0.05	0.80
LA 1.0 a-wave amplitudes	-0.07	0.72
LA 3.0 a-wave amplitudes	0.11	0.55
LA 10 a-wave amplitudes	0.16	0.39
LA 24 a-wave amplitudes	0.26	0.15

Table 3-3: Spearman's rank correlation for the LA a-wave implicit times with Log age. * = those which remain significant after the Adjusted Bonferroni.

Stimulus	r value	p value	Adjusted α value for significance
LA 0.3 a-implicit times	0.55	0.001*	<0.0125
LA 1.0 a-implicit times	0.39	0.02	<0.0167

LA 10 a-implicit times	0.39	0.02	<0.0167
LA 24 a-implicit times	0.30	0.03	<0.025
LA 3 a-implicit times	0.33	0.07	NA

3.5.2.1 LA a- wave amplitudes

The results of the correlation analysis revealed that none of the light-adapted ERG a-wave amplitudes were significantly associated with age (see Table 3-2). The mean estimates for the LA a-wave amplitudes of individuals aged from 7 to 33 years old are shown in Table 3-4.

Table 3-4: Distribution of light adapted a-wave amplitudes. * *CI* = confidence interval (1.96 x SD).

Age range (years)	**Stimuli**	**Mean (µv)**	**St. Deviation**	***95% CI****	
				Lower limit	**Upper limit**
7.1-33.4	LA 0.3 a-wave	20.1	6.9	6.6	33.6
7.1-33.4	LA 1.0 a-wave	32.8	14.5	4.4	61.2
7.1-33.4	LA 3.0 a-wave	44.0	19.6	5.6	82.4
7.1-33.4	LA 10 a-wave	59.1	19.6	20.7	97.5
7.1-33.4	LA 24 a-wave	62.0	19.9	22.9	101

3.5.2.2 LA a-wave implicit times

The rank correlation analysis showed that the LA a-wave implicit times were positively correlated with age, that is longer implicit times in older subjects. Adjusted Bonferroni correction[126] for the significant correlations revealed that a significant positive correlation with age was retained only for the dimmest stimulus, the LA 0.3 ERG (Table 3-3). This means that as age increases the implicit time of LA 0.3 increases (Figure 3-4). The rank correlations between age and LA ERGs for stronger stimuli showed similar trends however, these did not reach significance. Therefore, there was no evidence of maturation of the implicit times beyond 7 years of age for the LA 1.0, 3, 10, 24 ERGs. The mean estimates for the LA a-wave implicit times of individuals aged from 7 to 33 years old are indicated in Table 3-5. The medians and ranges for the LA a-wave 0.3 for the three age groups are shown in Table 3-6. This shows that the median implicit time for younger children (7-11 years) was 17ms and increased to approach the adult values with an implicit time reaching 18ms.

Table 3-5: Light adapted a-wave implicit times.

Age range (years)	**Stimulus strength cd.s.m^{-2}**	**Median**	**interquartile range**	**2.5th percentile**	**97.5th percentile**
7.1-33.4	LA 1.0	15	±1.5	13	17.11
7.1-33.4	LA 3.0	14.5	±1.4	12.5	16
7.1-33.4	LA 10	13.25	±1.0	11	14.5
7.1-33.4	LA 24	12.5	±1.0	11	13

Table 3-6: Median, and reference ranges of the light adapted a-wave (stimulus 0.3) implicit time for each group.

Age group	Stimulus strength cd.s.m^{-2}	Median (ms)	Range	
			Minimum	Maximum
7-11	LA 0.3	17	15	18
12-15		17.5	15	18
20-33		18	17	19

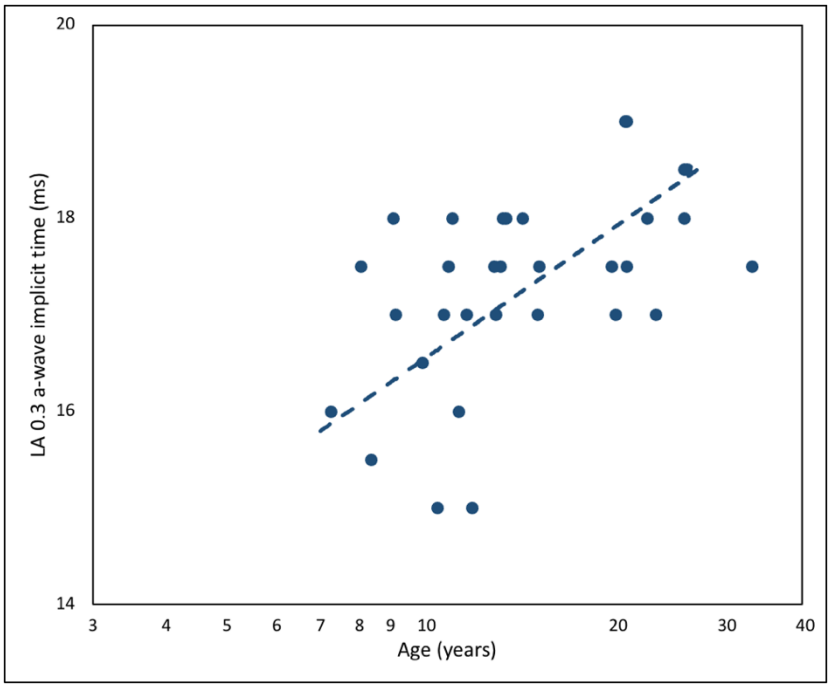

Figure 3-4: Scattergram of the LA 0.3 a-wave implicit time against age. Each point represents the average data for one participant. The linear regression line is shown as a dashed line and is representative of the trend although rank correlation was used for this non-normally distributed data.

3.5.3 Light adapted (LA) b-wave

The Shapiro-Wilk test showed that the light adapted b-wave amplitudes were normally distributed for all stimuli. Therefore, Pearson's correlation coefficient was used to analyze the amplitude data. However, the light adapted implicit times datasets were not normally distributed for any stimulus. Therefore, Spearman's rank correlation test was used to analyze those data. The correlation coefficients with age for LA b-wave amplitudes and implicit times are shown in Tables 3.7 and 3.8, respectively.

Table 3-7: Pearson correlation coefficient for the LA b-wave amplitudes with Log age.

Stimulus	r value	p value
LA 0.3 b-wave amplitudes	-0.23	0.21
LA 0.1 b-wave amplitudes	-0.25	0.31
LA 3.0 b-wave amplitudes	-0.06	0.74
LA 10 b-wave amplitudes	0.19	0.31
LA 24 b-wave amplitudes	0.19	0.35
LA 3/24 b-wave amplitudes	-0.315	0.08

Table 3-8: Spearman's rank correlation for the LA b-wave implicit times with age. * = those which remain significant after using the adjusted Bonferroni.

Stimulus	r value	p value
LA 1.0 b-wave implicit times	0.36	0.04*

LA 0.3 b-wave implicit times	-0.11	0.54
LA 3 b-wave implicit times	-0.06	0.73
LA10 b-wave implicit times	-0.02	0.91
LA 24 b-wave implicit times	0.07	0.72

3.5.3.1 LA b-wave amplitudes

The Pearson correlation analysis revealed that none of the ERG b-wave amplitudes were significantly associated with age (see Table 3-7). Therefore, age was found to have no significant effect on the LA b-wave amplitudes. The mean estimates for the LA b-wave amplitudes of individuals aged from 7 to 33 years old are indicated in Table 3-9. As a measure of the relative maturation of the ON and OFF pathways, the ratio of 3/24 b-wave amplitudes was used to test whether the ON and OFF pathways mature at different rates. The results of the correlation analysis showed that the ratio of 3/24 b-wave amplitudes was not significantly correlated with age, suggesting that the ON and OFF pathways are unlikely to mature at different times.

Table 3-9: Light adapted b-wave amplitudes. *CI* = confidence interval (1.96 x SD).

Age range (years)	**Stimuli cd.s.m^{-2}**	**Mean b-wave amplitude (μV)**	**St. Deviation μV**	***95% CI***	
				Lower limit	**Upper limit**
7.1-33.4	LA 0.3	58.5	17.9	23.4	93.6
7.1-33.4	LA 1.0	136.6	40.9	56.4	216.8
7.1-33.4	LA 3.0	196.6	60.4	78.2	314.9

7.1-33.4	LA 10	164.2	51.3	63.7	264.7
7.1-33.4	LA 24	116.1	35.6	46.3	185.9
7.1-33.4	LA 3/24	1.7	0.4	0.9	2.5

3.5.3.2 LA b-wave implicit times

The rank correlation analysis showed that the LA 1.0 ERG implicit time was significantly positively correlated with age ($r = 0.36$, $p= 0.04$, see Table 3.8) such that the implicit time was shorter for children compared to adults as it can be seen in Figure 3-5. However, the implicit times of none of the other stimuli were correlated with age (see Table 3.8). Thus, the implicit times for the LA 0.3, 3.,10 and 24 ERGs are unlikely to be influenced by age. The mean estimates for the LA b-wave implicit times of individuals aged from 7 to 33 years old are indicated in Table 3-10 and the age-related medians and ranges for the implicit time for the LA 1.00 b-wave are shown in Table 3-11.

Table 3-10: Light adapted b-wave implicit times (IT).

Age range (years)	**Stimuli ($cd.s.m^{-2}$)**	**Median IT (ms)**	**intra-quartile range**	**2.5^{th} percentiles**	**97.5^{th} percentiles**
7.1-33.4	LA 0.3 b-wave	25.0	±0.0	22	27.33
7.1-33.4	LA 3.0 b-wave	29.0	±1.9	27	31.33
7.1-33.4	LA 10 b-wave	33.0	±2.0	31	36
7.1-33.4	LA 24 b-wave	36.0	±2.5	33.5	40.45

Table 3-11: Median, and reference ranges of the light adapted 1.0 b-wave implicit time for each age group.

Age group	Stimulus ($cd.s.m^{-2}$)	Median (ms)	Range	
			Minimum	Maximum
7-11	LA 1.0	25	24	28
12-15		26.7	26	28
20-33		26.7	26	28.5

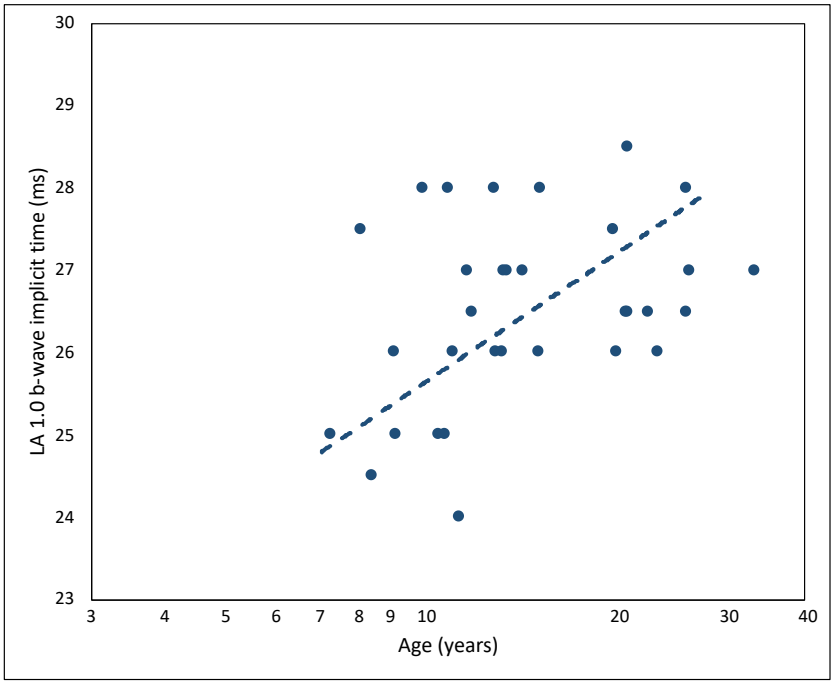

Figure 3-5: Scattergram of the LA 1.0 b-wave implicit time against age. Each point represents the average data for one participant. The linear regression line is shown as a dashed line and is representative of the trend although rank correlation was used for this non-normally distributed data.

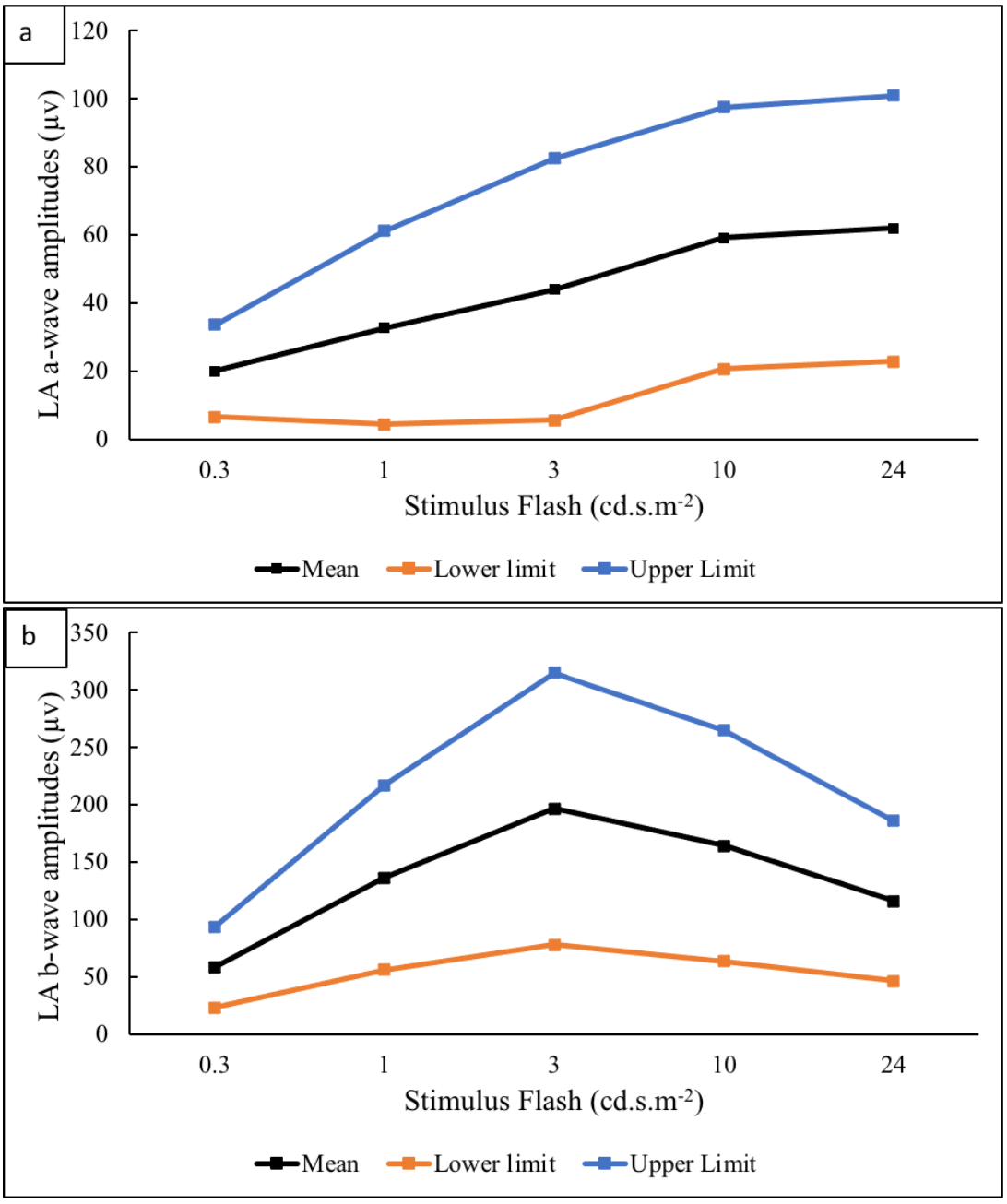

Figure 3-6: (a) The mean and 95% confidence interval for the LA a-wave amplitudes plotted against flash luminance. (b) The mean and 95% confidence interval for the LA b-wave amplitudes plotted against luminance intensities.

3.5.4 Dark adapted (DA) a-wave

The Shapiro-Wilk results showed that the dark-adapted a-wave amplitude data was normally distributed for all stimuli. Therefore, Pearson's correlation coefficient was used to analyze the amplitude data. However, the implicit times were not normally distributed for any stimulus. Therefore, Spearman's rank correlation was used to analyze the data. The correlation coefficients with age are shown in Table 3.12 and 3.13.

Table 3-12: Pearson correlation coefficient for the DA a-wave amplitudes with age.

Stimulus (cd.s.m^{-2})	**r value**	**p value**
DA 3.0 a-wave amplitudes	0.07	0.69
DA 10 a-wave amplitudes	0.08	0.68

Table 3-13: Spearman's rank correlation for the DA a-wave implicit times with age. * those which remain significant with the adjusted Bonferroni.

Stimulus (cd.s.m^{-2})	**r value**	**p value**	**Adjusted α value for significance**
DA 10	0.57	<0.001*	≤0.05
DA 3.0	0.57	0.001*	≤0.025

3.5.4.1 DA a-wave amplitudes

The correlation analysis failed to demonstrate any change with age for the amplitude of the DA 3.0 ERG or the DA 10 ERG (see Table 3.12). Therefore, the DA a-wave amplitudes are unlikely

to be influenced by age at least beyond 7 years of age. The mean estimates for the DA a-wave amplitudes of individuals aged from 7 to 33 years old are shown in Table 3-14.

Table 3-14: Dark-adapted a-wave amplitudes. *CI* = confidence interval (1.96 x SD).

Age range (years)	**Stimulus ($cd.s.m^{-2}$)**	**Mean (µv)**	**St. Deviation**	***95% CI***	
				Lower limit	**Upper limit**
7.1-33.4	DA 3.0 a-wave	216.0	48.1	121.7	310.3
7.1-33.4	DA 10 a-wave	190.0	41.5	108.7	271.4

3.5.4.2 DA a-wave implicit time

The rank correlation analysis showed that both the DA 3.0 ERG implicit time and the DA 10 implicit time increased with age (positive correlations). Adjusted Bonferroni correction showed that both these correlations remained significant (Table 3-13). As age increases the implicit times increase to approach adult values (Figures 3-7 and 3-8). The age-related medians and ranges are shown in Tables 3-15.

Table 3-15: DA a-wave implicit times: Median and reference ranges for each age group.

Age group	**Stimulus ($cd.s.m^{-2}$)**	**Median (ms)**	**Range**	
			Minimum	**Maximum**
7-11	DA 3.0	15	14	15.5
12-15		15	14.5	16
20-33		15	14	15.5

7-11	DA 10	13	12	14
12-15		13	11.5	14.5
20-33		13	12	14

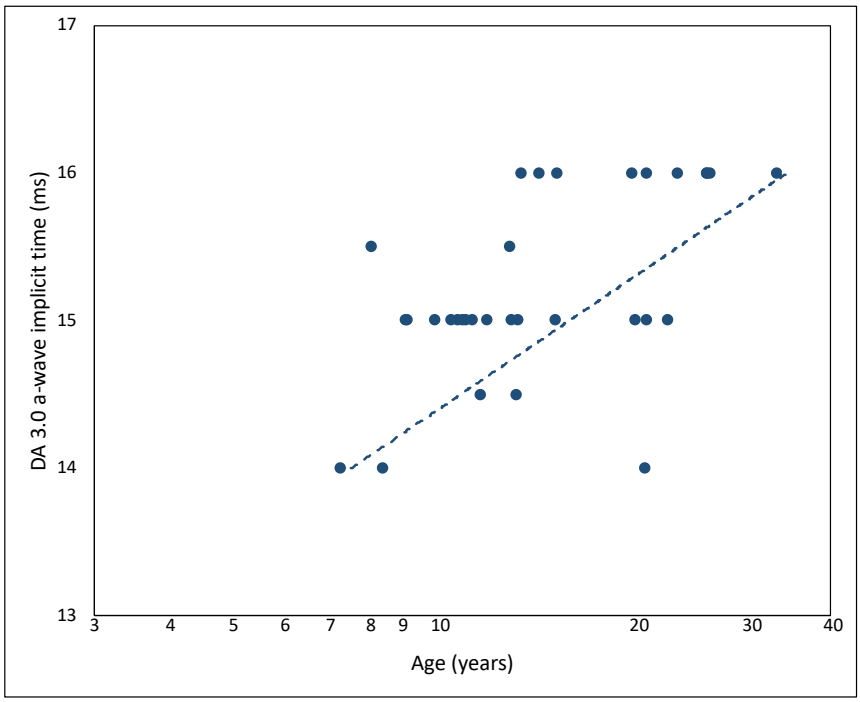

Figure 3-7: Scattergram of the DA 3.0 a-wave implicit time against age. Each point represents the average data for one participant. The linear regression line is shown as a dashed line and is representative of the trend although rank correlation was used for this non-normally distributed data.

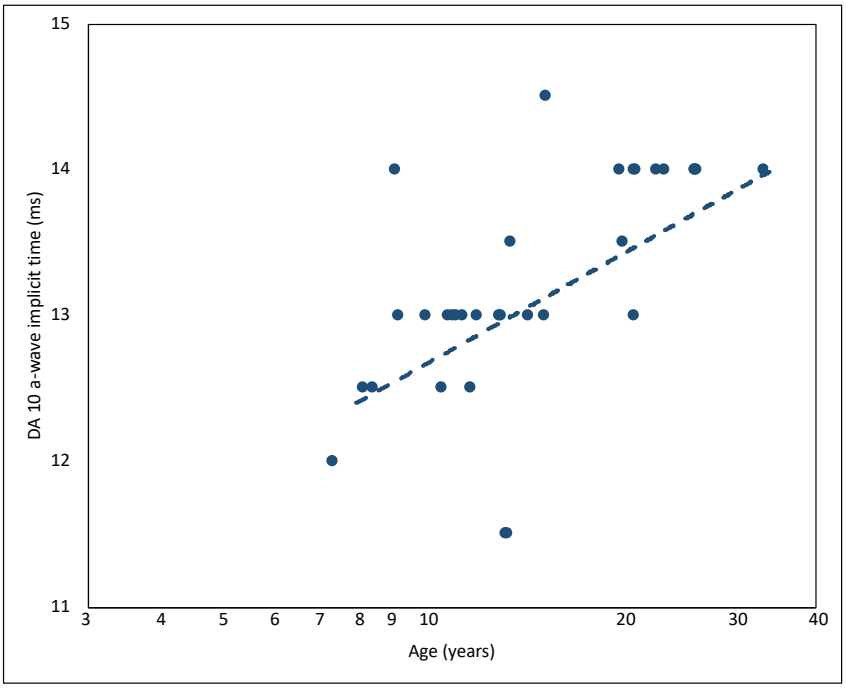

Figure 3-8: Scattergram of the DA 10 a-wave implicit time against age. Each point represents the average data for one participant. The linear regression line is shown as a dashed line and is representative of the trend although rank correlation was used for this non-normally distributed data.

3.5.5 Dark adapted (DA) b-wave

The Shapiro-Wilk results showed that the dark-adapted b-wave amplitudes were normally distributed for all stimuli. Therefore, Pearson's correlation coefficient was used to analyze the amplitude data. However, the implicit times were not normally distributed for all stimulus. Therefore, Spearman's rank correlation was used to analyze the data. The correlation coefficients with age are shown in Table 3.16 and 3.17.

Table 3-16: Pearson correlation coefficient for the DA b-wave amplitudes with age.

Stimulus	r value	p value
DA 0.01 b-wave amplitudes	-0.08	0.67
DA 3.0 b-wave amplitudes	0.19	0.29
DA 10 b-wave amplitudes	0.18	0.31

Table 3-17: Spearman's rank correlation for the DA b-wave implicit times with age. * = those which remain significant after the Adjusted Bonferroni.

Stimulus	r value	p value	Adjusted α value
DA 0.01 b-wave implicit times	0.60	<0.001*	0.025
DA 10 b-wave implicit times	0.44	0.01*	0.05
DA 3.0 b-wave implicit times	0.20	0.25	NA

3.5.5.1 DA b-wave amplitudes

The results of the correlation analysis showed that there was no significant relationship between age and the amplitude for any of the stimulus levels (see Table 3.16). Therefore, age was found to have no significant effect on the DA b-wave amplitudes. The mean estimates for the DA b-wave amplitudes of individuals aged from 7 to 33 years old are indicated in Table 3-18.

Table 3-18: Mean, standard deviation, and 95% confidence interval of the dark-adapted b-wave amplitudes. *CI* = confidence interval (1.96 x SD).

Age range (years)	Stimulus ($cd.s.m^{-2}$)	Mean b-wave amplitude (µv)	St. Deviation	*95% CI*	
				Lower limit	Upper limit
7.1-33.4	DA 0.01	325.68	72.56	183.5	467.9
7.1-33.4	DA 3.0	341.83	80.30	184.5	499.2
7.1-33.4	DA 10.0	238.48	57.54	125.7	351.3

3.5.5.2 DA b-wave implicit times

The rank correlation analysis showed that b-wave implicit times for both the DA 0.01 and the 10 ERG, but not the DA 3.0 ERG were significantly positively correlated with age (Table 3.17) such that the implicit time was shorter for children compared to adults as it can be seen in Figure 3-9 and Figure 3-10. Adjusted Bonferroni correction showed that these correlations remained significant. The reference ranges are given in Tables 3-19. There was no significant relationship with age for the 3.0 DA b-wave implicit time; the median and percentiles are given in Table 3.20.

Table 3-19: Reference ranges of the dark-adapted b-wave implicit times (IT) for each age group.

Age group	Stimulus ($cd.s.m^{-2}$)	Median b-wave IT (ms)	Range	
			Minimum	Maximum
7-11	DA 0.01	82	70	85
12-15		78.5	74.5	108

20-33		88.25	77.5	98
7-11	b-wave 10	30	25	33
12-15		31	25	40
20-33		33	31.5	45

Table 3-20: Table 3-20: b-wave implicit times (IT) for the DA 3.0 ERG

Age range (years)	**Stimulus strength (cd.s.m^{-2})**	**Median b-wave IT (µV)**	**interquartile range**	**2.5th percentiles**	**97.5th percentiles**
7.1-33.4	DA 3.0	37.5	±9.5	32	47.1

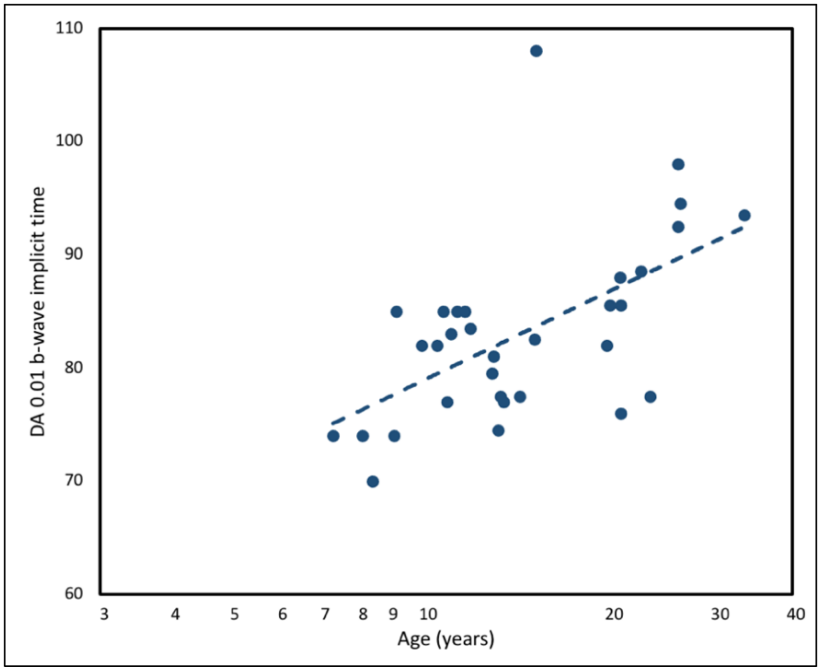

Figure 3-9: Scattergram of the DA 0.01 b-wave implicit time against age. Each point represents the average data for one participant. The linear regression line is shown as a dashed line and is representative of the trend although rank correlation was used for this non-normally distributed data.

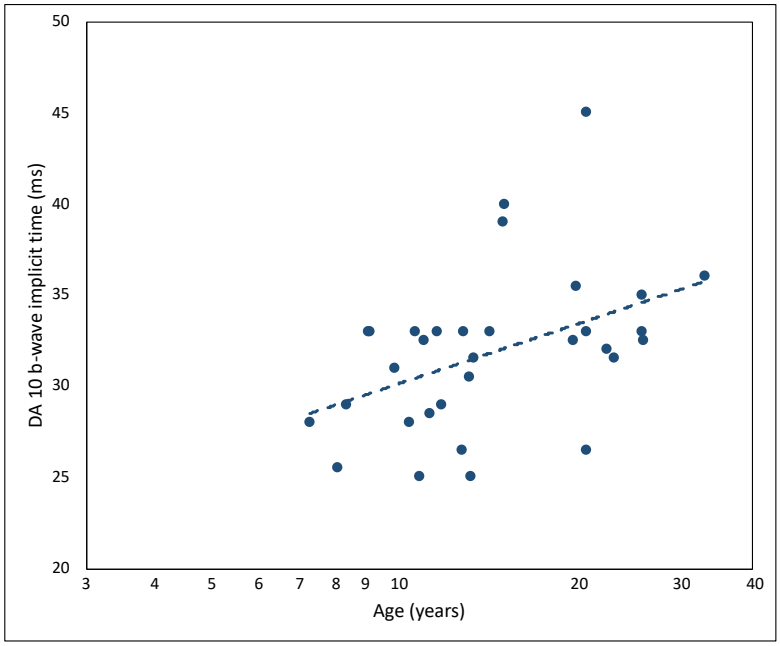

Figure 3-10: Scattergram of the DA 10 b-wave implicit time against age. Each point represents the average data for one participant. The linear regression line is shown as a dashed line and is representative of the trend although rank correlation was used for this non-normally distributed data.

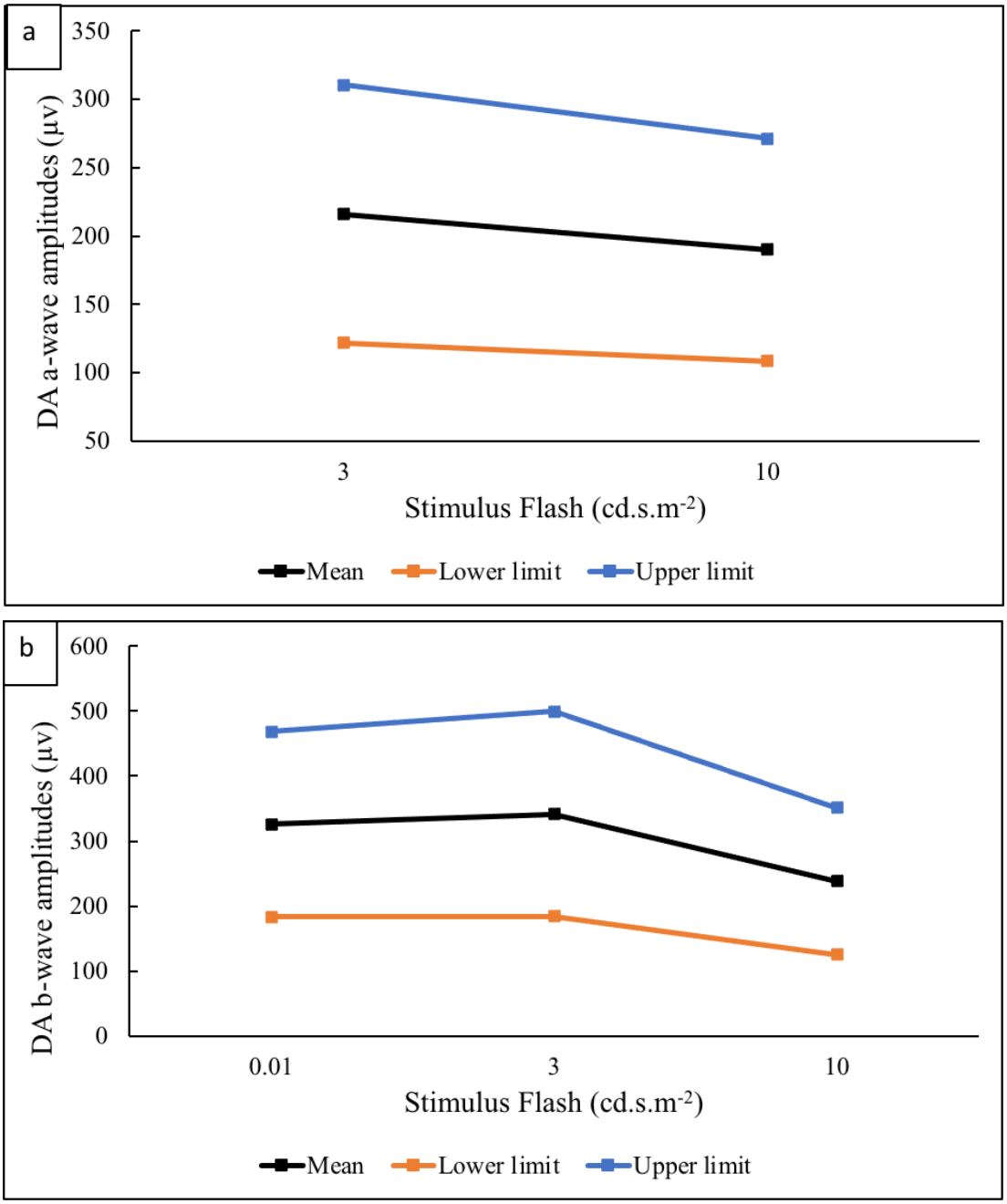

Figure 3-11: (a) The mean and 95% confidence interval for the DA a-wave amplitudes plotted against luminance intensities. (b) The mean and 95% confidence interval for the DA b-wave amplitudes plotted against luminance intensities.

3.6 Discussion

The purpose of the study was to acquire pediatric normative values for full-field standard ERGs and an extended LA ERG protocol. The study provides reference data to better understand the retinal functional changes during childhood, which can be used to evaluate clinical pediatric ERGs. The standard ISCEV protocol was used to acquire ERG normative data from children who are of European descent as a previous study has shown that ERG recordings might be influenced by fundus color such that darker fundi have smaller amplitudes compared to lighter fundi[127].

A direct comparison between the current study and existing studies is not possible as various techniques were used to record ERG waveforms. For instance, previous studies have used contact lens electrodes[48,49,53], skin electrodes and gold foil electrodes[128] to acquire ERG normative data, while in the present study, DTL electrodes were used. It has been previously shown that ERG amplitudes vary depending on the electrode types[129]. Additionally, Birch et al.[49] and Westall et al.[53] used a dimmer flash (of 2 cd.s.m^{-2}) for the DA 3.0 ERG, known previously as DA maximal response, while in the present study, we adopted the current ISCEV standard protocols. In a study conducted by Fulton et al. the data were collected from two laboratories, and each laboratory used different techniques to obtain ERGs (white flashes for the first lab, blue and red flashes for the second lab). Even though the study reported no significant differences for the comparable stimuli between the data collected from the two laboratories, chromatic ERGs are designed to improve isolation of rod versus cone-initiated responses compared to the white flashes. In the present study, white flashes were used as specified by the current ISCEV standard protocol. Finally, Westall et al.[53] used a logistic curve to describe the developmental changes of

the of the amplitudes for the ERG waveforms, whereas the present study used log-linear regression. A direct comparison is only possible if both studies do similar fitting. The sample size of the current study was not considered sufficiently large to undertake curve fitting. The Westall et al. study provided the equation for Naka Rushton parameters, but calculating the value for each age range has not been attempted.

The results of the present study indicated large inter-subject variability in the ERG amplitudes even for individuals within the same age group, particularly LA and DA b-wave amplitudes. Such large inter-subject variability is typical in ERG recordings[48,128,130,131]. Previous studies have indicated that peak to peak amplitude (b-wave) can demonstrate large variability between individuals with skin electrode[130], microfiber electrode[131], and contact lens electrode [48,128] for both adult and child populations. For instance, Fernandes et al.[131] used the microfiber electrode to report the standard ERG waveforms in normal adults. They found large inter-subject variability for the DA weak flash (SD ±40μv), standard flash (SD ± 49μv), and the LA standard flash (SD ±32μv). Similarly, Bardshaw et al.[128] used contact lens electrodes in a child population and reported inter-quartile ranges of (259-350μv) for the DA weak flash, and (379-624μv) for the standard flash. In the present study, the ERG was observed in real time, and individual ERGs were compared prior to averaging to establish the repeatability of the waveforms. A minimum of 20 responses at each luminance level was acquired. Thus, when the data had to be eliminated because of electrical noise, blinking or eye movements, we had adequate data to have at least three valid responses for each participant. Subsequently, we determined a- and b-wave amplitudes and implicit times using the average of the right and left eye values to compare age groups. This is justified as we did not obtain observations for the left and right eye for all

participants. On examining the interocular variability in ERG amplitudes, we found that the percentage difference between the left and right eye varied between 10% to 20% for all participants that had ERG recordings for both eyes (by observation, not statistically tested). Therefore, the large variation observed in the ERG amplitudes is likely to be normal variability between subjects (which may hide some real differences between age groups).

Previous findings documented that the immature retina is characterized by long implicit times that decrease systematically with age in young children. Fulton et al[48] reported that the dark-adapted b-waves' implicit time varies little with age for 0.01 ERG, whereas for the 3.0 ERG it decreases with age from 65ms during infancy to 47ms by 1-10 years, somewhat longer than the median of 37.5ms found across our entire age range of 7 to 33 years, which may be attributed to the weaker flash used by Fulton et al. Birch et al.[45] documented that implicit time is considerably longer in infancy and reaches maturity between 5-15 years old for both 0.01 and 3.0 ERGs. This difference between studies is likely due to different techniques being used to obtain the ERG recordings. The present study results indicated a significant effect of age for the implicit times of DA a- and b-waves. We observed that the implicit times of the 0.01 and10 DA b-wave and the 1.0 LA b-wave were significantly influenced by age. Similarly, the effect of age was significant for the implicit times of DA a-waves, including 3.0 and 10 ERGs and LA dim flash (0.3 ERG). The implicit times for children aged between 7-15 years increase with age and approach adult values. Therefore, the overall conclusion of the present study in conjunction with previously reported findings is that the implicit times initially decrease with age from early infancy (at birth) until about 5-6 years, and then increase again through 7-15 years. This may indicate overall immaturity in early infancy (prolonged ERG waveforms) and relative immaturity of the rod

system in childhood as ERGs primarily due to rod and rod pathway activity have longer implicit times than those from the cone system. Of note, these effects are limited to 1 or 2ms difference across the age range tested which may not be clinically significant, although it reached statistical significance.

Our finding for the light-adapted b-wave amplitudes (3.0 ERG) agrees with the previously published studies[48,49,53] that have found that adult-like values are reached somewhere between 1 and 10[48] or 5 and 15[49,53] years of age. However, the data in the majority of the previously reported studies[48,49] are grouped such that any developmental changes between older and younger children could not be identified. Fulton et al.[48] reported that the amplitudes of LA b-waves increase systematically with age in very young children until they fall within the lower limits of normal adult data by 15-52 weeks of age with an amplitude of 128μv. Westall et al documented that b-wave amplitudes overlap 95% of the adult data by five years of age. Similarly, Birch et al. found that the light-adapted b-wave amplitudes reached maturity by 5-15 years. In the present study, no evidence of further maturation of the LA 3.0 b-wave amplitudes beyond seven years of age was found, as the amplitude showed no significant change with age. This indicates that the postsynaptic neural activities of the depolarizing ON bipolar cells and hyperpolarizing OFF bipolar cells are sufficiently mature to be considered adult-like before 7-11 years of age. Similarly, we did not observe any developmental changes between adults and our children for the LA a-wave amplitudes. This is consistent with Fulton et al. who found the LA-a wave is within the adult range by 15-25 weeks of age. Our finding also indicates that the cone photoreceptors and the inner retinal activity postsynaptic to the cones, including hyperpolarizing OFF -bipolar neurons, are adult-like before 7-11 years of age.

Previously reported studies suggested that the DA b-wave amplitude of the 0.01 ERG was slower to reach maturity than other ERG waveforms. Birch et al. documented that DA 0.01 b-wave waveform was extremely immature at birth both in terms of amplitude and implicit time before it developed progressively reaching adult values by 5-15 years with a b-wave amplitude of 145μv and implicit time of 79.4ms. Similarly, Westall et al. found the amplitude of the 0.01 ERG reached half of the adult value by 19 months and approached a 95% overlap of the adult data by 7 years of age (307.6 μv). Fulton et al. concluded that the median amplitude of the b-wave approached the lower limit of the adult values by 1-10 years of age. In agreement with previously published studies, the present study finds that the amplitude of DA 0.01 ERG b-wave for a child over seven years of age did not differ significantly from those of adults. It has previously been shown that the DA 3.0 b-wave amplitude matures more rapidly than the ERG to weak stimuli which is dominated by the rod system. Birch et al. found that the DA 3.0 b-wave amplitude approaches the adult range of normal values (372uv) by 5-15 years. In comparison, Westall et al. reported that the DA-b-wave amplitude is adult-like by three years of age. Similarly, Fulton et al. documented that the median of the b-wave amplitude increases gradually from birth before reaching maturity between 1-10 years old. Thus, the present results agree with previous studies, showing that the b-wave amplitude is unlikely to be influenced by age for children older than seven years of age. Similarly, the present results revealed that the amplitude of the b-wave for the strong flash (DA-10 ERG) did not differ significantly between children and adults. We are not aware of any normative data in literature with which to compare this finding.

One limitation of the present study is that younger children (4-6 years) were not included in the analysis. This was because most children within this age range could not tolerate the Espion E3

visual electrophysiology system and the DTL electrodes. Subsequently, ERG data for younger children were collected using a hand-held ERG system with skin electrodes (the RETeval visual electrophysiology system, LKC® city country). But the ERG data for these younger children were not in included in the analysis as the data acquired using skin electrodes are substantially smaller and have earlier implicit times compared to those collected using DTL electrodes. As a result, we were not able to determine whether the developmental trend for this younger age group would agree with the previously published findings.

Another limitation is that demographic characteristics of the participants limits the generalization of the study findings to other ethnicities and racial groups as the study only included participants of European descent. However, if similar data were collected from other Ethnicities, then these separate data for different ethnicities would be a strength.

Lastly, we are unable to determine with certainty the age at which ERG recordings reach maturity owing to the small sample size that was included in the present study and that younger children were not included. Therefore, future studies could add to the present data to create larger sample size and possibly a wider age range with other ethnic groups to add important detail to the scope of these pediatric normative values.

In conclusion: the present study showed that the implicit time of the dark-adapted a- and b-waves are significantly influenced by age between 7 years of age and young adults, such that the implicit times were shorter for children than adults. In agreement with the literature, we find no evidence of the maturation of amplitude after 7 years.

Chapter 4: Normative Data for The Retinal Layer and Retinal Nerve Fiber Layer Thicknesses in Children of European Descent

4.1 Introduction

The human fovea is located in the center of the macula and it is the most important portion of the retina for high spatial resolution and color vision[132]. It has been suggested that it plays a major role in the maturation of the human visual cortex, regulation of the cortical maps[133] as well as calcarine fissure symmetry[134]. Despite its importance, there are surprisingly few studies that have documented the morphological changes of the human fovea from infancy until it becomes truly adult-like[2,3,9]. Most of our understanding regarding the maturation of the human fovea has relied heavily on histologic studies of the simian retina[5,6]. Nevertheless, histological findings may not always determine with certainty the developmental patterns or the time course for each retinal layer due to the fact that there are very few human histological samples available and samples could be affected by shrinking of the tissue or artifacts such as retinal detachment[78]. Additionally, existing histological studies vary in their conclusions: earlier studies reported that foveal development is complete between 11 months and five years of age[1–3,] but more recent studies indicated that it continues even after 12 years of age[8,9].

Optical coherence tomography (OCT) is a non-invasive imaging modality that has increasingly become an indispensable cornerstone of managing various ocular pathologies over the past few decades. The fundamental principles of the OCT evolved from the previously designed imaging system known as low coherence reflectometry, which utilized a broadband light source and a Michelson interferometer. In 1991, the application of transverse scanning (B-scan) enabled two-dimensional scanning of the retinal tissue known as time-domain OCT. The reliability of the

OCT technology has increased with the introduction of spectral-domain OCT (SD-OCT), which provides high-resolution scans and cross-section topographical images of the retina with a short acquisition time. Therefore, the procedure enables examination of the human retina without the need for sedation or anesthesia. Previous studies reported that the technique is repeatable and reproducible, and it can be used effectively to reflect the developmental changes of the retinal tissues[86,109,135]. Because of the short acquisition time, scans can be obtained in young children. The retinal layers detected in OCT correspond topographically with their histologically defined names except for the outer nuclear layers and outer plexiform layer. For these layers, the Henle fiber layer (the axons of the photoreceptors) is histologically part of the outer plexiform layer, whereas with OCT it has similar reflectivity as the outer nuclear layer and they are indistinguishable[80].

OCT has already added to our understanding of human retinal development, which occurs over a relatively long-time frame starting from early gestational age through early adulthood. For instance, even though the formation of the human macula has been reported as early as 11 weeks gestational age, it is still not completely developed at birth[1]. The development of the retinal layers is complex and involves two neural displacements that occur in opposite directions: the outward migration of the inner retinal layers away from the fovea and the inward migration of the cone photoreceptors towards the foveal centre. Maldonado et al.[78]established the timeline of the human foveal maturation *in vivo* using a hand-held OCT on premature infants aged between 31 to 41 weeks of gestation (i.e., 9 weeks preterm to 1-week post-term). This timeline was validated and expanded by investigating the foveal maturation in infants beyond term age[8,77]. During the infancy, the fovea has an immature appearance with prominent thick inner retinal

layers at the foveal center, overall thinner outer retinal layers and lack of photoreceptors sublayers including ellipsoid zone and interdigitation zone[78]. Lee et al.[77] found that the centrifugal displacement of the inner retinal layers is complete by 17.5 months of age while centripetal displacement of the outer retinal layers may continue until adulthood (beyond 12 years of age). This is in agreement with one histological study which revealed that the cone packing density is approximately half of adult values by 45 months of age indicating that the process is incomplete, although it must be noted that this was the retina of a single child[3].

Quantitative SD-OCT assessment is routinely used to detect and monitor the progression of the ocular pathologies. For example, OCT has been shown to be valuable in early detection and monitoring of glaucoma[82,107]. For the adult population, SD-OCT instruments typically compare the acquired retinal thickness values with an age-matched database to assess for normalcy and monitor the disease progression over time. However, the internal normative database provided by the SD-OCT (Heidelberg Engineering) used in this study only starts with individuals over 18 years and there are no reference data with which to compare the acquired numeric values in children. Knowledge of child normative thickness values is essential to detect and monitor retinal disorders that might affect the pediatric retina.

Previously, Yanni et al.[103] reported normative values for macular thickness and RNFL thickness in North American (mixed race) children aged from 5 to 15 years old using SD-OCT. The present study aims to expand on previously reported studies in two ways: (1) to obtain reference data from North American children who are of European descent (since ethnicity is one factor which influences OCT measurements[85,94]) (2) to compile a normative database for individual

retinal layers at the foveal, parafoveal, and perifoveal areas to add important detail to the scope of pediatric normative values.

4.2 Study participants

In this cross-sectional study, thirty-six participants of European descent with normal ocular and general health were recruited. The sample was a purposeful sample to include children evenly spread within the ages of 4-15 years. The final numbers were six participants between 4 and 7 years, nine between 8 and 11 years and ten between 12 and 15 years, and eleven adults between 20 and 33 years.

Recruiting strategies, inclusion criteria and screening test are described in detail in Chapter 3.

4.3 Optical Coherence Tomography measures

4.3.1 Equipment

The Spectralis SD-OCT (Heidelberg Engineering system, Heidelberg, Germany), available within the Optometry Clinic at the School of Optometry and Vision Science, was used to obtain OCT scans. The instrument consists of dual systems of SD-OCT and a confocal scanning laser ophthalmoscope to produce high-resolution cross-sectional imaging of the retina *in vivo* which is comparable to those obtained by histological analysis[8]. The acquisition rate of the instrument is 40,000 A-scans per second. Standard protocols for SD-OCT imaging were used to obtain a macular cube and a nerve fiber layer scan around the optic nerve. Central fixation was monitored through the live fundus image, and the quality score of the scan was determined by Spectralis® proprietary software as a signal-to-noise (SNR) ratio in decibels (dB). A-scans with a SNR above

20 decibels (dB) are considered to be of high quality as recommended by the manufacturer's guidelines. The Spectralis® segmentation software was used to acquire retinal layer thickness measurements. The accuracy of the automatic segmentation was assessed manually frame by frame to avoid any segmentation failure within the standard macular cube area (Figure 4-1).

4.3.2 Protocol

The study participants were asked to sit in front of the instrument and the table height as well as the chinrest were adjusted for comfort. Participants were asked to put their head in the headrest and the canthus marker was adjusted to be at eye level. Participants were directed to look at the fixation target and the camera of the instrument was moved toward the eye to obtain alignment, so the fundus was equally illuminated for optimum image quality. During the test, participants were instructed to minimize eye movement in order to acquire a high resolution of OCT scan. The image was acquired after selecting the desired OCT scans which included macular cube scan and nerve fiber layer scan.

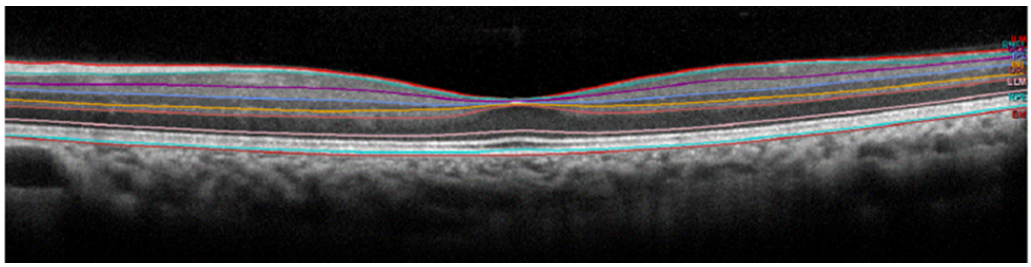

Figure 4-1: Automatic retinal layer segmentation by Spectralis SD-OCT software.

4.3.3 Nerve fiber layer scan

The nerve fiber layer scan is a series of B-scan images that are acquired from the retina around the optic nerve head to enable better visualization of the morphology and any pathology of the optic nerve head. The instrument uses a circle of predefined diameter centered at the optic nerve to measure the thickness of the retinal nerve fiber layer. The high-resolution mode was used to acquire the images which were circular B-scan (3.5 mm diameter, 768 pixels, 1536 A-scans/second) centered on the optic nerve. The peripapillary area was subdivided into 7 sectors; temporal superior sector (45 degrees), nasal superior sector (45 degrees), nasal sector (90 degrees), temporal sector (90 degrees), temporal inferior sector (45 degrees), nasal inferior sector (45 degrees), and global sector (360 degrees) (Figure 4-2). The instrument segmentation software was used to acquire the RNFL thickness automatically which was calculated from the distance between the internal limiting membrane and the RNFL.

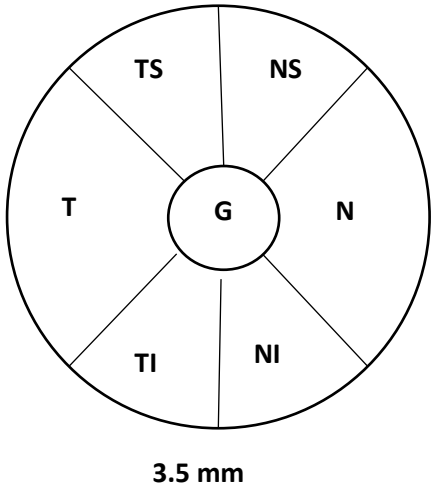

Figure 4-2: Peripapillary retinal nerve fiber layer thickness classification provided by the Spectralis for the nerve fiber layer scan. Temporal superior sector (TS), nasal superior sector (NS), nasal sector (N), temporal sector (T), temporal inferior sector (TI), and nasal inferior sector (NI).

4.3.4 Macular cube scan

Macular cube scans are 3D scans that allow a volumetric evaluation of the central retinal structure by acquiring a rapid sequence of cross-sectional B-scan images, mainly in a 6 mm × 6 mm area centered on the fovea. These scans are analyzed automatically to produce retinal layer thickness measurements enabling quantifying and mapping of the individual retinal layers at the macula. The thickness of each macular layer was measured for the entire cube and then sub-divided according to the sectors defined for the Early Treatment Diabetic Retinopathy Study (ETDRS)[75] within 3 concentric circles (Figure 4-3). The central circle (sector 1) represents the fovea and is 1.00 mm in diameter. The middle circle termed parafovea (3.00 mm outer diameter) is divided into 4 areas: superior sector (2), nasal sector (3), inferior sector (4) and temporal sector (5). The outer circle has an outer diameter of 6.00 mm (perifovea) and is divided into the superior sector (6), nasal sector (7), inferior sector (8) and temporal sector (9). The thickness of each retinal layer was calculated from the thickness map generated automatically by the instrument, which included overall retinal thickness (RT), retinal nerve fiber layer (RNFL), ganglion cell layer (GCL), inner plexiform layer (IPL), inner nuclear layer (INL), outer plexiform layer (OPL), outer nuclear layer (ONL), retinal pigment epithelium (RPE), inner retinal layer (IRL) and outer retinal layers (ORL).

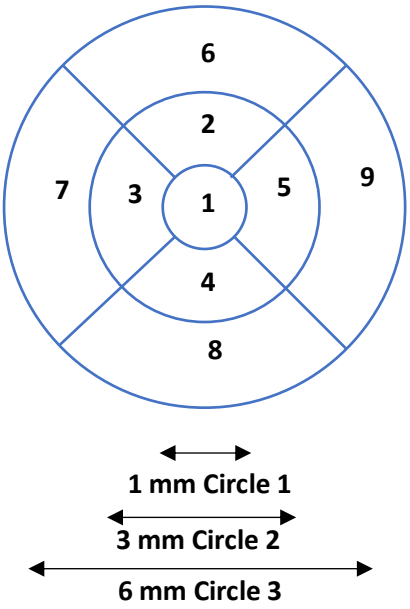

Figure 4-3: Early Treatment Diabetic Retinopathy Study (ETDRS) template used to measure macular thickness in different areas.

4.4 Data analysis

For the RNFL data, the average thickness measurements were calculated for each of the 6 RNFL sectors (temporal superior, nasal superior, nasal, nasal inferior, temporal inferior and temporal). Thus, there were six RNFL thickness measures for each participant plus the global thickness.

For the macular cube, for each participant, mean thicknesses were calculated for each of the nine ETDRS areas for each retinal layer and for the overall inner retina, overall outer retina and the overall retinal thickness.

Statistical analyses were conducted using SPSS (IBM SPSS Statistics 27) and Excel (Microsoft®Excel, Version 16.42). The Shapiro-Wilk test was used to test the distribution of the data for normality. Age was transformed into a log10 scale which spread the age range more

evenly and resulted in a normal distribution for age. Depending on whether the data for each layer/area were normally or not normally distributed, Pearson's correlation or Spearman's rank correlation tests, respectively, were used to determine the correlation between age and the retinal thickness values for each layer. The adjusted Bonferroni correction for multiple comparisons was applied within data sub-groups (Jaccard and Wan[126]). The 95-confidence intervals (mean ±1.96xSD) were calculated for the data that were not correlated with age, and which were normally distributed. For those data that were not correlated with age and not normally distributed, the median and 2.5th, 50th and 97.5th percentiles were calculated for all ages together. For the data that were significantly correlated with age, scatterplots were created, and the mean/ median and reference ranges were calculated for each age participant group. Standard deviations or percentiles were not attempted when there was a correlation with age because of the small sample size when divided into age sub-groups.

Results 4.5

4.5.1 Population Demographics

A total of 36 participants were included in the study. The sample included 11 adult participants (median age = 23.4, ranging from 20 to 33.42 years), 10 older children (median age = 13.3 ranging from 12.08 to15.33), 9 intermediate-aged (mean age = 10.5 ranging from 8 to 11.17 years), and 6 young children (median age = 5.4 ranging from 3.92 to 7.17 years) .

All participants participated in the screening, met the eligibility criteria as described in Chapter 3 and successfully completed the study's procedure.

4.5.2 Peripapillary RNFL thickness

As described above, the peripapillary RNFL thickness values were automatically measured by the Spectralis SD-OCT, providing a global average, and average thickness measurements for each quadrant including temporal, temporal-superior, temporal- inferior, nasal, nasal superior, nasal inferior quadrants. The images were of high quality (average SNR values were 31.69 range 22-41 dB), see Figure 4-4.

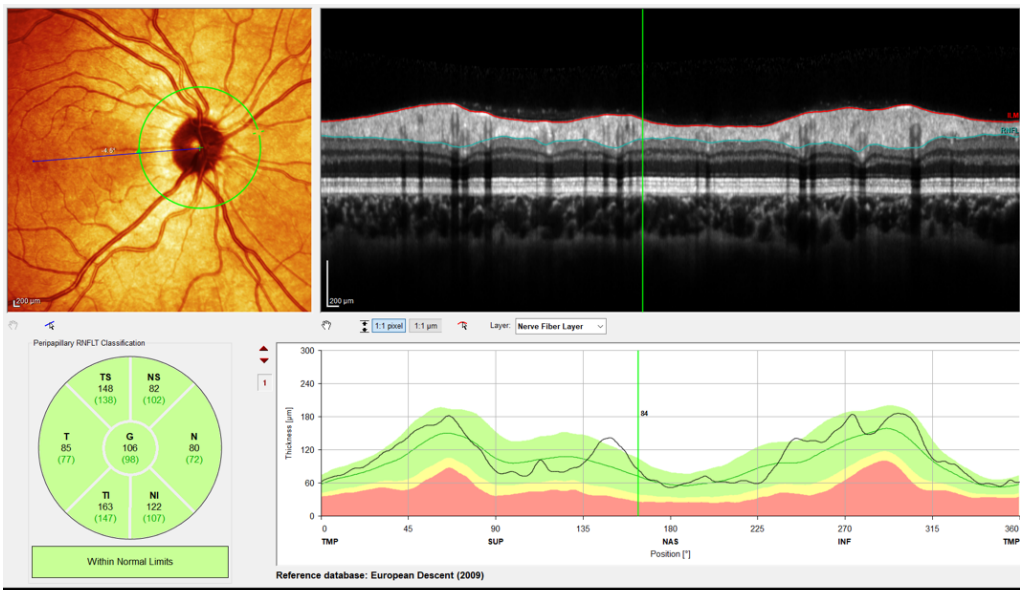

Figure 4-4: Upper figure. A representative example of RNFL report generated by Spectralis SD-OCT for RNFL scan for a 15-year-old healthy participant. Lower figure. Bold numbers under each sector indicate the average RNFL thickness. Numbers in parentheses are the adult's normative database provided by the Spectralis SD-OCT**.**

The results of the Shapiro-Wilk test showed that the data were normally distributed for the global, temporal, temporal inferior, nasal and nasal inferior sectors. Therefore, Pearson's correlation coefficient was used to test the correlation between age and the RNFL thickness for these sectors and the results are shown in Table 4-1. The results of the correlation analysis failed to demonstrate any change with age in the average RNFL thickness of the global measurement,

the temporal sector, the temporal inferior sector, the nasal sector, or in the nasal inferior sector. The mean and 95% confidence interval for the thickness of each sector are indicated in Table 4-2.

Table 4-1: The correlation between Log age and RNFL sectors.

RNFL sector	**r value**	**p value**
Global	-0.22	0.18
Temporal	-0.06	0.70
Temporal superior	-0.28	0.08
Nasal superior	-0.37	0.02
Nasal	-0.03	0.79
Nasal inferior	-0.07	0.64
Temporal inferior	-0.14	0.40

Table 4-2: RNFL thickness by sector for sectors which do not change with age.

Age range (years)	**RNFL area**	**Mean thickness (µm)**	**St. Deviation**	**95% CI (1.96xSD)**	
				Lower limit	**Upper limit**
3.92-33.42	Global RNFL	104.8	9.4	86.4	123.2
3.92-33.42	RNFL temporal	72.5	12.2	48.6	96.4
3.92-33.42	RNFL nasal	83.8	14.2	55.9	111.6

3.92-33.42	RNFL nasal inferior	123.0	22.9	78.1	167.9
3.92-33.42	RNFL temporal inferior	143.0	20.2	103.4	182.6
	RNFL area	**Median thickness (µm)**	**Interquartile range**	**2.5th percentiles**	**97.5th percentiles**
3.92-33.42	RNFL temporal superior	146.3	18.6	121.6	190.8

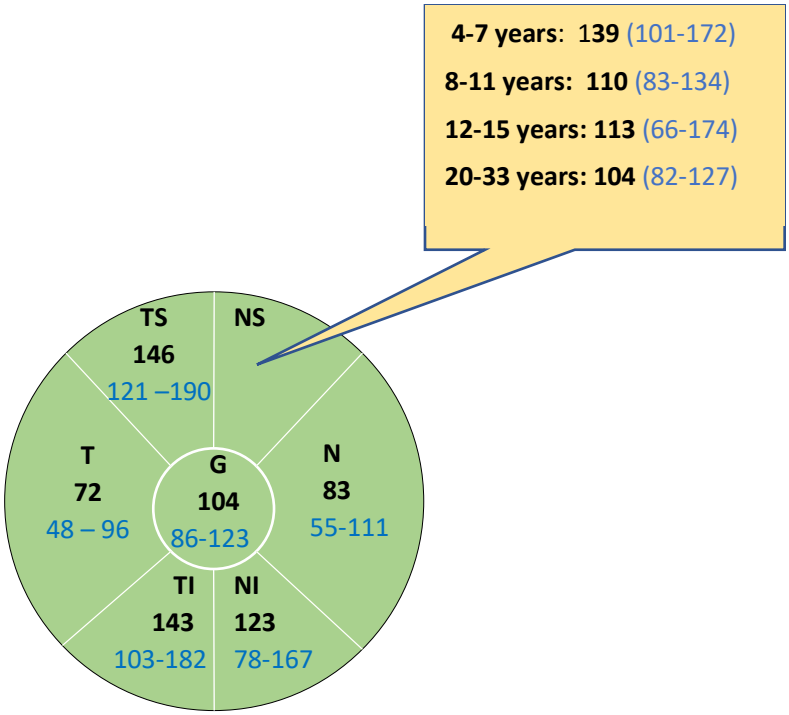

Figure 4-5: Peripapillary RNFL thickness measurements for each sector generated by the Spectralis SD-OCT. Bold numbers i.n each sector indicate the average RNFL thickness. Numbers in blue indicate the normal (2.5-97.5%) range. For the nasal superior sector, which was affected by age, the normal range (2.5-97.5%) for each age group is indicated in a callout box.

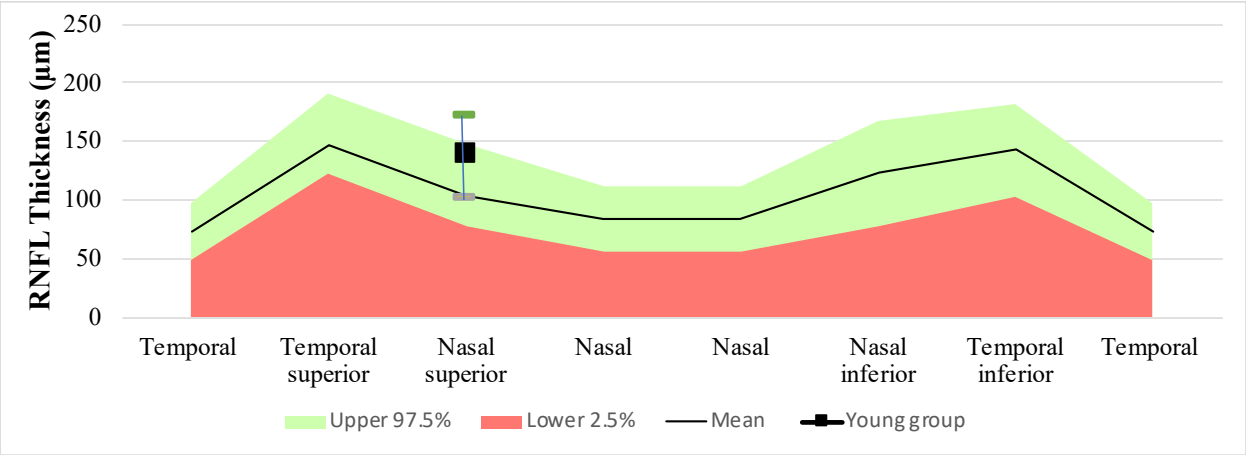

Figure 4-6: The mean (or median) and 2.5%, to 97.5% range for the peripapillary retinal nerve fiber layer. The green area indicates the normal (2.5-97.5%) range and the red area indicates measures that are below the 2.5% range. For the nasal superior, which was affected by age, the range is for participants aged 8 to 33 years and the black square indicates the median thickness measurements of young children (4-7 years) and the error bar indicates the lower 2.5% and the upper 97.5% range for the 4-7-year olds.

The data were not normally distributed for the nasal superior and temporal superior sectors and Spearman's rank correlation was used for these sectors. The results of these correlation analyses revealed that the average RNFL thickness in the nasal superior sector was significantly negatively correlated with age, so that the RNFL thickness decreases with age ($r = -0.37$, $p = 0.02$). Since only one correlation result was significant among the RNFL data, it remains significant with the Adjusted Bonferroni. Table 4-3 shows that the median value for young children (4-7) was 139.50µm compared to 104µm for adults. There was no significant correlation between the average RNFL thickness at the temporal superior sector and age ($r = -0.289$, $p = 0.088$). The median, 2.5 and 97.5 percentiles for the RNFL thickness in the temporal superior sector are indicated in Table 4-2.

Table 4-3: RNFL thickness for the nasal superior sector for each age group.

Age group	Median (um)	Range	
		Minimum	Maximum
4-7 (n= 6)	139.5	101	172
8-11 (n= 9)	110	83	134
12-15 (n= 10)	113	66	174
20-33 (n=11)	104	82	127

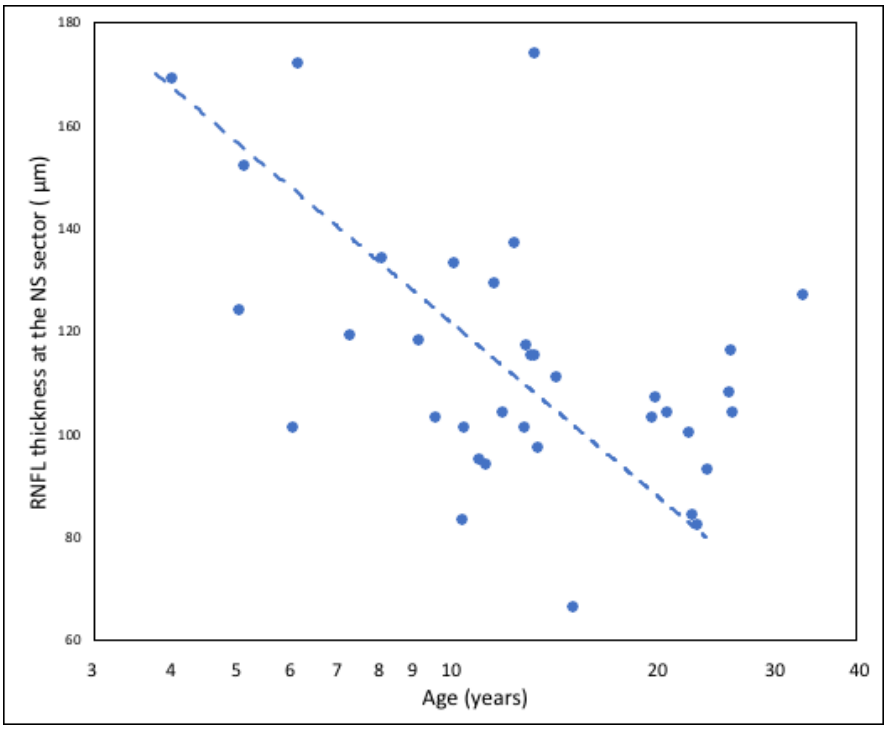

Figure 4-7: Scattergram of the RNFL thickness for the nasal superior sector against age. Each point represents the average data for one participant. Dashed linear regression line is representative of the trend although rank correlation was used for this non-normally distributed data, rho= -0.379, p= 0.023.

4.5.3 Macular cube: Overall retinal thickness

The results of the Shapiro-Wilk test showed that the data were normally distributed across all regions including the foveal, parafoveal and perifoveal areas. Therefore, Pearson's correlation coefficient test was used to test the correlation between age and the average retinal thickness measurements in these areas. The correlation results are shown in Table 4-4.

Table 4-4: Pearson correlation coefficient for the total retinal layer measurements in the foveal, para and perifoveal areas with age. *= remains significant after adjusted Bonferroni.

Retinal region	**r value**	**Unadjusted p value**	**α value for significance with adjusted Bonferroni**
Whole foveal area	0.487	0.003*	0.0125
Superior parafovea	0.391	0.018	0.017
Nasal parafovea	0.388	0.019	0.025
Temporal parafovea	0.3.83	0.021	0.05
Inferior parafovea	0.323	0.054	NA
Nasal perifovea	0.166	0.333	NA
Inferior perifovea	0.109	0.528	NA
Temporal perifovea	-0.046	0.790	NA
Superior perifovea	-0.019	0.941	NA

4.5.3.1 Overall retinal thickness in the foveal area

The results of the correlation analysis revealed that there was a significant positive correlation between age and the overall retinal thickness at the foveal area ($r = 0.487$, $p = 0.003$). Adjusted Bonferroni correction for the significant correlation (age vs retinal thickness) showed that the correlation remained significant (Table 4-4). Therefore, as age increases the overall retinal thickness values increase (Figure 4-9). The mean values of the overall foveal thickness increase with age from a mean thickness of 245.33µm for children (4-7 years) to 275.91 µm for adults (Table 4-5).

Table 4-5: Full retinal thickness values of the foveal area for each age group.

Age group	**Macular area**	**Mean (µm)**	**Range**	
			Minimum	**Maximum**
4-7 (n= 6)	Fovea	245.3	235	266
8-11 (n=9)	Fovea	270.1	244	320
12-15 (n=10)	Fovea	281.5	366	307
20-33 (n=11)	Fovea	275.9	255	302

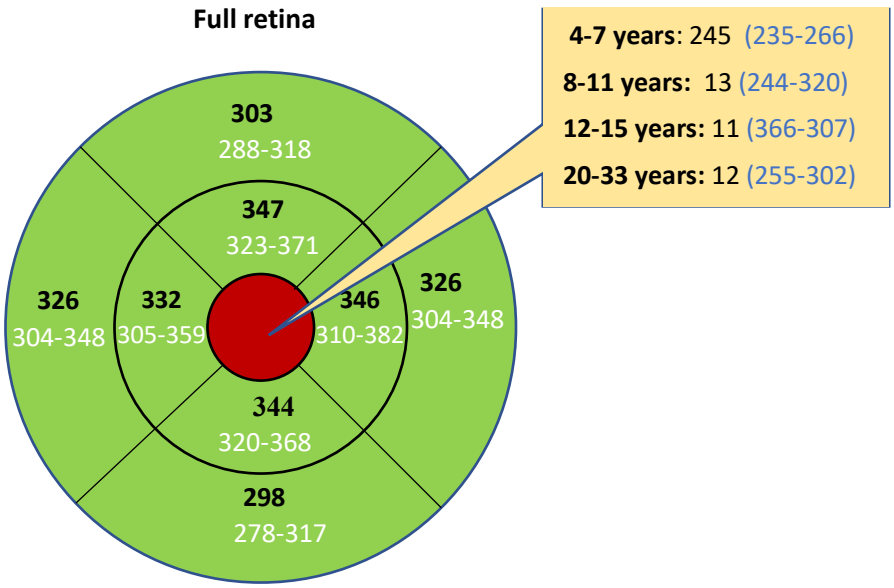

Figure 4-8: Early Treatment Diabetic Retinopathy study (ETDRS) thickness map for the full retinal thickness. The mean is given in black and the lower and upper 95% confidence intervals in white. The red area indicates areas where the retinal thickness did change with age while the green areas indicates retinal areas that do not change with age.

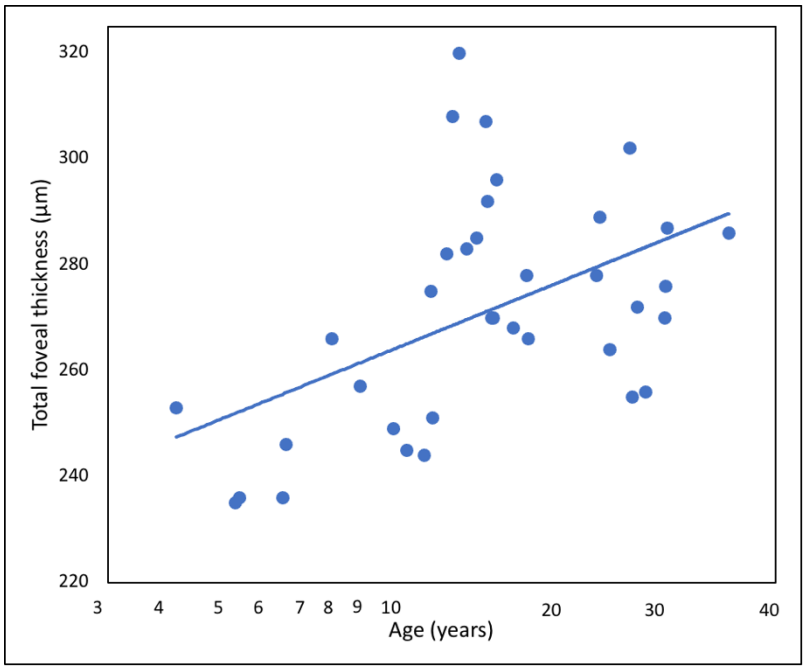

Figure 4-9: Scattergram of the overall foveal thickness against age. Each point represents the average foveal thickness for one participant. The regression line shown is: Thickness = 45.378 * Log(age) + 220.53, $r^2 = 0.24$, p=0.003.

4.5.3.2 Overall retinal thickness at the parafoveal and perifoveal areas

The results of the individual correlation analyses between age and overall retinal thickness of the parafoveal areas in the nasal, temporal and superior sectors suggested that the retinal thickness values were positively correlated with age (see Table 4.4). However, these correlations with age did not remain significant after using the adjusted Bonferroni (Table 4-4). There was no significant correlation between age and the retinal thickness values in the inferior sector.

The correlation analysis demonstrated no significant relationship between age and retinal thickness for any of the perifoveal sectors. Therefore, the retinal thickness values in the perifoveal area are unlikely to change with age. The mean and 95% confidence interval for the macular thickness values for each sector of the 3mm and 6mm diameter circles are indicated in Table 4-6.

Table 4-6: Full retinal thickness in the para and perifoveal region.

Age range (years)	**Retinal region**	**Mean overall retinal thickness (µm)**	**Standard Deviation**	**95% CI (1.96xSD)**	
				Lower limit	**Upper limit**
3.9-33.4	Temporal parafovea	332.8	13.8	305.7	359.9
3.9-33.4	Superior parafovea	347.8	12.2	323.9	371.7
3.9-33.4	Nasal parafovea	346.1	18.4	310.0	382.2
3.9-33.4	Inferior parafovea	344.2	12.30	320.1	368.3

3.9-33.4	Temporal perifovea	288.4	9.3	270.2	306.6
3.9-33.4	Superior perifovea	303.6	7.6	288.7	318.5
3.9-33.4	Nasal perifovea	326.3	11.3	304.2	348.4
3.9-33.4	Inferior perifovea	298.2	10.1	278.4	317.9

4.5.4 Inner retinal layers

The Shapiro-Wilk test showed that the inner retinal layer thickness values were normally distributed across all regions except RNFL measurements at the foveal, parafoveal and perifoveal areas.

4.5.4.1 Total inner retinal layer (IRL) thickness

The correlation results are shown in Table 4-7.

Table 4-7: Pearson correlation coefficient for the total inner retinal layer measurements in the foveal, para and perifoveal area with Log age. *= remains significant after adjusted Bonferroni.

Total inner retinal layers region	**r value**	**Unadjusted p value**	**α value for significance with adjusted Bonferonni**
fovea	0.490	0.002*	0.025
parafovea	0.369	0.027*	0.05
perifovea	0.042	0.807	NA

There was a significant positive correlation between age and total inner retinal layer thickness at the foveal ($r = 0.49$, $p= 0.002$) and parafoveal areas ($r = 0.37$, $p= 0.027$). Adjusted Bonferroni correction revealed that these correlations remained significant. These relationships can be seen in Figures 4-11 and 4-12, respectively. However, there was no significant correlation between age and overall inner retinal layers thickness values at the perifoveal area. While the mean thickness of the IRLs at foveal area was 156µm for young children (Table 4-8), it was 188µm for the adults (Table 4-8). Interestingly, the mean thickness of total IRLs at the fovea and parafovea increased initially in thickness until 12-15 years and did not increase further between 15 years and adults (Table 4-8 and Table 4-9, respectively).

Table 4-8: Total inner retinal layers thickness values of the foveal area for each age group.

Age group	**Macular area**	**Mean (µm)**	**Range**	
			Minimum	**Maximum**
4-7 (n= 6)	Fovea	156	143	182
8-11 (n=9)	Fovea	167	153	228
12-15 (n=10)	Fovea	189	178	221
20-33 (n=11)	Fovea	188	166	210

Table 4-9: Total inner retinal layers thickness values of the parafoveal area for each age group.

Age group	**Macular area**	**Mean (µm)**	**Range**	
			Minimum	**Maximum**
4-7 (n= 6)	Parafovea	248.7	233.0	267.7

8-11 (n=9)	Parafovea	262.4	243.0	282.0
12-15 (n=10)	Parafovea	267.3	252.2	281.0
20-33 (n=11)	Parafovea	264.9	254.7	278.2

Table 4-10: Total inner retinal layers thickness values in the perifoveal area.

Age range (years)	**Retinal region**	**Mean overall retinal thickness (µm)**	**Standard Deviation**	**95% CI (1.96xSD)**	
				Lower limit	**Upper limit**
3.9-33.4	Perifovea	342.7	13.6	333.3	352.1

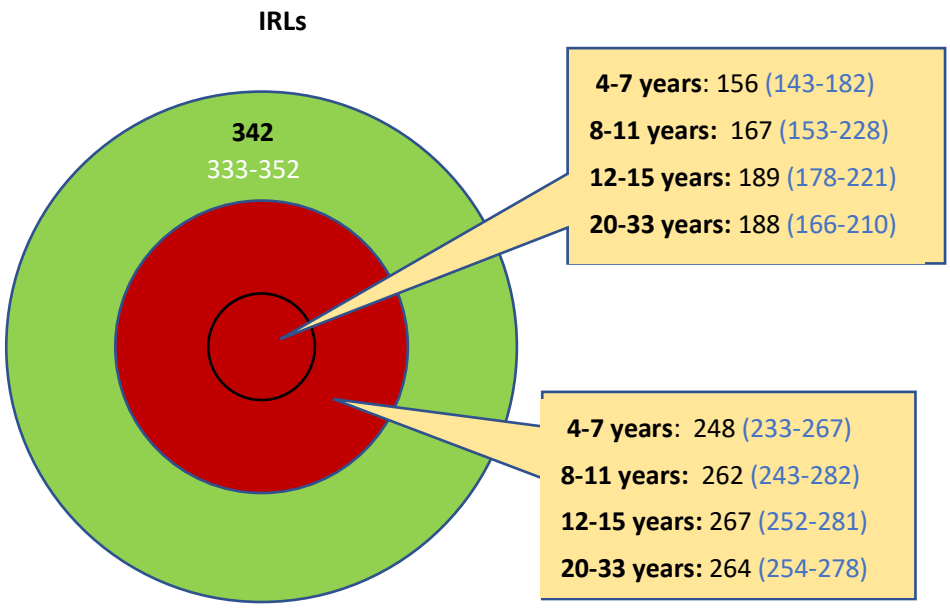

Figure 4-10: Early Treatment Diabetic Retinopathy study (ETDRS) thickness map for the total inner retinal layers (IRLs). The mean is given in black and the lower and upper 95% confidence intervals in white. The red area indicates areas where the retinal thickness did change with age while the green areas indicates retinal areas that do not change with age.

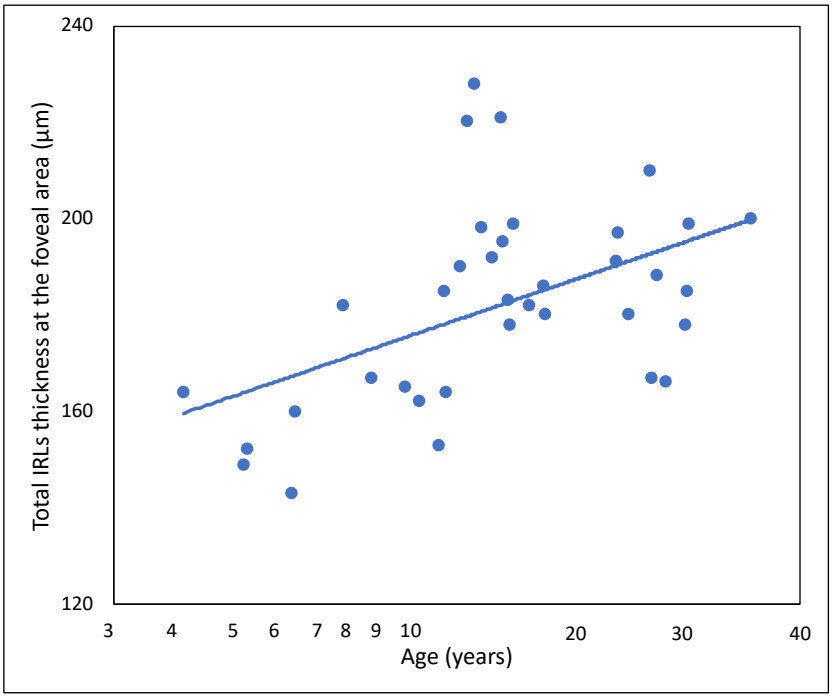

Figure 4-11: Scattergram of the total inner retinal layers thickness in the foveal area against age. Each point represents the average data for one participant. The regression line shown is: Thickness = 43.283 *Log(age) + 134.13, $r^2 = 0.24$, p=0.002.

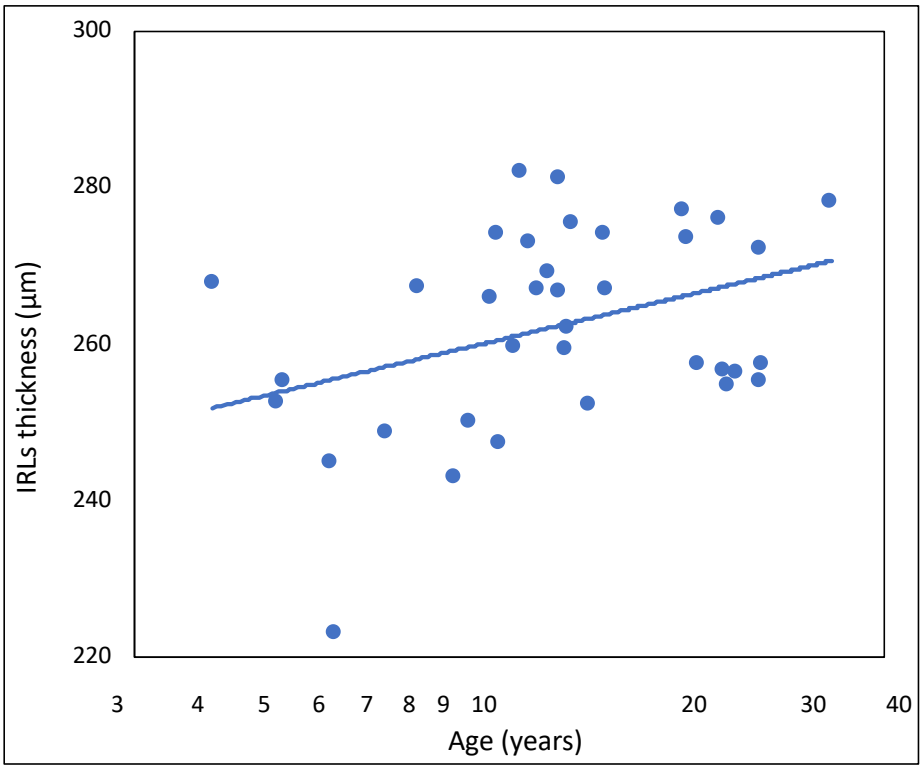

Figure 4-12: Scattergram of the total inner retinal layers thickness in the parafoveal area against age. Each point represents the average data for one participant. The regression line shown is: Thickness = 20.199 *Log(age) + 239.86, $r^2 = 0.13$, p=0.027.

4.5.4.2 Individual Inner Retinal layers

The correlation results are shown in Table 4-11.

Table 4-11: The correlation between the inner retinal layer measurements in the foveal, para and perifoveal areas with age. *= remains significant after adjusted Bonferroni.

Retinal region	r value	Unadjusted p value	α value for Adjusted Bonferroni
RNFL in the fovea	0.557	<0.001*	0.0055
IPL in the parafovea	0.495	0.002*	0.006
RNFL in the parafovea	0.474	0.004*	0.007
INL in the fovea	0.452	0.006*	0.008
IPL in the fovea	0.419	0.011	0.01
INL in the perifovea	-0.409	0.013	0.0125
GCL in the parafovea	0.408	0.014	0.0167
GCL in the perifovea	0.363	0.029	0.025
RNFL in the perifovea	0.343	0.041	0.05
IPL in the perifovea	0.099	0.564	NA
INL in the parafovea	0.053	0.761	NA
GCL in the fovea	-0.042	0.807	NA

The data for some inner retinal layer thickness values were not correlated with age, including the nerve fiber layer (RNFL) at the perifovea, ganglion cell layer (GCL) at all foveal regions, inner plexiform layer

(IPL) at the fovea and perifovea, and inner nuclear layer (INL) at the parafovea and perifovea, are summarized in Table 4-12.

Table 4-12: Inner retinal layer thicknesses for the fovea, parafovea and perifovea areas. Mean, standard deviation and 95% confidence limits are given for the normally distributed data. Medians, interquartile ranges, 2.5 and 97.5 percentiles are given. for data which was not normally distributed. RNFL= nerve fiber layer; GCL = ganglion cell layer; IPL = inner plexiform layer; INL = inner nuclear layer.

Age range	**Retinal area**	**Median (µm)**	**intra-quartile range**	**2.5 percentiles**	**97.5 percentiles**
3.9-33.4	RNFL at the perifoveal area	34.2	3.9	29.0	45.2
Age range (years)	**Retinal area**	**Mean thickness (µm)**	**St. Deviation**	**95%**	**CI (1.96xSD)**
				Lower limit	**Upper limit**
3.9-33.4	GCL at the foveal area	16.2	4.8	6.8	25.6
3.9-33.4	IPL at the foveal area	20.9	3.4	14.2	27.6
3.9-33.4	GCL at parafoveal area	52.7	3.8	45.2	60.1
3.9-33.4	INL at the parafoveal area	40.6	3.3	34.1	47.1
3.9-33.4	GCL at the perifoveal area	37.1	1.8	33.6	40.6
3.9-33.4	IPL at the perifoveal area	30.2	1.3	27.7	32.7
3.9-33.4	INL at the perifoveal area	34.2	3.3	27.7	40.7

Retinal nerve fiber layer (RNFL)

After adjusted Bonferroni, the correlation analysis showed that the RNFL thickness was significantly positively correlated with age at the fovea ($r = 0.557$, $p<0.001$) and parafovea ($r=0.474$, $p = 0.004$), but not at the perifoveal area. The RNFL thickness values at the foveal and parafoveal areas for each age group are shown in Tables 4-13 and 4-14. The mean and 95% confidence interval for the RNFL thickness for the perifoveal are shown in Table 4-12.

Table 4-13: RNFL thickness values in the foveal area for each age group.

Age group	**Macular area**	**Median (µm)**	**Range**	
			Minimum	**Maximum**
4-7 (n= 6)	Fovea	9	8	12
8-11 (n=9)	Fovea	13	11	14
12-15 (n=10)	Fovea	11	9	14
20-33 (n=11)	Fovea	12	10	15

Table 4-14: RNFL thickness values at the parafoveal area for each age group.

Age group	**Macular area**	**Median (µm)**	**Range**	
			Minimum	**Maximum**
4-7 (n= 6)	Parafovea	18.8	18.2	20.7
8-11 (n=9)	parafovea	19.5	18.7	24.5

12-15 (n=10)	Parafovea	20	18.2	22.5
20-33 (n=11)	Parafovea	21	18.0	25

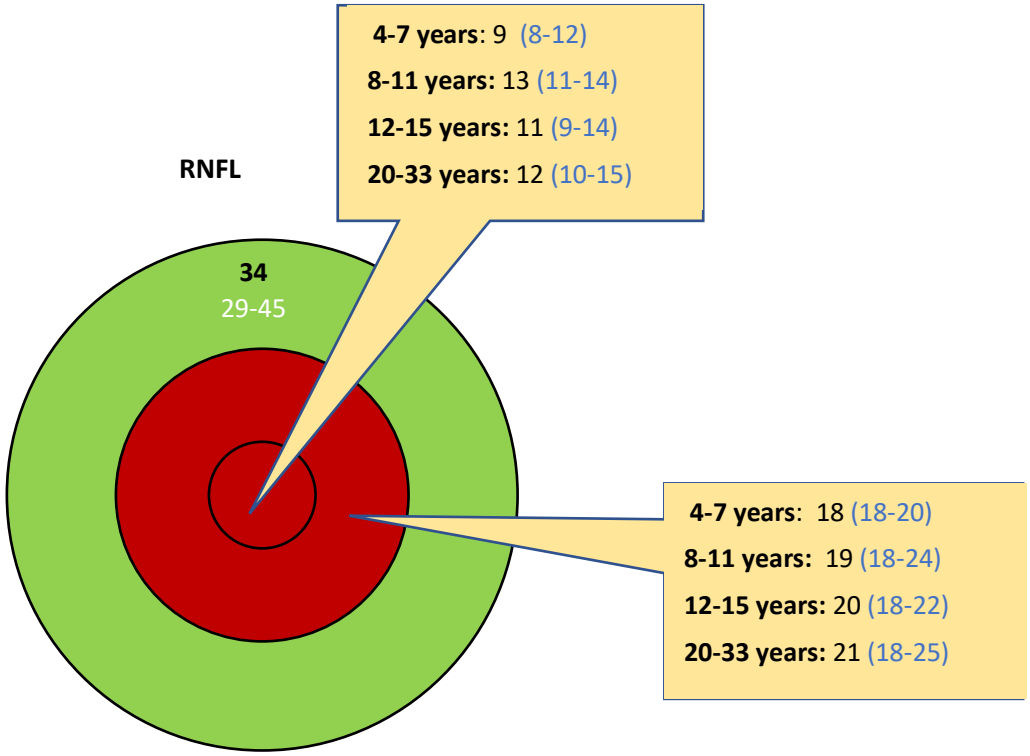

Figure 4-13: Early Treatment Diabetic Retinopathy Study (ETDRS) thickness map for the nerve fiber layer (RNFL). The median is given in black and the 2.5% and 97.5% in white. The red area indicates areas where the retinal thickness did change with age while the green areas indicates retinal areas that do not change with age.

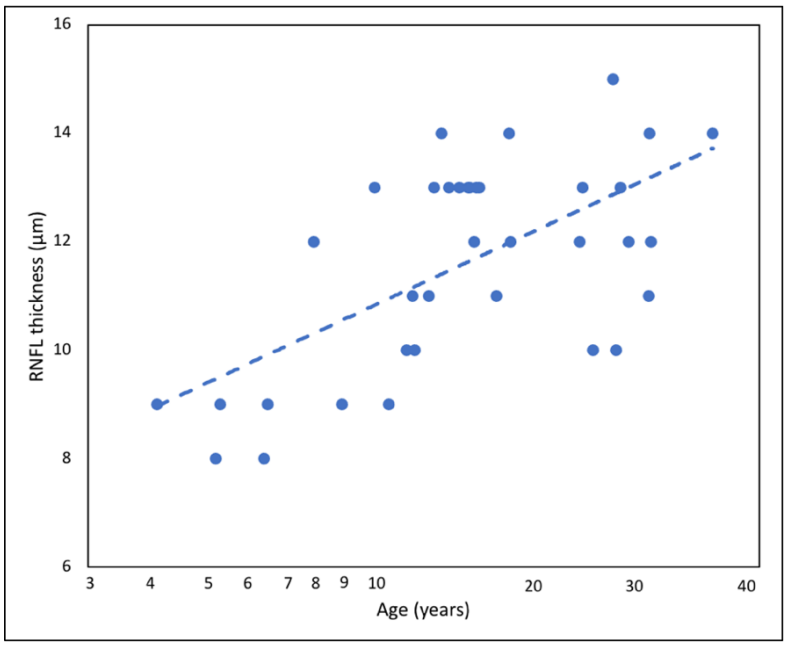

Figure 4-14: Scattergram of the RNFL thickness at the foveal area against age. Each point represents the average data for one participant. The dashed linear regression line is representative of the trend although rank correlation was used for this non-normally distributed data.

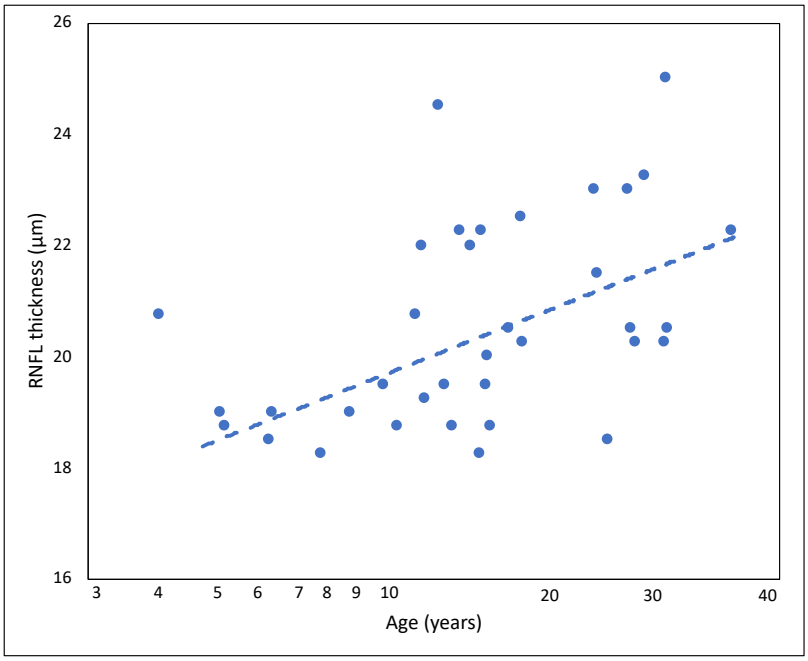

Figure 4-15: Scattergram of the RNFL thickness at the parafoveal area against age. Each point represents the average data for one participant. The dashed linear regression line is representative of the trend although rank correlation was used for this non-normally distributed data.

Ganglion cell layer thickness

The results of the correlation analysis with the adjusted Bonferroni correction revealed that the GCL thickness at the fovea, perifoveal and parafovea were not significantly correlated with age. However, it is noteworthy that the correlations with age at the parafovea and perifovea were borderline significant with the adjusted Bonferroni. The mean and 95% confidence interval for the GCL thickness values are shown in Table 4-12.

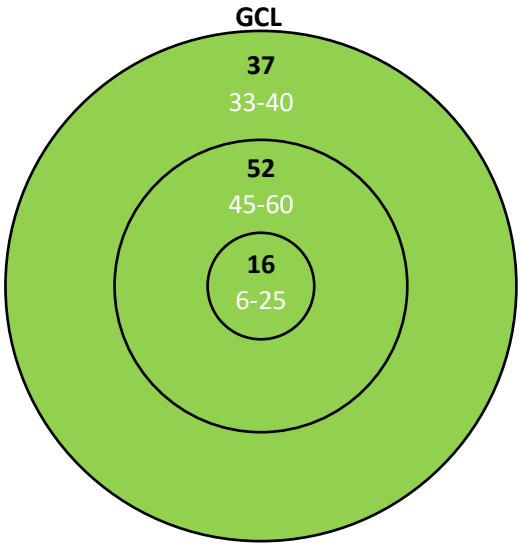

Figure 4-16: Early Treatment Diabetic Retinopathy study (ETDRS) thickness map for the ganglion cell layer (GCL). The mean is given in black and the lower and upper 95% confidence intervals in white. The green areas indicate retinal areas that do not change with age.

Inner plexiform layers

The results of the correlation analysis with the adjusted Bonferroni correction revealed a significant positive correlation between age and the IPL thickness values in the parafovea ($r = 0.495$, $p = 0.002$) (Figure 4-18 and Table 4-15). However, the correlation analysis showed no change with age in the IPL thickness values in the fovea and perifoveal areas (Table 4-11). The mean and 95% confidence interval for the IPL thickness values in the fovea and perifoveal areas are indicated in Table 4-12. Table 4-15 shows that the mean thickness of the IPL in the parafoveal area increased from 39.2µm for younger children to 43.6 during adulthood. It is noteworthy that the correlation with age at the fovea was borderline significant with the adjusted Bonferroni.

Table 4-15: IPL thickness values in the parafoveal area for each age group.

Age group	**Macular area**	**Mean (µm)**	**Range**	
			Minimum	**Maximum**
4-7 (n= 6)	parafovea	39.2	34	41.3
8-11 (n=9)	parafovea	42.0	38.5	47.5
12-15 (n=10)	Parafovea	44.0	40	46
20-33(n=11)	parafovea	43.6	40	48.8

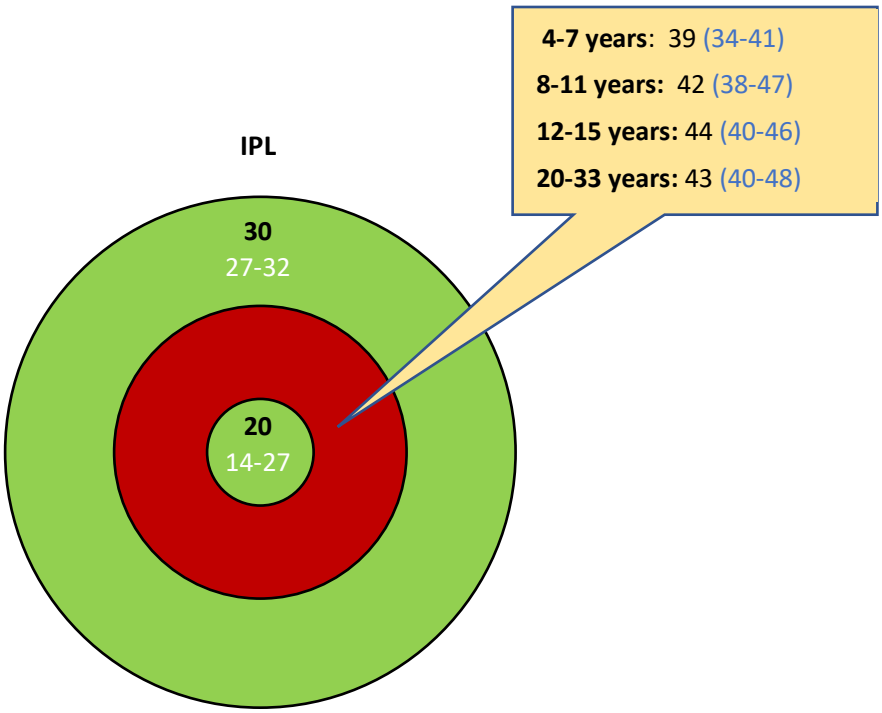

Figure 4-17: Early Treatment Diabetic Retinopathy study (ETDRS) thickness map for the inner plexiform layer (IPL). The mean is given in black and the lower and upper 95% confidence intervals in white. The red area indicates areas where the retinal thickness did change with age while the green areas indicates retinal areas that do not change with age.

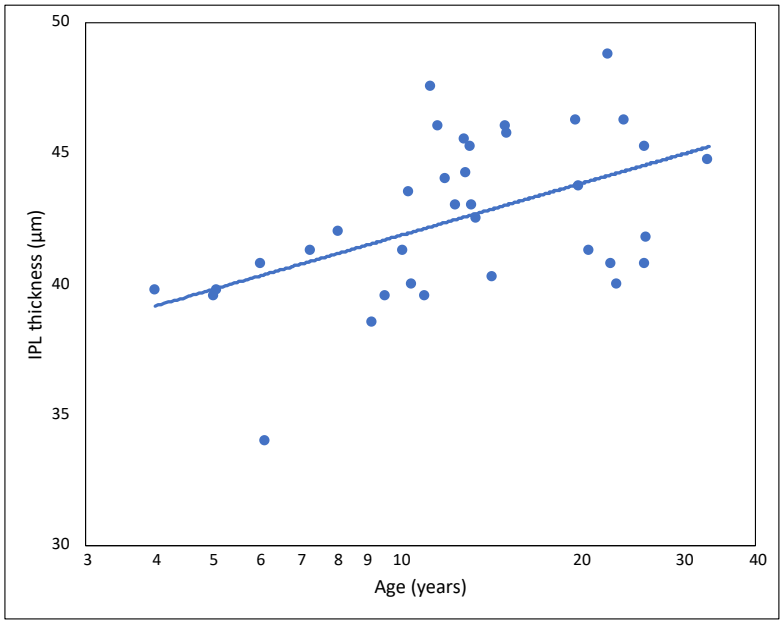

Figure 4-18: Scattergram of the IPL thickness at the parafoveal area against age. Each point represents the average data for one participant. Each point represents the average data for one participant. The regression line shown is: Thickness = 6.54 *Log(age) + 35.287, $r^2 = 0.24$, p=0.002.

Inner nuclear layer

The results of the correlation analysis after the adjusted Bonferroni correction revealed a significant positive correlation between age and INL thickness in the foveal area ($r = 0.45$, $p = 0.006$). However, neither the correlation of the INL in the parafovea nor in the perifovea was significant. The mean and 95% confidence interval for the INL thickness values in the para and perifovea are shown in Table 4-12. Table 4-16 shows that the average value of the INL at the foveal area for younger children was 12.8µm which increased to 18.11µm for the intermediate age group of children before it reached approximately 19µm for older children and adults. It is noteworthy that the correlations with age at the perifovea was borderline significant with the adjusted Bonferroni.

Table 4-16: Mean, and range values of INL thickness values at the fovea for each group.

Age group	**Macular area**	**Mean (µm)**	**Range**	
			Minimum	**Maximum**
4-7 (n= 6)	Fovea	12.8	11	16
8-11 (n=9)	Fovea	18.1	12	27
12-15 (n=10)	Fovea	19.4	15	24
20-33 (n=11)	Fovea	19.0	12	28

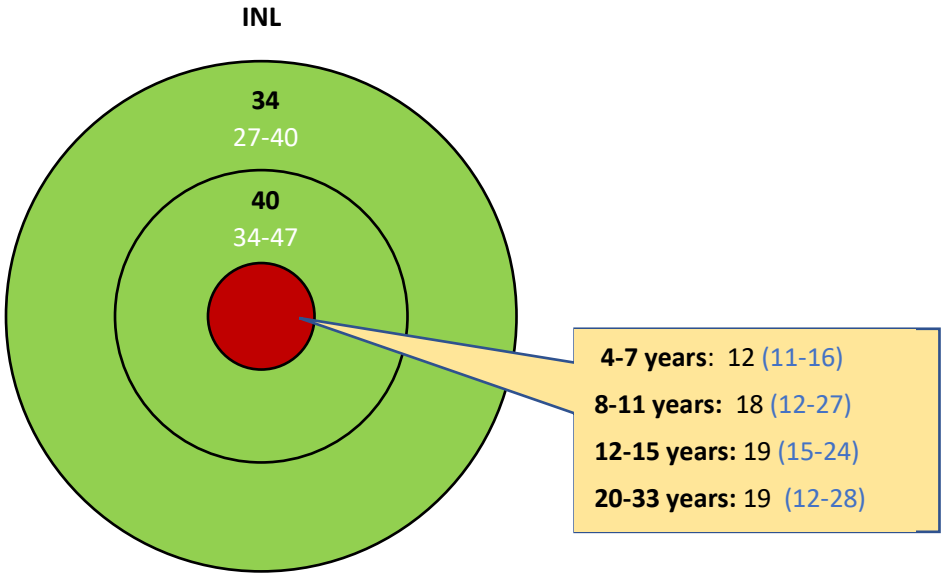

Figure 4-19: Early Treatment Diabetic Retinopathy study (ETDRS) thickness map for the inner nuclear layer (INL). The mean is given in black and the lower and upper 95% confidence intervals in white. The red area indicates areas where the retinal thickness did change with age while the green areas indicates retinal areas that do not change with age.

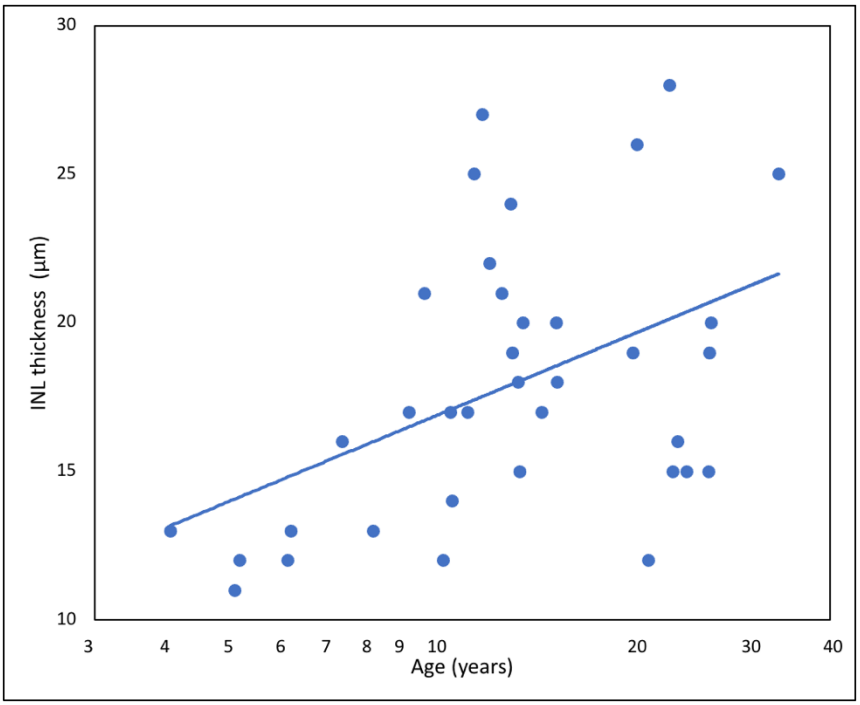

Figure 4-20: Scattergram of the INL thickness in the foveal area against age. Each point represents the average data for one participant. Age in Log 10 scale. The regression line shown is: Thickness = 9.1076 *Log(age) + 7.7759, $r^2 = 0.20$, p=0.006.

4.5.5 Outer retinal layers

The Shapiro-Wilk test showed that the outer retinal layers thickness values were normally distributed across all regions.

4.5.5.1 Overall outer retinal layers

The correlation results are shown in Table 4-17

Table 4-17: Pearson correlation coefficient for the total outer retinal layer measurements in the foveal, para and perifoveal area with age.

Total outer retinal layers region	r value	p value
fovea	0.14	0.41
parafovea	0.29	0.08
perifovea	0.11	0.52

The results of the correlation analysis failed to demonstrate any change with age in the overall outer retinal thickness measurements in any of the areas. Therefore, the overall outer retinal layers thickness values are unlikely to be influenced by age (Table 4-17).

The mean estimates for the outer retinal layer thickness values in the foveal, parafoveal, and perifoveal areas are summarized in Table 4-18.

Table 4-18: Total outer retinal layer thickness values in the foveal, parafoveal and perifoveal areas.

Age range (years)	Retinal area	Mean thickness (µm)	St. Deviation	95% CI (1.96xSD)	
				Lower limit	Upper limit
3.9-33.4	Total outer retinal layers at the fovea	88.9	3.7	81.6	96.2
3.9-33.4	Total outer retinal layers in the parafovea	80.5	2.0	76.6	84.4
3.9-33.4	Total outer retinal layers in the perifovea	77.7	2.3	73.2	82.2

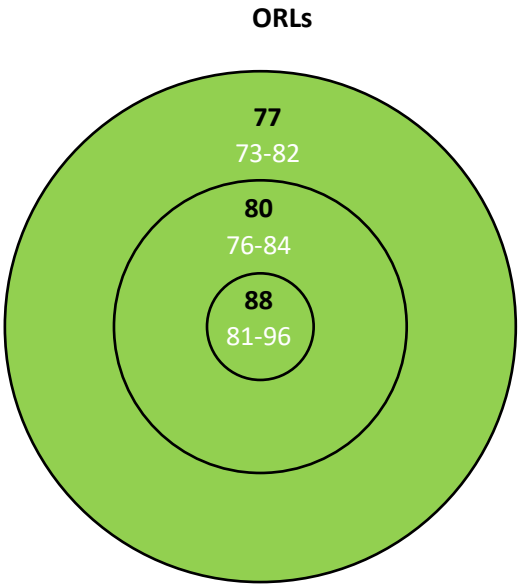

Figure 4-21: Early Treatment Diabetic Retinopathy study (ETDRS) thickness map for the outer retinal layers (ORLs). The mean is given in black and the lower and upper 95% confidence intervals in white. The green areas indicate retinal areas that do not change with age.

4.5.5.2 Individual outer retinal layers

The correlation results are shown in Table 4-19.

Table 4-19: Pearson correlation coefficient for the outer retinal layer measurements in the foveal, para and perifoveal areas with age. *= remains significant after adjusted Bonferroni.

Retinal region	r value	p value	α value for adjusted Bonferroni
OPL in the parafovea	- 0.394	0.017*	0.025
RPE in the fovea	0.387	0.020*	0.05
ONL in the fovea	0.301	0.075	NA
RPE in the parafovea	0.301	0.075	NA
OPL in the perifovea	-0.257	0.130	NA
ONL in the parafovea	0.227	0.184	NA
OPL in the fovea	0.213	0.212	NA
RPE in the perifovea	0.076	0.697	NA
ONL in perifovea	0.023	0.893	NA

The mean estimates for some outer retinal layers thickness values including the outer plexiform layer (OPL) at the fovea and perifovea, the outer nuclear layer (ONL) in all foveal areas, and retinal pigment epithelium layer (RPE) at the parafovea and perifovea are summarized in Table 4-20.

Table 4-20: Thickness for outer retinal layers in the foveal, parafoveal and perifoveal areas including OPL, ONL and RPE. OPL = outer plexiform layer; ONL = outer nuclear layer; RPE = retinal pigment epithelium.

Age range (years)	Retinal area	Mean thickness (µm)	St. Deviation	95% CI (1.96xSD)	
				Lower limit	Upper limit
3.9-33.4	OPL at the fovea	25.4	4.0	17.6	33.2
3.9-33.4	ONL at the fovea	90.4	8.3	74.1	106.6
3.9-33.4	ONL in the parafovea	72.7	7.1	58.8	86.6
3.9-33.4	RPE in the parafovea	14.1	1.1	11.9	16.3
3.9-33.4	OPL in the perifovea	27.1	1.5	24.2	30.0
3.9-33.4	ONL in the perifovea	62.4	7.1	48.9	76.3
3.9-33.4	RPE in the perifovea	12.9	1.1	10.8	15.1

Outer plexiform layer

There was no significant correlation between macular thickness values and age in the foveal and perifoveal areas (Table 4-19). However, the retinal thickness in the parafoveal area was significantly negatively correlated with age ($r = -0.394$, $p = 0.017$) (Figure 4-23). Thus, as age increases the OPL thickness decreases. The thickness values for the OPL in the parafoveal area for each age group are indicated in Table 4-21.

Table 4-21: Mean, and range values of OPL thickness measurements at the parafoveal area for each age group.

Age group	Macular area	Mean (um)	Range	
			Minimum	Maximum
4-7 (n= 6)	parafovea	34.8	33.2	36.0
8-11 (n=9)	parafovea	33.4	30.3	37.2
12-15 (n=10)	parafovea	33.6	28	39.2
20-33 (n=11)	Parafovea	31.2	27.7	36.7

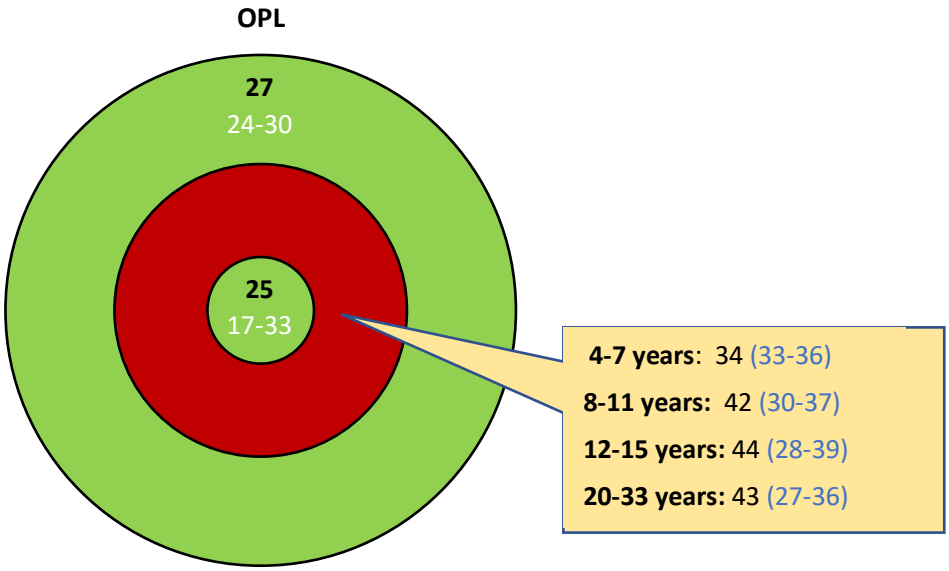

Figure 4-22: Early Treatment Diabetic Retinopathy study (ETDRS) thickness map for the outer plexiform layer (OPL). The mean is given in black and the lower and upper 95% confidence intervals in white. The red area indicates areas where the retinal thickness did change with age while the green areas indicates retinal areas that do not change with age.

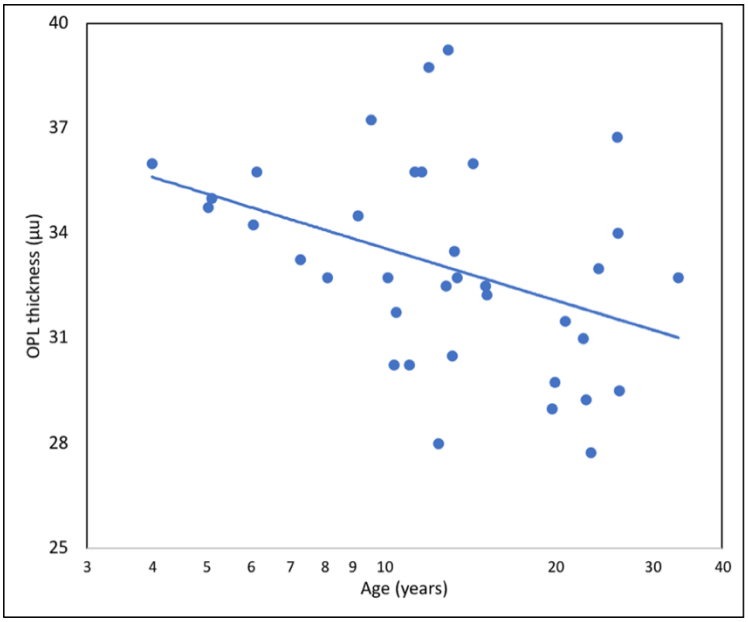

Figure 4-23: Scattergram of the OPL thickness at the parafoveal area against age. Each point represents the average data for one participant. The regression line shown is: Thickness = - 4.958 *Log(age) +38.532, $r^2 = 0.15$, p=0.006.

Outer nuclear layer

The results of the correlation analysis failed to demonstrate any change in thickness according to age in any of the areas (Table 4-19). Therefore, the outer nuclear thickness measurements are unlikely to be influenced by age.

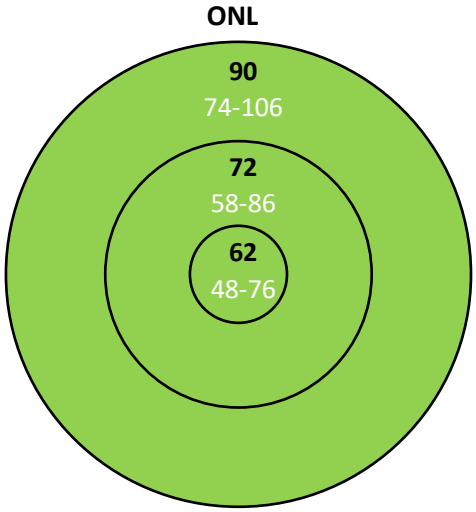

Figure 4-24: Early Treatment Diabetic Retinopathy study (ETDRS) thickness map for the outer nuclear layer (ONL). The mean is given in black and the lower and upper 95% confidence intervals in white. The green areas indicate retinal areas that do not change with age.

Retinal pigment epithelium layer

There was a significant positive correlation between the macular RPE thickness values in the foveal area and age (r = 0.387, p = 0.020) (Figure 4-26). Therefore, as the age increases the RPE thickness values increase (Table 4-22). However, the RPE thickness was not significantly correlated with age in the parafoveal and perifoveal and the normative values are shown in Table 4-20.

Table 4-22: RPE thickness at the foveal area for each group.

Age group	Macular area	Mean (µm)	Range	
			Minimum	Maximum
4-7 (n= 6)	Fovea	15	12	17
8-11 (n=9)	Fovea	17.1	15	20
12-15 (n=10)	Fovea	17	16	19
20-33 (n=11)	Fovea	17.2	15	20

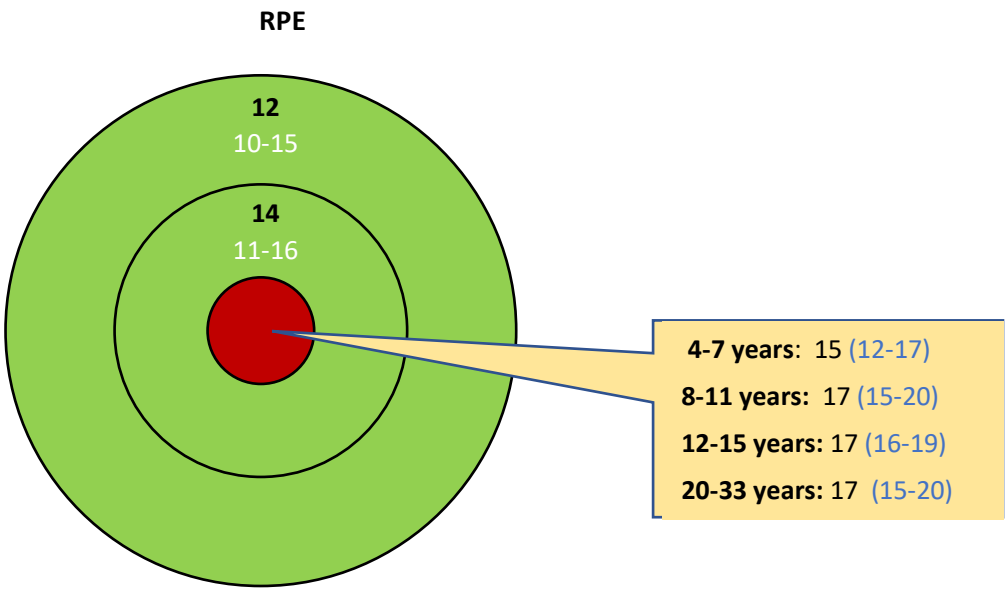

Figure 4-25: Early Treatment Diabetic Retinopathy study (ETDRS) thickness map for the retinal pigment epithelium layer (RPE). The mean is given in black and the lower and upper 95% confidence intervals in white. The red area indicates areas where the retinal thickness did change with age while the green areas indicates retinal areas that do not change with age.

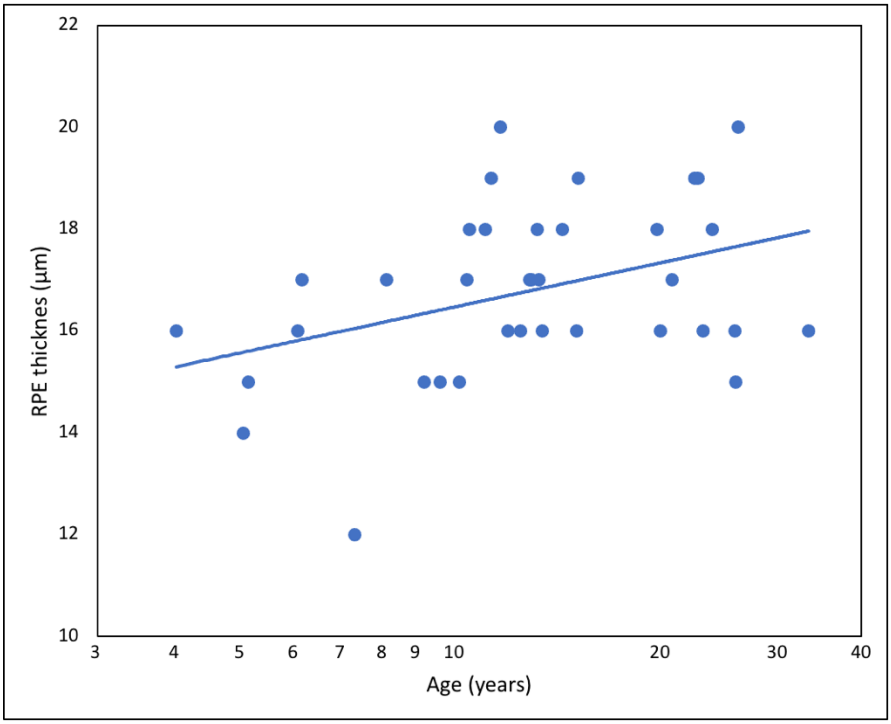

Figure 4-26: Scattergram of the RPE thickness in the foveal area against age. Each point represents the average data for one participant. The regression line shown is: Thickness = 2.8563 *Log(age) + 13.606, r^2 = 0.14, p=0.020.

4.6 Discussion

Spectral-domain optical coherence tomography (SD-OCT) is increasingly being used as an early diagnostic indicator to assess and monitor the progression of ocular disorders that may affect the pediatric retina, including genetic disorders such as retinitis pigmentosa. Its applicability among pediatric patients is due to its short acquisition time and eye-tracking system that enables a high-quality scan (with SNRs > 20 dB) from children as young as four years of age. Nevertheless, for the scan to be most beneficial for monitoring retinal disorders, quantitative measurements from the pediatric population have to be compared to an age-matched database. Currently, the manufacture's normative values are only available for individuals older than 18 years, and it may not be appropriate to compare children's findings with the normative values in the standard dataset. On examining the literature, most studies which used SD-OCT have focused on documenting a pediatric reference database for overall retinal thickness and peripapillary RNFL thickness. Therefore, a comprehensive pediatric normative dataset documenting ETDRS thickness map measurements for each retinal sublayer is still lacking. The main purpose of the study was to provide a pediatric normative dataset of ETDRS thickness maps measurements for each of the seven layers that are automatically generated by SD-OCT (Heidelberg Spectral is, Eye Explorer software version 1.9.10.0). Since thickness values may be affected by levels of pigmentation, the additional purpose was to provide reference values for each sector of the peripapillary RNFL thickness in healthy children of European descent. Data from children of other ethnicities would be added later. The findings of the present study revealed that overall retinal thickness, several retinal sublayers, and the nasal superior sector of the RNFL thickness are influenced by age.

4.6.1 Nerve fiber layer scan

The majority of peripapillary RNFL studies with OCT have been performed in the adult population, and only a few studies have been reported on children[81,82]. Consequently, some degree of uncertainty exists as to when peripapillary RNFL thickness becomes adult-like. This uncertainty is partly due to the variations in methods and distribution of the samples that have influenced the studies' outcomes. For instance, a variety of OCT techniques (TD-OCT vs. SD-OCT) were used, and some used the standard protocol while others used the fast scan protocol. Knight et al. reported that the RNFL thickness measurement acquired by TD-OCT yields relatively thicker values compared to SD-OCT, and differences might also occur between different versions of SD-OCT instruments[88]. Therefore, thickness values may vary depending on the OCT model used. Previous adult studies found that the average peripapillary RNFL thickness varies between 85 and 150μ and such thickness decreases with age[100–102]. Available RNFL studies with children vary in their conclusions about the effect of age on the peripapillary RNFL thickness. Some studies documented a significant positive relationship with age[82,83] while the majority of studies documented that the RNFL thickness is not influenced by age[85,103,107]. However, those studies that found the RNFL is influenced by age, reported a weak relationship, indicating that age has a limited effect in the child population. Using TD-OCT, Huynh et al.[85] documented the largest population-based study in six-year-old Australian children of mixed ethnicity, and they found that the average global RNFL thickness was 104μm. In another TD-OCT study performed by Samarawickrama et al.[136] the global RNFL thickness was found to be 104.5μm. Turk et al.[99] conducted the first peripapillary RNFL thickness study using SD-OCT on Turkish children and reported the global RNFL thickness as 106.45μm. In an SD-OCT study on North American children, Yanni et al.[103] reported the global RNFL thickness as 107.6μm.

Recently, Turan et a.l[137] found that the average global RNFL thickness among Turkish children aged from 8 to 11 years was 98.75µm. In accordance with the previously reported studies, we found that the effect of age on RNFL thickness was limited, and the 95% overlap with adults' values reached 104µm for the global sector. However, the present study results indicated a weak negative correlation between age and thickness in the nasal superior quadrant, suggesting that the RNFL in the nasal superior sector thins during childhood, whereas the other sectors do not change significantly. Previous SD-OCT studies have reported the average RNFL thickness in the NS sector for children (5-15 years) to vary between 104 to 116µm, which is significantly lower than 139µm reported in the present study for children aged between 4 to 7 years. This correlation between age and nasal superior quadrant needs to be studied further with a larger sample size to determine with certainty the developmental pattern of the RNFL NS sector with age.

4.6.2 Macular cube

Previous studies have reported the total retinal thickness in the foveal area (central macular thickness) within 1mm diameter of the ETDRS thickness maps using both SD-and TD OCTs. Using TD-OCT, Samarawickrama et al.[136] found that the average central macular thickness (CMT) was 192.5µm for six-year-old children compared to 197.5µm for older children (12 years). In a study by El-Dair et al.[86] using TD-OCT the CMT was found to be 198µm for eight-year-old children. Turk et al.[99] used SD-OCT and found that CMT was 211.39µm for children age between 6 and 16 years, which is comparable to the finding reported by Yanni et al[103] (271.2µm) for children aged between 5 and 15 years. Varied conclusions have been suggested about the effect of age on the CMT in the pediatric population. Turk et al. reported that CMT was not significantly correlated with age, whereas Yanni et al. found that the average CMT was

significantly positively correlated with age. Similarly, Barrio-Barrio et al.[138] and Turanan et al.[137] found that CMT was significantly positively correlated with age. In accordance with the previously reported studies, the present study found the CMT was significantly positively correlated with age so that the average CMT for children (4-7 years) was 245.3µm, considerably lower than 270µm observed for children aged from 8 to 11 years and 275.9µm for adults (Table 4-5). A recent adult study using similar techniques to acquire retinal thickness measurements among the white adult population aged from 20 to 74 years[139] is in agreement. The study found the average CMT was 280µm, which is significantly higher than 245µm for children aged between 4-7 years and comparable to adult values (275.91µm) reported in the present study. This developmental trend agrees with previously reported histological studies[3,9] indicating continued maturation of the fovea beyond four years of age.

The present study results indicated that the overall inner retinal thickness at the foveal and parafoveal areas significantly increased with age. The average thickness of the foveal area is within the lower range of the adult values by 8-11 years of age, reaching an average macular thickness of 167µm (Table 4-8). A similar developmental trend was observed in the parafovea, such that the average thickness values for younger children (4-7 years) was 250µm and the average thickness in the parafovea entered the lower range of the adult value by 8 to 11 years approaching thickness values of 265.75µm (Table 4-9). Of note, available child SD-OCT studies have not reported the total thickness of the inner retinal layers (IRLs) in the foveal and parafoveal areas as reported in the present study. Therefore, a direct comparison with the existing studies is not possible. Using a hand-held OCT, Maldonado et al.[78] documented that the total IRL thickness in the foveal area for children (2-15 years) was 10µm. Similarly, Lee et al.[77] used a

hand-held OCT and found that the average IRL thickness values for children aged between 4 to 6 years to range between 7.93 and 11μm in the foveal area and 17-19μm at the parafoveal area. These differences between the present study results and previously published studies could be attributed to the algorithm used to obtain retinal thickness values. Each OCT instrument may use a different built-in algorithm that generates different numeric values depending on the ability of the software to identify sub-retinal layers and calculate retinal thickness. Additionally, in the study conducted by Lee et al., the para and perifovea were defined as 2mm and 4mm in diameter respectively. Similarly, Maldonado et al. defined the parafoveal area as a distance measured at 1mm away from the foveal center (2mm in diameter). In contrast, in the present study, we used ETDRS thickness maps to acquire retinal thickness measurements. The center ring is 1mm in diameter and defined as fovea, the middle ring is 3mm in diameter (parafovea), and the outer ring was 6mm in diameter (perifovea). Therefore, the studies described above measured the IRL thickness values at a distance closer to the foveal center where the IRLs are fused into a single layer owing to the migration of the IRLs away from the fovea. Thus, they reported considerably lower thickness values than the present study.

The effect of aging on the individual inner retinal layers has been previously explored using hand-held and SD- OCTs with controversial findings, including no correlation[103] or not measurable at the fovea[77,78]. However, a recent study has documented a specific developmental trajectory of each retinal layer using a hand-held OCT. In particular, in a cohort of more than 261 child participants, Lee et al[77] found that the centrifugal displacement of the retinal layers is complete by 17.5 months. The outward displacement of the GCL from the fovea reaches 95% of normal adult values by 10.6 months, whereas the IPL and INL reach mature thickness levels by

18.7 and 17.6 months, respectively. In contrast, the parafoveal and perifoveal areas' developmental pattern reached maturity by 31.4 and 39 months for the RNFL and IPL, respectively[77]. The GCL and INL reach 95% of the adult values by 65- and 41-months, respectively. In another hand-held OCT study, Maldonado et al. concluded that the inner retinal layers are not measurable or barely detectable in the foveal area for children aged between 2-15 years and for adults. Similarly, Yanni et al. using SD-OCT, found that the inner retinal layers are not measurable in the foveal area, and the thickness measurements of the inner retinal layers in the parafoveal area are not significantly influenced by age for children aged between 5-15 years. The results of the present study do not agree with these previously reported findings. Unlike the previous studies where custom segmentation software was used to obtain retinal thickness measurements, we used the automatic segmentation software provided by the OCT instrument and found that the inner retinal layers in the foveal area are measurable according to the ETDRS thickness map, which is in agreement with Invernizzi et al.[139] in another previously reported adult study.

We found that the RNFL in the foveal area is immature for children aged between 4-7 years and the mean value of the foveal RNFL thickness enters the lower range of adult values by 8-11 years. Despite the positive correlation between age and RNFL thickness at the middle ring (parafovea), the median RNFL thickness for younger children (4-7) was within the lower limit of adult values. When comparing our findings with a previously reported adult study[139], we found that the average foveal thickness of the RNFL in the previous study was 12.8µm, which is slightly higher than 9µm for children (4-7years) and comparable to adult values (12µm) reported in the present study. However, the median RNFL thickness values at the parafoveal area for

younger children (4-7) reported in the present study (21µm) were comparable to those reported in an adult study[139] (23µm).

In agreement with the previously reported studies[77,103], we did not find any evidence of a further maturation of the GCL beyond four years of age. This is also in a good agreement with previously reported histological findings[2,3] indicating that the GCL may be considered mature by 3.8 years.

Significant positive correlations between age and the thickness of the inner plexiform layer in the parafoveal area, as well as of the inner nuclear layer thickness (foveal area) were also observed. These findings do not agree with Lee et al. who report that the IPL and INL were considered mature by 18 and 17 months, respectively at the foveal area and by 39- and 41-months at the parafoveal area, respectively. Similarly, Yanni et al., found that the IPL and INL thicknesses were not influenced by age. These differences between the present study results and the previously published findings could be due to the variety of the techniques used to acquire retinal thickness measurements. Additionally, available studies used different age ranges to calculate retinal thickness measurement. For instance, in the study by Yanni et al., a mean thickness measurement of 45µm for the inner plexiform at the parafoveal area was reported for children aged between 5-15 years. In the present study, we divided this age range into three separate groups and acquired mean inner plexiform layer thickness measurements of 39.16µm for younger children (4-7 years), 41.97µm of intermediate age (8-11 years), and 43.95µm for older children (12-15 years).

The results of the present study showed that the thickness values of the outer nuclear layer (ONL) were not influenced by age at the foveal, parafoveal, and perifoveal areas, which is inconsistent with the findings reported by Yanni et al. The present study's findings do not agree with findings documented by Lee et al. In their study they used the hand-held OCT and concluded that the development of the ONL at the perifoveal area might continue beyond 12 years of age. Similarly, histological studies suggested that the thickness of the ONL increases with time (until approximately 13 years) as the cone outer segments continue to become tightly packed at the center of the fovea. This, as well as the elongation of the photoreceptor axons, makes the foveal ONL become thicker with time reaching maturity by 13 years of age. However, this developmental pattern was not observed in the present study, likely due to the lack of sensitivity of the currently used OCT to detect small changes of single cells. Additionally, the terms para and perifovea were defined differently in the present study and previously reported hand-held OCT studies[77,78]. Finally, the fact that Lee et al. reported the immaturity of the ONL in the perifovea and not in the foveal area might indicate the limitation of the OCT instruments to detect small changes of single cells. For instance, histological studies have shown that the ONL in the foveal pit is formed of a single layer of cone cell bodies at birth, and it continues to increase in thickness with time in the foveal center reaching adult-like values by 13 years of age as the foveal cone cell bodies are packed 12 cells deep[3,9]. This developmental change means that the ONL changes from a single layer of cones at birth to approximately 12 cone cell bodies deep by 13 years of age and these changes at the level of individual cells may be too small for the resolution of current OCT instruments and are not included in the OCT segmentation, and so have not been reported in OCT studies.

A significant correlation between age and the outer plexiform layer (OPL) thickness was observed in the present study. The average thickness of the OPL approached the lower limit of the adult values by 8-11 years of age, with an average mean thickness reaching 33.44µm. In comparison, Yanni et al. did not report the thickness measurements for the OPL, while Lee et al. concluded that there was no evidence of a plateau in the development of OPL in the temporal parafovea, and the OPL on the nasal side reached maturity by 11.6 months. When comparing our findings with a previously reported adult study[139], the present study found that the average thickness of the OPL was 33.1µm for the white adult population. This finding is comparable to the OPL thickness measurements for children aged 8-11 with an average thickness approaching 33.4µm and significantly higher than the 24µm for younger children (4-7 years) reported in this study. Therefore, the OPL thickness in the parafoveal area may not be mature for children 4-7 years and is likely to be adult-like by 8-11 years.

It is known that RPE metabolism is significantly influenced by age. The content of the RPE lipofuscin increases with age owing to the shedding of photoreceptor outer segments[140] as well as the accumulation of extracellular basal deposits within the RPE and Bruch's membrane[141]. Both of these changes are likely to cause a considerable thickening of the RPE with time. In agreement with the above-described studies, we found that the retinal pigment epithelium (RPE) thickness in the foveal area was significantly influenced by age. Nevertheless, Yanni et al. documented that the RPE was not affected by age for children aged between 5-15 years and Lee et al. found that the RPE thickness reaches maturity by 54 months (4.5 years).

The main limitation of the present study is that the sample size was not sufficient to determine with certainty the developmental trajectory of the retinal layers. Therefore, we are unable to determine the age at which the retinal layers reach maturity.

Another limitation of the present study is that the automatic segmentation software provided by the SD-OCT does not provide the thickness measurements for the photoreceptor's inner and outer segments. Therefore, we are unable to test whether the present study results would agree with the previous SD-OCT findings reported by Yanni et al. who found that children have approximately 36% thinner outer segment compared to adults.

Another limitation of the study is that the axial length was not measured. Nevertheless, the axial has a limited effect on retinal thickness values. All the participants in the present study had normal visual acuity and refractive error for their age, so that they are unlikely to have an atypical axial length.

In conclusion: the present study provides a pediatric normative dataset of ETDRS thickness map measurements for each of the seven layers that were automatically generated by SD-OCT as well as reference values for each sector of the peripapillary RNFL thickness in children of European descent. The thickness measurements of certain retinal layers were influenced by age. Overall, the findings of the present study suggest that both the inner and outer retinal layers were influenced by age over the ages 4 years to adulthood except for the ganglion cells layer and outer nuclear layer. This developmental trend appears primarily driven by younger children as the average thickness values of other age groups appear comparable and are considerably different

from the younger children. Therefore, the development of the retinal layers may not be mature for younger children (4-7 years) and is likely to become adult-like by 8-11 years old. Clinicians can compare their clinical measurements with the expected central retinal thickness measurements norms for each age range provided herein. Future studies with a larger sample size, wider age range and other ethnicities are needed in order to have more accurate pediatric reference data to easily detect disease processes that may affect the pediatric retina.

Chapter 5: Overall Discussion and Conclusion

5.1 Maturation of ERGs in children

Knowledge of the normal development of the standard ERG waveforms from childhood until adulthood is critical to better understand the disease processes that might influence a child's retina. Therefore, this study aimed to provide a pediatric normative dataset for the standard ERGs to be used for clinical interpretations for children with suspected retinal diseases. The ERGs recorded in the present study included ISCEV Standard dark-adapted ERGs (DA 0.1, DA 3, DA 10) and a LA ERG series with flash strengths of 0.3, 1.0, 3.0, 10 & 24 cd.secs/m^2 (this includes the Standard LA 3.0). On examining the literature, only a few studies have documented the development of the standard ERG waveforms from childhood and existing studies used a variety of techniques to obtain ERG recordings. Studies that used contact lens electrodes to acquire ERGs showed general agreement in terms of the maturation of the ERG waveforms[48,49,53]. It is known that different electrodes elicit different ERG amplitudes. We wanted to broaden the scope of the pediatric normative dataset by providing reference data using DTL electrodes for the standard ERG waveforms.

In the present study we found that the implicit times of both DA a-wave (3.0 and 10 ERGs) and DA b-wave (0.01and10 ERGs) were influenced by age. However, the LA implicit times for both a- and b-waves were only significant for the dim flashes including (0.3 for the a-wave and 1.0 for the b-wave). So, the implicit time for children aged between 7-15 years increased with age and approach adult values. Nevertheless, determining the exact age of maturity was not possible owing to the small sample size that was included in the present study. Therefore, the DA ERG

findings might indicate immaturity of the rod and rod pathway activities. Previous studies that used contact lens electrodes reported that immature retina is characterized by long implicit times in the first three years of life that decrease systematically with age reaching maturity somewhat between 1-15 years of age[48,49]. It should be noted that the previously reported data are sparse so that determining the exact age of maturity was not possible. Nevertheless, Rodriguez et al.[142] used a skin electrode and non-standard ERG stimuli to investigate the maturation of the ERG waveforms from childhood until adulthood. They found that approximately 85% of the b-wave and almost 45% of the a-wave changes occur from birth to the first six months of life. While the implicit time of the a-wave reached maturity by 3 years of age, the implicit time of the b-wave underwent a progressive increase from six months to 3 years and then continued to increase slowly, reaching maturity somewhere between 18-21 years[142]. Putting the previous and current studies together, the implicit times first decrease until about 5-6 years, and then increase again until adulthood.

The present study results indicate that the none of the a- or b-wave amplitudes of either LA or DA stimuli were affected by age. This suggested that the neural activities responsible for generating a- and-b-wave amplitudes are considered mature by age 7 years. It is known that the DA a-wave is primarily due to photoreceptor activities whereas the DA b-wave is due to depolarizing ON rod bipolar cell responses that generate the extraretinal light current. Furthermore, the LA a-wave reflects the cone photoreceptor activities, in addition to a considerable contribution from hyperpolarizing OFF bipolar neurons. The LA b-wave is generated by depolarizing ON bipolar cell and hyperpolarizing OFF bipolar cell activities, in addition to some contribution from the electrical activities of horizontal cells with moderation by

Muller cells. The findings of the present study agreed with previous reports that have found that adult-like values are not reached until somewhere between 1 and 10[48] or 5 and 15[49,53] years of age. Rodriguez et al.[142] found that the amplitude of the a-wave is adult-like by 3 years of age while the amplitude of the b-wave increased progressively from childhood until reaching maturity somewhere between 7-8 to 12-14 years.

5.2: Maturation of retinal layer thickness in children

The main purpose of the second study was to provide pediatric reference ranges for the retinal layer thicknesses as measured using the SD-OCT according to the ETDRS thickness maps in healthy children of European descent. Also, the study aimed to establish a normative dataset of peripapillary retinal nerve fiber layer thickness (RNFL). The SD-OCT has increasingly become an indispensable cornerstone of detecting and evaluating various retinal diseases over the past few decades. However, for the technique to be most useful in detecting retinal diseases at early stages in children, normative retinal thickness values from populations of children needs to be developed. The available normative dataset provided by the SD-OCT is only for adults and it is not correct to compare children thickness values with adult's reference ranges before the age at which is becomes adult-like. Only a few studies have reported children's reference values for each retinal layer and the majority of these studies have used the hand-held OCT to acquire pediatric retinal thickness measurements[77,78,80,103]. Therefore, a comprehensive pediatric normative dataset documenting ETDRS thickness map measurements for each retinal sublayer is still lacking. The present study provides evidence that the morphological development of the retinal layers may not be mature between 4 to 15 years of age. However, determining the exact age of maturation is limited by the small sample size included in the current study. Therefore, it

is appropriate to provide separate age norms for separate ages under the age of 15 years for these parameters, which is the approach taken in this thesis.

5.2.1 Nerve fiber layer scan

Age is considered a significant factor influencing RNFL thickness, with most previous findings indicating that RNFL thickness decreases with age in older adult populations[100,101,108], whereas child studies varied in their conclusions. Some publications reported a significant positive correlation of retinal thicknesses with age during childhood[82,83], while others reported no significant correlation with age[85,103,107]. Nevertheless, the reported r values in the studies that found any significant correlations with age were relatively small, indicating a considerable variation in the data in pediatric populations. From the previously reported studies, we can conclude that the average global RNFL thickness using SD-OCT for white children aged between 5 and 16 years of age ranges between 100 and 107μm, indicating very little change with age. In agreement with the previously reported studies, the present study showed the global RNFL thickness was not influenced by age, reaching an average thickness for the 95% overlap with the adult values of 104μm. There was no effect of age for the other sectors, except for a weak negative correlation between age and the nasal superior sector (NS) and this finding needs to be confirmed with further studies ideally with a larger sample size. Previous SD-OCT studies have reported the average RNFL thickness at the NS sector for children (5-15 years) to vary between 104 and 116μm[99,103], significantly lower than 139.5μm reported in this study for children aged between 4 and 7 years.

5.2.2 Macular cube: Overall retinal thickness

The vast majority of studies that used SD-OCT have focused on documenting a pediatric reference database for overall retinal thickness. These studies varied in their conclusions about the effect of age on the overall macular thickness. While Turk et al.[99] documented that the total macular thickness in the foveal area is not influenced by age (from 6 to 16 years), other studies reported a significant positive correlation with age (3-15 years)[103,137]. These studies concluded that the average retinal thickness in the foveal area ranges between 271.2µm and 209µm (5-16 years). In contrast with the previous findings, the total retinal thickness in the foveal area in the present study was influenced by age. The average macular thickness for younger children was 245.3µm and increased with age, reaching 275.9µm for young adults.

5.2.3 Inner retinal layers

The maturation of the individual retinal layers has been previously reported using various techniques such as different instruments (SD-OCT and HH-SDOCT), different age ranges, and ethnicities[77,78,80,103]. The present study results indicated that the overall inner retinal thickness at the foveal and parafoveal areas significantly increased with age. However, a direct comparison with previous studies is limited. For instance, Lee et al.[77] and Maldonado et al.[78] used the HH-SDOCT. They concluded that the average total inner retinal layer (IRLs) thickness at the foveal area varies between 10 to 7µm for children aged between 2-15 years and the values decrease with age. In the present study, the average IRLs thickness at the fovea was significantly positively influenced by age, so that the average thickness in young children (4-7 years) was 156µm and increased significantly with age reaching 188µm for adults. A similar developmental trend was observed in the parafoveal area such that the thickness measurements increase

progressively with age from a mean thickness of 248.7µm (4-7 years) to 264.9µm for adults. The thickness values reported in the present studies are significantly higher than previously reported findings. This is likely because previous studies which measured the foveal thickness included a smaller area defined as the fovea, so that they have a different definition for the para and perifoveal areas compared to the present study. In these studies, the parafovea and perifovea were measured at 1mm and 2mm from the foveal center (2mm and 4mm diameter) respectively whereas in the present study the ETDRS thickness maps was used to obtain thickness measurements (1mm diameter for the foveal area, 3mm for the parafoveal area and 6mm for the perifoveal area).

We found that in some regions the individual inner retinal layers, except for the ganglion cell layer (GCL), were significantly influenced by age. This correlation might be driven by the thinner inner retinal layers in younger children (4-7 years). When comparing the mean values of younger children with other age groups, with our adult group and with another adult study[139], it can be seen that young children have thinner mean values (in all the inner retinal layers) compared to older age groups. However, we are unable to determine the exact age of maturity because the small sample size limits the study. These observed findings may indicate that the ongoing migration of the inner retinal layers away from the foveal center is not complete in children up to 15 years.

5.2.4 Outer retinal layers

Similarly, a couple of retinal thickness measurements of the outer retinal layers were significantly influenced by age (not including the outer nuclear layer). Lee et al.[77] reported that

the outer plexiform layer (OPL) reaches maturity by 11.6 months in the nasal parafovea. However, they documented that the outer nuclear layer in the perifoveal area matures by 12 years, and the retinal pigment epithelium layer (RPE) is mature by 4.5 years. In comparison, Yanni et al.[103] found that only the outer segment layer was influenced by age for children age from 5 to 15 years and thickness values of the RPE did not significantly change with age (5 to 15 years) . Nevertheless, the data in the present study suggested that the OPL in the parafoveal area decreases with age, and the retinal thickness of the OPL found in our adult group was 31.2μm compared to 34.8μm for the 4 to 7 years old children. In accordance with the previous reports that suggested the RPE thickens with age[140,141], the findings of the present study indicated the RPE at the fovea is not mature for children age from 4 to 15 and increases with age.

5.3 The correlation between retinal structure and function

In the present study, the SD-OCT was used to investigate the developmental changes of the individual retinal layers' thickness with age within the macular area, including fovea, parafovea, and perifovea. Additionally, the full-field ERG was used to investigate the maturation of the retinal activities in response to flash stimuli, particularly within the area of the photoreceptor layer and neurons postsynaptic to the photoreceptors. The correlation between the OCT and ERG measures was explored to investigate whether there are associations between the maturation of the retinal structure and function among individuals, independent from any maturation with age.

5.3.1 Structure-Function relationships - LA and DA a-wave vs. the outer retina

The correlation between the a-wave as assessed by the full-field ERG and thickness measurements of the outer retinal layers across the macular area includes fovea, parafovea, and

perifovea was tested. This area was selected because the ERGs are dominated by the extramacular rod and cone photoreceptors' activity. The outer retinal thickness was measured from the inner border of the RPE to the inner border of the OPL; thus, the measurements reflect all the photoreceptor layers, including the outer nuclear layer, inner and outer segment, which is the closest measurement in the current data which would reflect photoreceptor activity. Pearson's correlation was used to analyze the correlation between the LA a-wave (24 ERG) and the outer retinal thickness and the correlation between DA a-wave (10 ERG) and the outer retinal thickness. The results of the correlation analysis revealed that neither of the LA and DA ERGs a-wave amplitudes were significantly associated with the outer retinal thickness measurements (LA 24 ERG [r = 0.07, p = 0.705], DA10 ERG [r = -0.024, p = 0.897]), see Figure 5-1.

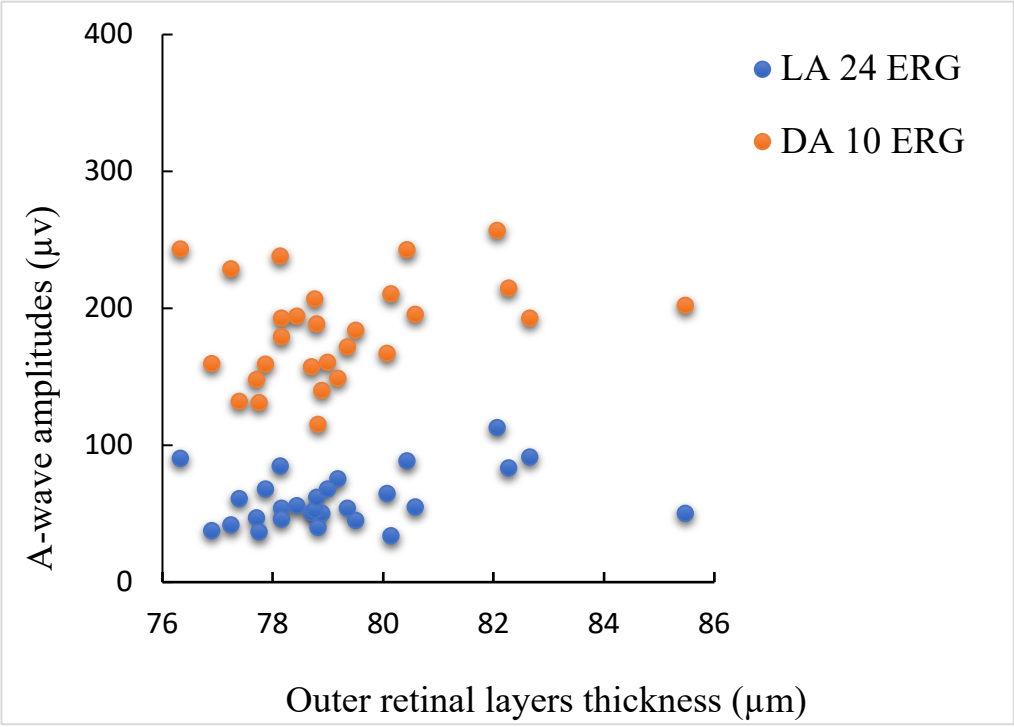

Figure 5-1: Scattergram of the LA and DA a-wave amplitudes against the outer retinal layers thickness measurements. Each point represents the average data for one participant.

It is known that the descending portion of the DA a-wave reflects the activity of the photoreceptors (rods and cones) while the LA a-wave receives a considerable contribution from OFF bipolar neurons in addition to the cone photoreceptors contributions. Therefore, the present study's findings suggest that the cone and rod related functions are unlikely to be influenced by thickness measurements of the whole outer retinal layers as measured by OCT of the macular cube.

5.3.2 Structure-Function relationships - LA and DA b-wave vs. the outer retina

The relationship between the neural mechanism responsible for generating b-wave and thickness measurements of the outer nuclear layers across the whole region, including the fovea, parafovea, and perifovea, was explored. The outer nuclear layer was measured from the outer border of the inner plexiform layer to the inner border of the outer plexiform layer within the macular area. The INL includes the cell bodies of bipolar, horizontal, Muller, and amacrine cells; hence this area reflects the neural activates postsynaptic to the photoreceptors responsible for generating LA and DA b-wave. Pearson's correlation was used to analyze the correlation between LA b-wave (3 ERG) and the thickness of inner nuclear layer and similarly the correlation between DA b-wave (10 ERG) and the thickness of the inner nuclear layer. The correlation analysis demonstrated no significant relationship between the amplitudes of b-wave for LA and DA ERGs and thickness measurements of the inner nuclear layer (LA 3 ERG [$r = 0.24$, $p = 0.192$], DA10 ERG [$r = 0.024$, $p = 0.895$]), see Figure 5-2.

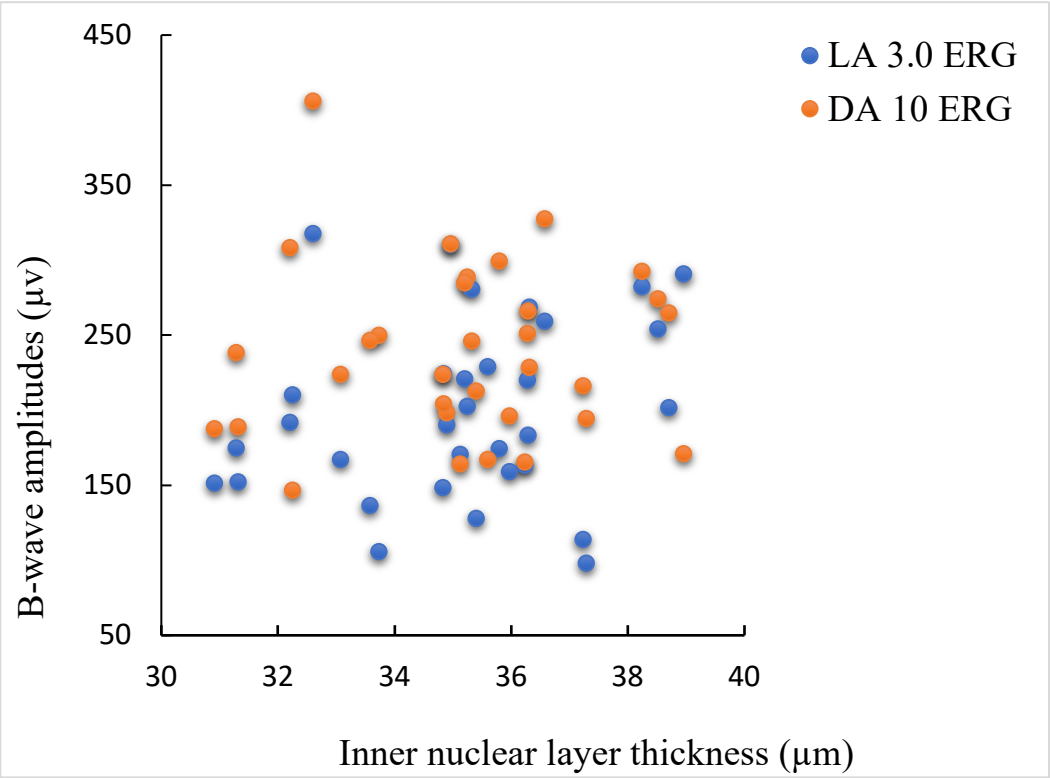

Figure 5-2: Scattergram of the LA and DA b-wave amplitudes against the inner nuclear layer thickness measurements. Each point represents the average data for one participant.

The morphology of the DA b-wave is defined by the interaction between the photoreceptor's activity and inner retinal layer activity, particularly ON-bipolar cell responses. In contrast, the LA b-wave received a considerable contribution from the horizontal cells, OFF bipolar cells, in addition to the ON-bipolar cell activity. Hence, the findings of the present study showed that the neural mechanism responsible for generating LA and DA b-wave is unlikely to be affected by the thickness of the inner nuclear layer within the macular cube.

5.4 Examples of the clinical application of ERG and OCT

5.4.1 Application of normative ERG data to HARS syndrome: case examples

The prime motivator of the present study was to obtain a pediatric dataset for OCT scans and ERG recordings to investigate the retinal structure, function, and pathological processes associated with the mutation of histidyl t-RNA synthetase gene (HARS) (described in Chapter 1). Hence, I will qualitatively compare the HARS OCT and ERG findings with healthy children.

The typical ERG recording for the DA 0.01 ERG has a prominent b-wave but almost no or very small a-wave. This is because the electrical activity generated by the rods in response to a dim light stimulus is too small to be identified as an a-wave. However, the rod signal is greatly amplified by the depolarizing ON bipolar neural pathway in the inner retina. The typical dark-adapted standard flash ERG (3.0 ERG) has prominent a- and b-waves (Figure 5-3a). The a-wave mainly reflects the activity of the photoreceptors (rods and cones) and the b-wave is primarily due to depolarizing ON rod bipolar cell responses that generate the extraretinal light current. The typical oscillatory potentials (OPs) consist of a series of high frequency and low amplitude wavelets, approximately 6-4 wavelets, and receive contributions from both rod and cone pathways. The earlier wavelets (cone-mediated) are likely due to ON neural pathway while the later wavelets (rods mediated) are associated with the OFF pathways (Figure 5-3a). In comparison, the ERGs for a 12-year-old HARS affected patient who has not experienced severe fever showed preserved DA ERGs but severely depressed DA b-waves and OPs (Figure 5-3b). However, patients with HARS who have experienced severe fever show more retinopathy changes and may have undetectable DA ERGs above the noise (Figure 5-3c). These findings

indicate that the abnormalities in HARS syndrome do affect the rods' neural activities and rod pathways.

On the other hand, the typical light-adapted 3.0 ERG has distinct a- and b-waves. The trough of the a-wave receives a considerable contribution from the inner retinal activity, including hyperpolarizing OFF-bipolar neurons, in addition to the cone photoreceptor contributions. In contrast, the LA b-wave is formed by the depolarizing ON bipolar cell activities and hyperpolarizing OFF bipolar cells as well as some contribution from the electrical activities of horizontal cells with moderation by Muller cells. Typically, the steady-state waveform of the flicker ERG is due to the ON and OFF pathways with large phase differences between the pathways so that they partly cancel each other out (Figure 5-1a). In comparison, an affected HARS patient with no fever had disproportionate depressions of LA ERGs, including flash and flicker ERGs (Figure 5-3b). A fifteen years old female who had experienced a previous severe fever showed undetectable LA ERGs above the noise (Figure 5-3c). Therefore, the ERG clinical findings in HARS syndrome suggest that the neural activities of the cones and cones pathways are more affected than the rod and rod pathways. Hence, the full-field ERG can be effectively used to detect and monitor the progression of the retinal changes in HARS syndrome.

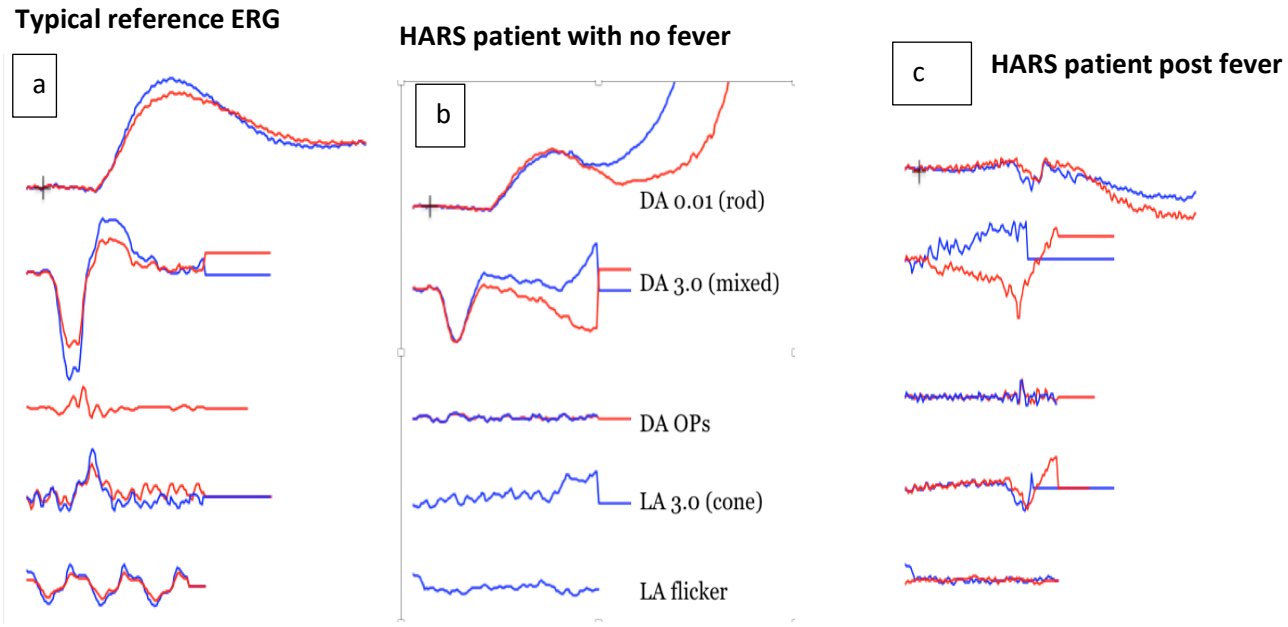

Figure 5-3*:* A typical ERG recording from a healthy participant. (b) an example from a 12-year-old girl with HARS showing the five ISCEV standard ERG waveforms. A typical ERG recording from a healthy participant. (b) an example from a 12-year-old girl with HARS showing the five ISCEV standard ERG waveforms, which illustrate that oscillatory potentials and cone-related ERGs are undetectable, although there is minimal retinopathy. Dark-adapted ERGs are relatively preserved but the DA 3.0 b-wave is reduced. (c) ERGs for a HARS patient who had experienced a severe fever showing that all 5 ISCEV Standard ERGS are undetectable above the noise. *These ERG recordings were taking by Dr. Daphne McCulloch.*

Clearly, the undetectable ERGs demonstrated abnormality of retinal function in both cases. For the child with HARS and no previous severe fever, the LA ERGs and OPs were undetectable and the DA 0.01 ERG b-wave amplitude of 87.15µv was considerably below the lower limit of normal (183.5µv). The DA 3.0 ERG had a clearly abnormal a-wave amplitude (22.41µv) and implicit time (20ms), and her b-wave amplitude (77.16µv) was below the lower limit of normal for the age range of 7-15 defined in this study (184.5µv). The implicit time of her DA b-wave of 49ms was slightly later than the typical normal range of 32 to 47.1ms (Table 5-1).

Table 5-1: Normative ERG values (from Tables 3-14, 3-15, 3-18, 3-19 and 3-20) and HARS ERG recordings for the patient with no previous severe fever.

Age (years) Typical individuals	**Stimulus strength cd.s.m^2**	**Mean Amplitude (µV)**	**Normal limits**		**Age (years) HARS patient**	**HARS ERG recordings (µV)**
			Lower	**Upper**		
7-33	DA 0.01 b-wave amplitude	325.7	183.5	467.9	12	87.2
7-33	DA 3.0 a-wave amplitude	216	121.7	310.3	12	22.4
7-33	DA 3.0 b-wave amplitude	341.8	184.5	499.2	12	77.2

Age (years)	**Stimulus strength cd.s.m^2**	**Median Implicit time (ms)**	**Normal limits**		**Age (years) HARS patient**	**HARS ERG recordings (ms)**
			Lower	Upper		
12-15	DA 0.01 b-wave implicit time	78.5	74.5	108	12	85.5
12-15	DA 3.0 a-wave implicit time	15	14.5	16	12	20

12-15	DA 3.0 b-wave implicit time	37.5	32	47.1	12	49

5.4.2: Qualitative comparison of OCT images in HARS syndrome

The OCT is a non-invasive diagnostic imaging technique that is commonly used to assess a wide range of retinal diseases. Interpretation of OCT anatomy includes both qualitative and quantitative assessments, and both are essential to evaluate an OCT image thoroughly. In qualitative evaluation, individual B-scans (line-scans) of the targeted area in the retina are qualitatively reviewed to assess the presence or absence of retinal pathology based on the knowledge of typical OCT anatomy. Generally, the retinal layers are divided into zones based on the relative reflectivity of the retinal layers. (Figure 5-4a). It should be noted that the inner retinal layers are fused into a single layer in the foveal center and are indistinguishable. Both IPL and GCL have a similar appearance so that they appear merged together. In comparison, the OCT findings of a 12-year-old HARS patient who had not experienced severe fever episodes showed a localized disturbance (hyper-reflectivity) that extends from the ONL to the RPE in both nasal and temporal retinae within the foveal and parafoveal areas. This is likely due to the distinct lesion that sometimes shows on ophthalmoscopy as a “beaten-metal” appearance observed in the affected HARS patients. In the perifovea, the outer retinal layers appear to be relatively intact and preserved. Unlike the normal control where the ellipsoid and interdigitation zones are present throughout the macular area, the patient’s ellipsoid and interdigitation zones were absent throughout the scan except for a small segment under the perifovea. Thus, both rod and cone photoreceptors would be expected to be affected (Figure 5-4b). Furthermore, there is a prominent

overall foveal thinning - the inner retinal layers appear to be relatively preserved but are thinner compared to a normal individual of the same age group (Figure 5-4 a&b). Therefore, these findings likely indicate that the affected patient has cone and rod dystrophy and visual impairment.

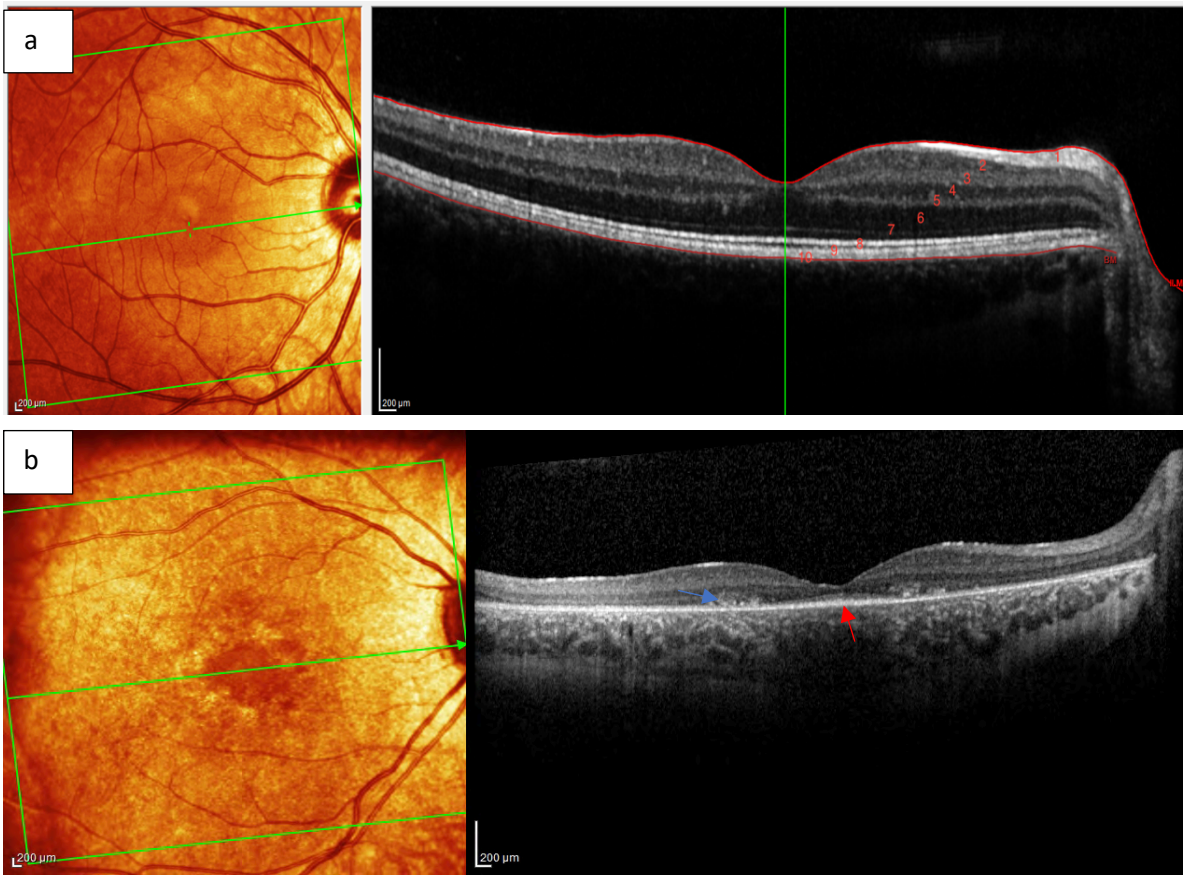

Figure 5-4: (a) A typical OCT scan of an 11-yearold healthy child. SD-OCT bands 1-10 are shown in the scan. 1 = RNFL; 2 = GCL; 3 = IPL; 4 = INL; 5 = OPL; 6 = ONL; 7 = ELM; 8 = EZ; 9 = interdigitation zone; 10 = RPE. (b) a representative example of an OCT scan from a 12-year-old affected patient showing disturbance of the area from RPE to ONL at both nasal parafovea and temporal parafovea (blue arrow), and interruption of the area of the ellipsoid zone (red arrow). The HARS image is courtesy of Natalie Hutchings.

The OCT findings of the 13-year-old patient who had experienced severe fever revealed that the ellipsoid and interdigitation zones were not visible across the foveal and parafoveal areas. The area from RPE to ONL was disrupted and appears to be hyper-reflective. It extends to a greater area compared to the individual who has not experienced severe fever. This is likely due to the distinct lesion causing a decreased visualization of the outer retinal tissues. In addition, there is an overall foveal thinning, although the foveal pit is relatively preserved. The inner retinal layers are relative preserved, but they appear thinner compared to an individual of the same age group (Figure 5-5 a&b). Therefore, these findings likely indicate that the affected patient has cone and rod dystrophy and loss of visual acuity. To conclude, the OCT finding of both patients showed relatively preserved inner retinal layers. However, quantitative assessment and comparison with pediatric normative data will determine with certainty whether the inner retinal thicknesses show normal retinal development or have been impacted by the disease process. The outer retinal layers are clearly affected in these example cases.

Figure 5-5: (a) A typical OCT scan of a 14-year-old healthy child. (b) an OCT scan of 15-year-old HARS patient post fever indicating overall foveal thinning and disruption from the RPE to ONL (blue arrow). Note that the Ellipsoid zone is not visible (red arrow). The HARS image is courtesy of Natalie Hutchings.

5.5 Limitations

One limitation of the first study is that the younger children (4-6 years) were not included in the ERG analysis. This was because most children within this age range could not tolerate the Espion E3 visual electrophysiology system and the DTL electrode. In fact, it is well established that skin electrodes elicit smaller amplitudes and earlier implicit times compared to the DTL

electrodes. As a result, we were not able to determine whether the developmental trend for this age group would agree with the previously published findings.

There are many factors that might influence the ERG recordings that could be tested which are not included in the present study. We did not test whether the ocular pigmentation is associated with differences in ERG amplitudes for the lightly pigmented people of European descent. This is justified as we did not obtain fundus photographs for each participant to determine with certainty the association between fundus pigmentation and ERG amplitudes.

Another limitation of the study is that the axial length was not measured. Nevertheless, the axial length has a limited effect on retinal thickness values[99,143]. All the participants in the present study had normal visual acuity and refractive error for their age, so that they are unlikely to have had an increased axial length.

Another limitation for the study is that the sample only included individuals of European descent. This is because the prime motivator was the need of such data when studying children with HARS syndrome (observed in several individuals of Old Order Amish). This population is white and of European descent. Therefore, generalization of the results to people with different ethnic and racial groups cannot be done. These other groups still need to be investigated.

The main limitation of the present thesis is that the sample size was not sufficient to determine

with certainty the developmental trajectory of the retinal layers as well as the standard ERG waveforms. Therefore, we are unable to determine the exact age at which these parameters reach maturity.

5.6 Future directions

The results of the present study lead to potential future research:

1- Further investigation to support the current negative association between age and OCT RNFL in the nasal superior sector. Studies might include a larger sample size to test this correlation, comparisons with ocular dimensions to determine if the layer thins with ocular growth, and long-term studies to determine with certainty if the thinning is present in individuals.

2- Future studies could investigate the developmental changes of the photoreceptor's inner and outer segments with age using a custom designed program as the average thickness values for these bands are not provided by SD-OCT (Heidelberg Spectrals, Eye Explorer software version 1.9.10.0).

3- A similar study could also be conducted for other ethnicities and racial groups to broaden the pediatric normative data and to investigate whether the developmental trend of the retinal structure and function is associated with differences for other ethnicities.

4- Future studies with larger sample size are necessary to determine with certainty the age at which retinal structure and function reach maturity. With more data, future studies could do a curve fitting or fit two straight lines; one will be a flat plateau for the adults and the other will be a sloping line for children to determine where these lines intersect.

5- The correlation between the retinal layers thickness measurements at the fovea and visual acuity/contrast sensitivity could also be investigated. The outer retinal layers significantly contribute to the maturation of visual acuity particularly the outer nuclear layer.[77]

6- Future work would be to analyze the OPs and flicker ERGs data that have already collected but were not included in this thesis owing to the limitation of time. Also, it would be interesting to quantitively analyze the HARS data for both OCT scans and ERG recordings (as far as is possible since some ERG recordings were non-recordable, and some OCT scans would be difficult to quantify the thickness of the layers).

5.7 Conclusions

Several conclusions are drawn in this thesis and are as follows

1- Although it is well established that ERGs from the immature retina up to 5 years of age are characterized by implicit times that decrease with time, this study shows that for participants aged 7 to approximately15 years, DA ERG and some of the LA implicit times increase with age to approach adult values. This indicates that the rod system is still relatively immature until at least 7-11 years.

2- The thickness measurements of some retinal layers (mainly in the inner retina) measured by OCT show changes with age in some retinal regions in this cross-sectional study. Therefore, the present study provides evidence that the morphological development of the

retinal layers is not mature before the age of 4-7 years. However, determining the exact age of maturation is limited by the small sample size included in the current study.

3- The peripapillary RNFL thickness in most segments was not influenced by age in this sample of 4 to 33 years of age. However, there was a weak negative correlation between age and thickness in the nasal superior quadrant, suggesting that the RNFL in the nasal superior sector thins during childhood, whereas the other sectors do not change significantly.

4- Both OCT and ERG techniques can be applied in children as young as 4 years old and can be used effectively to investigate children with HARS. Quantitative assessment of the OCT scans will help to follow the progression of the disorder as well as to determine with certainty whether the inner retinal layers are associated with abnormalities for HARS patients.

Bibliography

1. Abramov I, Gordon J, Hendrickson A, Hainline L, Dobson V, Labossiere E. The retina of the newborn human infant. *Science*. 1982;217(4556):265-267. doi:10.1126/science.6178160
2. Hendrickson AE, Yuodelis C. The morphological development of the human fovea. *Ophthalmology*. 1984;91(6):603-612. doi:10.1016/S0161-6420(84)34247-6
3. Yuodelis C, Hendrickson A. A qualitative and quantitative analysis of the human fovea during development. *Vision Res*. 1986;26(6):847-855. doi:10.1016/0042-6989(86)90143-4
4. Hendrickson A, Possin D, Vajzovic L, Toth CA. Histologic development of the human fovea from midgestation to maturity. *Am J Ophthalmol*. 2012;154(5):767-778.e2. doi:10.1016/j.ajo.2012.05.007
5. Hendrickson A. A morphological comparison of foveal development in man and monkey. *Eye*. 1992;6(Pt 2):136-144. doi:10.1038/eye.1992.29
6. Dorn EM, Hendrickson L, Hendrickson AE. The appearance of rod opsin during monkey retinal development. *Invest Ophthalmol Vis Sci*. 1995;36(13):2634-2651.
7. Dubis AM, Costakos DM, Subramaniam CD, et al. Evaluation of normal human foveal development using optical coherence tomography and histologic examination. *Arch Ophthalmol*. 2013;130(10):1291-1300. doi:10.1001/archophthalmol.2012.2270.Evaluation
8. Vajzovic L, Hendrickson AE, O'Connell R V., et al. Maturation of the human fovea: correlation of spectral-domain optical coherence tomography findings with histology. *Am J Ophthalmol*. 2012;154(5):779-789.e2. doi:10.1016/j.ajo.2012.05.004
9. Hendrickson A, Possin D, Vajzovic L, Toth CA. Histologic Development of the Human

Fovea From Midgestation to Maturity. *Am J Ophthalmol*. 2012;154(5):767-778.e2. doi:10.1016/j.ajo.2012.05.007

10. Polyak S. *The Retina*. 1st ed. Chicago: Univ. Chicago Press; 1941.
11. Xiao M, Hendrickson A. Spatial and temporal expression of short, long/medium, or both opsins in human fetal cones. *J Comp Neurol*. 2000;425(4):545-559. doi:10.1002/1096-9861(20001002)425:4<545::AID-CNE6>3.0.CO;2-3
12. Parness-Yossifon R, Mets MB. The electroretinogram in children. *Curr Opin Ophthalmol*. 2008;19(5):398-402. doi:10.1097/ICU.0b013e32830abf11
13. Lam BL, ed. *Electrophysiology of Vision*. 1st ed. Boca Raton: Taylor & Francis; 2005. doi:10.1201/b14209
14. Michael F, Marmor ZE. Introduction to the ISCEV Standards. In: Heckenlively, John, Arden, Geoffrey, eds. *Principles and Practice of Clinical Electrophysiology of Vision*. 2nd ed. Cambridge: MIT Press; 2006:287-288.
15. McCulloch DL, Marmor MF, Brigell MG, et al. ISCEV Standard for full-field clinical electroretinography (2015 update). *Doc Ophthalmol*. 2015;130(1):1-12. doi:10.1007/s10633-014-9473-7
16. Smith C. Phototransduction and photoreceptor physiology. In: Heckenlively, Arden, Geoffrey, John, eds. *Principles and Practice of Clinical Electrophysiology of Vision*. 2nd ed. Cambridge: MIT Press; 2006:65-75.
17. Peachey NS, Alexander KR, Derlacki DJ, Fishman GA. Light adaptation, rods, and the human cone flicker ERG. *Vis Neurosci*. 1992;8(2):145-150. doi:10.1017/S0952523800009305
18. Frishman. Origins of the electroretinogram. In: Heckenlively, Arden, Geoffrey, John, eds.

Principles and Practice of Clinical Electrophysiology of Vision. 2nd ed. Cambridge: MIT Press; 2006:139-176.

19. Falk G. Signal transmission from rods to bipolar and horizontal cells: A synthesis. *Prog Retin Res*. 1988;8(C):255-279. doi:10.1016/0278-4327(88)90028-4

20. Steinberg, Frishman, Sieving. Negative components of the electroretinogram from proximal retina and photoreceptor. *Prog Retin Res*. 1991;10:121-160.

21. Penn RD, Hagins WA. Signal transmission along retinal rods and the origin of the electroretinographic a-Wave. *Nature*. 1969;223(5202):201-204. doi:10.1038/223201a0

22. Qiu H, Fujiwara E, Liu M, Lam BL, Hamasaki DI. Evidence that a-wave latency of the electroretinogram is determined solely by photoreceptors. *Jpn J Ophthalmol*. 2002;46(4):426-432. doi:10.1016/S0021-5155(02)00505-1

23. Pugh EN, Lamb TD. Amplification and kinetics of the activation steps in phototransduction. *Biochim Biophys Acta*. 1993;1141(2-3):111-149. doi:10.1016/0005-2728(93)90038-H

24. Jamison JA, Bush RA, Lei B, Sieving PA. Characterization of the rod photoresponse isolated from the dark-adapted primate ERG. *Vis Neurosci*. 2001;18(3):445-455. doi:10.1017/S0952523801183112

25. Gurevich L, Slaughter MM. Comparison of the waveforms of the ON bipolar neuron and the b -wave of the electroretinogram. *Vision Res*. 1993;33(17):2431-2435. doi:10.1016/0042-6989(93)90122-D

26. Miller RF, Dowling JE. Intracellular responses of the Müller (glial) cells of mudpuppy retina: their relation to b-wave of the electroretinogram. *J Neurophysiol*. 1970;33(3):323-341. doi:10.1152/jn.1970.33.3.323

27. Newman EA, Odette LL. Model of electroretinogram b-wave generation: A test of the K+ hypothesis. *J Neurophysiol*. 1984;51(1):164-182. doi:10.1152/jn.1984.51.1.164

28. Stockton RA, Slaughter MM. B-wave of the electroretinogram: A reflection of ON bipolar cell activity. *J Gen Physiol*. 1989;93(1):101-122. doi:10.1085/jgp.93.1.101

29. Brown GC, Eagle RC, Shakin EP, Gruber M, Arbizio V V. Retinal toxicity of intravitreal gentamicin. *Arch Ophthalmol*. 1990;108(12):1740-1744. doi:10.1001/archopht.1990.01070140094037

30. Hood DC, Birch DG. Phototransduction in human cones measured using the a-wave of the ERG. *Vis Res*. 1995;35(20):2801-2810. doi:10.1016/0042-6989(95)00034-W

31. Hood DC, Birch DG. Human cone receptor activity: The leading edge of the a-wave and models of receptor activity. *Vis Neurosci*. 1993;10(5):857-871. doi:10.1017/S0952523800006076

32. Whitten DN, Brown KT. The time courses of late receptor potentials from monkey cones and rods. *Vision Res*. 1973;13(1):107-135. doi:10.1016/0042-6989(73)90168-5

33. Bush RA, Sieving PA. A proximal retinal component in the primate photopic ERG a-wave. *Invest Ophthalmol Vis Sci*. 1994;35(2):635-645.

34. Sieving PA, Murayama K, Naarendorp F. Push-pull model of the primate photopic electroretinogram: A role for hyperpolarizing neurons in shaping the b-wave. *Vis Neurosci*. 1994;11(3):519-532. doi:10.1017/S0952523800002431

35. Baron WS, Boynton RM. Response of primate cones to sinusoidally flickering homochromatic stimuli. *J Physiol*. 1975;246(2):311-331. doi:10.1113/jphysiol.1975.sp010892

36. Baron WS, Boynton RM, Hammon RW. Component analysis of the foveal local

electroretinogram elicited with sinusoidal flicker. *Vision Res*. 1979;19(5):479-490. doi:10.1016/0042-6989(79)90132-9

37. Bush RA, Sieving PA. Inner retinal contributions to the primate photopic fast flicker electroretinogram. *J Opt Soc Am A Opt image Sci Vis*. 1996;13(3):557-565. doi:10.1364/josaa.13.000557

38. Kondo M, Sieving PA. Post-photoreceptoral activity dominates primate photopic 32-Hz ERG for sine-, square-, and pulsed stimuli. *Invest Ophthalmol Vis Sci*. 2002;43(7):2500-2507.

39. Peachey NS, Alexander KR, Fishman GA. Rod and cone system contributions to oscillatory potentials: An explanation for the conditioning flash effect. *Vision Res*. 1987;27(6):859-866. doi:10.1016/0042-6989(87)90002-2

40. Janáky M, Goupland SG, Benedek G. Human oscillatory potentials: Components of rod origin. *Ophthalmologica*. 1996;210(6):315-318. doi:10.1159/000310731

41. Lachapelle P, Rousseau S. The electroretinogram recorded at the onset of dark-adaptation: understanding the origin of the scotopic oscillatory potentials. *Doc Ophthalmol*. 1999;99(2):135-150. doi:10.1023/a:1002679932462

42. Wachtmeister L. Oscillatory potentials in the retina: What do they reveal. *Prog Retin Eye Res*. 1998;17(4):485-521. doi:10.1016/S1350-9462(98)00006-8

43. Birch D, Birch E, Spencer R. Electroretinographic testing in infants and children. In: Reynolds J, Olitsky S, eds. *Pediatric Retina*. Springer; 2012.

44. Brigell M, Bach M, Barber C, Moskowitz A, Robson J. Guidelines for calibration of stimulus and recording parameters used in clinical electrophysiology of vision. *Doc Ophthalmol*. 2003;107(2):185-193. doi:10.1023/A:1026244901657

45. Birch DG, Birch EE, Hoffman DR, Uauy RD. Retinal development in very-low-birth-weight infants fed diets differing in omega-3 fatty acids. *Invest Ophthalmol Vis Sci*. 1992;33(8):2365-2376.

46. Mactier H, Dexter JD, Hewett JE, Latham CB, Woodruff CW. The electroretinogram in preterm infants. *J Pediatr*. 1988;113(3):607-612. doi:10.1016/S0022-3476(88)80663-2

47. Mactier H, Turner TL, Hamilton R, Bradnam MS, Dudgeon J. Contact lens electroretinography in preterm infants from 32 weeks after conception: A development in current methodology. *Arch Dis Child Fetal Neonatal Ed*. 2000;82(3):F233-6. doi:10.1136/fn.82.3.f233

48. Fulton AB, Hansen RM, Westall CA. Development of ERG responses: The ISCEV rod, maximal and cone responses in normal subjects. *Doc Ophthalmol*. 2003;107(3):235-241. doi:10.1023/B:DOOP.0000005332.88367.b8

49. Birch DG, Anderson JL. Standardized full-field electroretinography: normal values and their variation with age. *Arch Ophthalmol*. 1992;110(11):1571-1576. doi:10.1001/archopht.1992.01080230071024

50. Berezovsky A, Bueno Moraes N, Nusinowitz S, Salomão S. Standard full-field electroretinography in healthy preterm infants. *Doc Ophthalmol*. 2003;107(3):243-249. doi:10.1023/B:DOOP.0000005333.76622.c2

51. Mets MB, Smith VC, Pokorny J, Pass A. Postnatal retinal development as measured by the electroretinogram in premature infants. *Doc Ophthalmol*. 1995;90(2):111-127. doi:10.1007/BF01203332

52. Leaf A, Gosbell A, McKenzie L, Sinclair A, IFavilla I. Long chain polyunsaturated fatty acids and visual function in preterm infants. *Early Hum Dev*. 1996;45(1-2):35-53.

53. Westall CA, Panton CM, Levin A V. Time courses for maturation of electroretinogram responses from infancy to adulthood: ERG responses mature at different ages. *Doc Ophthalmol*. 1998;96(4):355-379. doi:10.1023/A:1001856911730

54. Moskowitz A, Hansen RM, Fulton AB. ERG oscillatory potentials in infants. *Doc Ophthalmol*. 2005;110(2-3):265-270. doi:10.1007/s10633-005-1983-x

55. Birch DG, Anderson JL, Fish GE. Yearly rates of rod and cone functional loss in retinitis pigmentosa and cone-rod dystrophy. *Ophthalmology*. 1999;106(2):258-268. doi:10.1016/S0161-6420(99)90064-7

56. Berson EL, Sandberg MA, Rosner B, Birch DG, Hanson AH. Natural course of retinitis pigmentosa over a three-year interval. *Am J Ophthalmol*. 1985;99(3):240-251. doi:10.1016/0002-9394(85)90351-4

57. Marlhens F, Bareil C, Griffoin JM, et al. Mutations in RPE65 cause Leber's congenital amaurosis. *Nat Genet*. 1997;17(2):139-141. doi:10.1038/ng1097-139

58. Perrault I, Rozet JM, Calvas P, et al. Retinal-specific guanylate cyclase gene mutations in Leber's congenital amaurosis. *Nat Genet*. 1996;14(4):461-464. doi:10.1038/ng1296-461

59. Smith RJH, Berlin CI, Hejtmancik JF, et al. Clinical diagnosis of the Usher syndromes. *Am J Med Genet*. 1994;50(1):32-38. doi:10.1002/ajmg.1320500107

60. Well D, Blanchard S, Kaplan J, et al. Defective myosin VIIA gene responsible for Usher syndrome type IB. *Nature*. 1995;374(6517):60-61. doi:10.1038/374060a0

61. Weston MD, Eudy JD, Fujita S, et al. Genomic structure and identification of novel mutations in Usherin, the gene responsible for Usher syndrome type IIa. *Am J Hum Genet*. 2000;66(4):1199-1210. doi:10.1086/302855

62. Aarem A Van, Wagenaar M, Pinckers AJLG, et al. Ophthalmologic findings in Usher

syndrome type 2a. *Ophthalmic Genet*. 1995;16(4):151-158. doi:10.3109/13816819509057856

63. Piazza L, Fishman GA, Farber M, Derlacki D, Anderson RJ. Visual Acuity Loss in Patients With Usher's Syndrome. *Arch Ophthalmol*. 1986. doi:10.1001/archopht.1986.01050210090031

64. Bharadwaj AK, Kasztejna JP, Huq S, Berson EL, Dryja TP. Evaluation of the myosin VIIA gene and visual function in patients with Usher syndrome type I. *Exp Eye Res*. 2000;71(2):173-181. doi:10.1006/exer.2000.0863

65. Seeliger MW, Zrenner E, Apfelstedt-Sylla E, Jaissle GB. Identification of Usher syndrome subtypes by ERG implicit time. *Invest Ophthalmol Vis Sci*. 2001;42(12):3066-3071.

66. Zysk AM, Nguyen FT, Oldenburg AL, Marks DL, Boppart SA. Optical coherence tomography: a review of clinical development from bench to bedside. *J Biomed Opt*. 2007;12(5):51-403. doi:10.1117/1.2793736

67. Bezerra HG, Costa MA, Guagliumi G, Rollins AM, Simon DI. Intracoronary optical coherence tomography: a comprehensive review clinical and research applications. *JACC Cardiovasc Interv*. 2009;2(11):1035-1046. doi:10.1016/j.jcin.2009.06.019

68. Adhi M, Duker JS. Optical coherence tomography-current and future applications. *Curr Opin Ophthalmol*. 2013;24(3):213-221. doi:10.1097/ICU.0b013e32835f8bf8

69. Mangalesh S, Jayadev C, Maldonado RS, Bauer N, A T. Retinal imaging of infants on spectral domain optical coherence tomography. *Biomed Res Int*. 2015;2015:782420.

70. Trichonas G, Kaiser PK. Optical coherence tomography imaging of macular oedema. *Br J Ophthalmol*. 2014;98(Suppl. 2):24-29. doi:10.1136/bjophthalmol-2014-305305

71. Huang D, Swanson EA, Lin CP, et al. Optical coherence tomography. *Science (80-)*. 1991. doi:10.1126/science.1957169

72. Duker JS, Waheed N, Goldman D. *Handbook of Retinal OCT: Optical Coherence Tomography*. 1st ed. Philadlphia: Saunders; 2014.

73. Bhende M, Shetty S, Parthasarathy M, Ramya S. Optical coherence tomography: A guide to interpretation of common macular diseases. *Indian J Ophthalmol*. 2018;66(1):20-35. doi:10.4103/ijo.ijo_902_17

74. Aumann S, Donner S, Fischer J, Müller F. Optical coherence tomography (OCT): Principle and technical realization. In: Bille J, ed. *High Resolution Imaging in Mcroscopy and Ohthalmology*. 3rd ed. Springer; 2019.

75. Early Treatment Diabetic Retinopathy Study design and baseline patient characteristics. ETDRS report number 7. *Ophthalmology*. 1991;98(5 Suppl):741-756. doi:10.1016/S0161-6420(13)38009-9

76. Anger EM, Unterhuber A, Hermann B, et al. Ultrahigh resolution optical coherence tomography of the monkey fovea. Identification of retinal sublayers by correlation with semithin histology sections. *Exp Eye Res*. 2004;78(6):1117-1125. doi:10.1016/j.exer.2004.01.011

77. Lee H, Purohit R, Patel A, et al. In vivo foveal development using optical coherence tomography. *Invest Ophthalmol Vis Sci*. 2015;56(8):4537-4545. doi:10.1167/iovs.15-16542

78. Maldonado RS, O'Connell R V., Sarin N, et al. Dynamics of human foveal development after premature birth. *Ophthalmology*. 2011;118(12):2315-2325. doi:10.1016/j.ophtha.2011.05.028

79. Vinekar A, Avadhani K, Sivakumar M, et al. Macular edema in premature infants. *Ophthalmology*. 2012;119(6):1288-9.e1. doi:10.1016/j.ophtha.2012.03.029

80. Vajzovic L, Hendrickson AE, O'Connell R V., et al. Maturation of the human fovea: correlation of Spectral-Domain Optical Coherence Tomography findings with histology. *Am J Ophthalmol*. 2012;154(5):779-789. doi:10.1016/j.ajo.2012.05.004

81. Larsson E, Eriksson U, Alm A. Retinal nerve fibre layer thickness in full-term children assessed with Heidelberg retinal tomography and optical coherence tomography: Normal values and interocular asymmetry. *Acta Ophthalmol*. 2011;89(2):151-158. doi:10.1111/j.1755-3768.2009.01680.x

82. Qian J, Wang W, Zhang X, et al. Optical coherence tomography measurements of retinal nerve fiber layer thickness in Chinese children and teenagers. *J Glaucoma*. 2011;20(8):509-513. doi:10.1097/IJG.0b013e3181f7b16c

83. Salchow DJ, Oleynikov YS, Chiang MF, et al. Retinal nerve fiber layer thickness in normal children measured with optical coherence tomography. *Ophthalmology*. 2006;113(5):786-791. doi:10.1016/j.ophtha.2006.01.036

84. Repka MX, Kraker RT, Tamkins SM, Suh DW, Sala NA, Beck RW. Retinal nerve fiber layer thickness in amblyopic eyes. *Am J Ophthalmol*. 2009;142(2):247-251. doi:10.1016/j.ajo.2009.01.015

85. Huynh SC, Wang XY, Rochtchina E, Mitchell P. Peripapillary retinal nerve fiber layer thickness in a population of 6-Year-old children. Findings by optical coherence tomography. *Ophthalmology*. 2006;113(9):1583-1592. doi:10.1016/j.ophtha.2006.02.067

86. El-Dairi MA, Holgado S, O'Donnell T, Buckley EG, Asrani S, Freedman SF. Optical coherence tomography as a tool for monitoring pediatric pseudotumor cerebri. *J AAPOS*.

2007;11(6):564-570. doi:10.1016/j.jaapos.2007.06.018

87. Knight OJ, Chang RT, Feuer WJ, Budenz DL. Comparison of retinal nerve fiber layer measurements using time domain and dpectral domain optical coherent tomography. *Ophthalmology*. 2009;116(7):1271-1277. doi:10.1016/j.ophtha.2008.12.032

88. Leite MT, Rao HL, Weinreb RN, et al. Agreement among spectral-domain optical coherence tomography instruments for assessing retinal nerve fiber layer thickness. *Am J Ophthalmol*. 2011;151(1):85-92.e1. doi:10.1016/j.ajo.2010.06.041

89. Ahn HC, Son HW, Kim JS, Lee JH. Quantitative analysis of retinal nerve fiber layer thickness of normal children and adolescents. *Korean J Ophthalmol*. 2005;19(3):195-200. doi:10.3341/kjo.2005.19.3.195

90. Altintas Ö̈, Yüksel N, Özkan B, Çaglar Y. Thickness of the retinal nerve fiber layer, macular thickness, and macular volume in patients with strabismic amblyopia. *J Pediatr Ophthalmol Strabismus*. 2005;42(4):216-221. doi:10.3928/01913913-20050701-03

91. Hess DB, Asrani SG, Bhide MG, Enyedi LB, Stinnett SS, Freedman SF. Macular and retinal nerve fiber layer analysis of normal and glaucomatous eyes in children using optical coherence tomography. *Am J Ophthalmol*. 2005;139(3):509-517. doi:10.1016/j.ajo.2004.10.047

92. Yoon SW, Park WH, Baek SH, Kong SM. Thicknesses of macular retinal layer and peripapillary retinal nerve fiber layer in patients with hyperopic anisometropic amblyopia. *Korean J Ophthalmol*. 2005. doi:10.3341/kjo.2005.19.1.62

93. Kee SY, Lee SY, Lee YC. Thicknesses of the fovea and retinal nerve fiber layer in amblyopic and normal eyes in children. *Korean J Ophthalmol*. 2006;20(3):177-181. doi:10.3341/kjo.2006.20.3.177

94. Kim TW, Kim TW, Park KH, Kim DM. An unexpectedly low Stratus optical coherence tomography false-positive rate in the non-nasal quadrants of Asian eyes: Indirect evidence of differing retinal nerve fibre layer thickness profiles according to ethnicity. *Br J Ophthalmol*. 2008;92(6):735-739. doi:10.1136/bjo.2007.129502

95. Park SH, Park KH, Kim JM, Choi CY. Relation between axial length and ocular parameters. *Ophthalmologica*. 2009;224(3):188-193. doi:10.1159/000252982

96. Schweitzer KD, Ehmann D, García R. Nerve fibre layer changes in highly myopic eyes by optical coherence tomography. *Can J Ophthalmol*. 2009;44(3):e13-6. doi:10.3129/i09-058

97. Kashiwagi K, Tamura M, Abe K, Kogure S, Tsukahara S. The influence of age, gender, refractive error, and optic disc size on the optic disc configuration in Japanese normal eyes. *Acta Ophthalmol Scand*. 2000;78(2):200-203. doi:10.1034/j.1600-0420.2000.078002200.x

98. Manassakorn A, Chaidaroon W, Ausayakhun S, Aupapong S, Wattananikorn S. Normative database of retinal nerve fiber layer and macular retinal thickness in a Thai population. *Jpn J Ophthalmol*. 2008;52(6):450-456. doi:10.1007/s10384-008-0538-6

99. Turk A, Ceylan OM, Arici C. Evaluation of the nerve fiber layer and macula in the eyes of healthy children using spectral-domain optical coherence tomography. *Am J Ophthalmol*. 2012;153(3):552-559.e1.

100. Ramakrishnan R, Mittal S, Ambatkar S, Kader MA. Retinal nerve fibre layer thickness measurements in normal Indian population by optical coherence tomography. *Indian J Ophthalmol*. 2006;54(1):11-15. doi:10.4103/0301-4738.21608

101. Schuman JS, Hee MR, Puliafito CA, et al. Quantification of nerve fiber layer thickness in normal and glaucomatous eyes using optical coherence tomography: A pilot study. *Arch*

Ophthalmol. 1995;113(5):586-596. doi:10.1001/archopht.1995.01100050054031

102. Varma R, Bazzaz S, Lai M. Optical tomography-measured retinal nerve fiber layer thickness in normal latinos. *Invest Ophthalmol Vis Sci*. 2003;44(8):3369-3373. doi:10.1167/iovs.02-0975

103. Yanni SE, Wang J, Cheng CS, et al. Normative reference ranges for the retinal nerve fiber layer, macula, and retinal layer thicknesses in children. *Am J Ophthalmol*. 2013;155(2):354-360.e1. doi:10.1016/j.ajo.2012.08.010

104. Cohen MJ, Kaliner E, Frenkel S, Kogan M, Miron H, Blumenthal EZ. Morphometric analysis of human peripapillary retinal nerve fiber layer thickness. *Invest Ophthalmol Vis Sci*. 2008;49(3):941-944. doi:10.1167/iovs.07-0621

105. Jonas JB, Gusek GC, Naumann GOH. Optic disc, cup and neuroretinal rim size, configuration and correlations in normal eyes. *Invest Ophthalmol Vis Sci*. 1988;29(7):1151-1158.

106. Budenz DL, Anderson DR, Varma R, et al. Determinants of normal retinal nerve fiber layer thickness measured by Stratus OCT. *Ophthalmology*. 2007;115(3):472. doi:10.1016/j.ophtha.2006.08.046

107. Leung MMP, Huang RYC, Lam AKC. Retinal nerve fiber layer thickness in normal Hong Kong Chinese children measured with optical coherence tomography. *J Glaucoma*. 2010;19(2):95-99. doi:10.1097/IJG.0b013e3181a98cfa

108. Alamouti B, Funk J. Retinal thickness decreases with age: An OCT study. *Br J Ophthalmol*. 2003;87(7):899-901. doi:10.1136/bjo.87.7.899

109. Park KA, Oh SY. Retinal nerve fiber layer thickness in prematurity is correlated with stage of retinopathy of prematurity. *Eye*. 2015;29(12):1594-1602.

doi:10.1038/eye.2015.166

110. Wang CY, Zheng YF, Liu B, et al. Retinal nerve fiber layer thickness in children: The Gobi Desert children eye study. *Invest Ophthalmol Vis Sci*. 2018;59(12):5285-5291. doi:10.1167/iovs.18-25418

111. Puffenberger EG, Jinks RN, Sougnez C et al. Genetic mapping and exome sequencing identify variants associated with five novel diseases. *PLoS One*. 2012;7(1):e28936. doi:10.1371/journal.pone.0028936. Epub 2012 Jan 17

112. Leat SJ, McCulloch D, Hutchings N SV. Visual function in HARS syndrome. *Am Acad Optom*. 2018.

113. Badalato L, Leat SJ, Chakrabarti R, et al. Natural history of the multisystem disease associated with homozygous Y454S variants in histidyl tRNA synthetase (HARS). *Am J Med Genet Genomics*. 2020.

114. Meyer-Schuman R, Antonellis A. Emerging mechanisms of aminoacyl-tRNA synthetase mutations in recessive and dominant human disease. *Hum Mol Genet*. 2017;26(R2):R114-R127. doi:10.1093/hmg/ddx231

115. Yao P, Fox PL. Aminoacyl-tRNA synthetases in medicine and disease. *EMBO Mol Med*. 2013;5(3):332-343. doi:10.1002/emmm.201100626

116. Pierce SB, Chisholm KM, Lynch ED, et al. Mutations in mitochondrial histidyl tRNA synthetase HARS2 cause ovarian dysgenesis and sensorineural hearing loss of Perrault syndrome. *Proc Natl Acad Sci U S A*. 2011;108(16):6543-6548. doi:10.1073/pnas.1103471108

117. Brozkova D, Deconinck T, Griffin L, et al. Loss of function mutations in HARS cause a spectrum of inherited peripheral neuropathies. *Brain*. 2015;138(8):2161-2172.

doi:10.1093/brain/awv158

118. McCulloch DL, Leat SJ, Hutchings N, Siu VM. Retinal dystrophy in HARS Syndrome. 2017.

119. Granit R, Riddell LA. The electrical responses of light- and dark-adapted frogs' eyes to rhythmic and continuous stimuli. *J Physiol*. 1934;81(1):1-28. doi:10.1113/jphysiol.1934.sp003112

120. van Genderen M, Riemslag F, Jorritsma F, Hoeben F, Meire F, Stilma J. The key role of electrophysiology in the diagnosis of visually impaired children. *Acta Ophthalmol Scand*. 2006;84(6):799-806. doi:10.1111/j.1600-0420.2006.00717.x

121. Vedantham V, Jethani J, Vijayalakshmi P. Electroretinographic assessment and diagnostic reappraisal of children with visual dysfunction: A prospective study. *Indian J Ophthalmol*. 2007;55(2):113-116. doi:10.4103/0301-4738.30704

122. Dawson WW, Trick L, Litzkow CA. Improved electrode for electroretinography. *Invest Ophthalmol Vis Sci Vis Sci*. 1979;18(9):988-991.

123. Fulton AB, Hansen RM, Petersen RA, Vanderveen DK. The rod photoreceptors in retinopathy of prematurity: An electroretinographic study. *Arch Ophthalmol*. 2001;119(4):499-505. doi:10.1001/archopht.119.4.499

124. Fulton AB, Hansen RM. Photoreceptor function in infants and children with a history of mild retinopathy of prematurity. *J Opt Soc Am A*. 1996. doi:10.1364/josaa.13.000566

125. Mactier, Dexter, Hewett, Latham, Woodruff. The electroretinogram in preterm infants. *J Pediatr*. 1988;113(3):607-612. doi:0.1016/s0022-3476(88)80663-2

126. Jaccard J, CK W. Quantitative applications in social sciences. LISREL approaches to interaction effects in multiple regression. *Thousand Oakes*. 1996;114:112.

127. Al Abdlseaed A, McTaggart Y, Ramage T, Hamilton R, McCulloch DL. Light- and dark-adapted electroretinograms (ERGs) and ocular pigmentation: Comparison of brown- and blue-eyed cohorts. *Doc Ophthalmol*. 2010;121(2):135-146. doi:10.1007/s10633-010-9240-3

128. Bradshaw K, Hansen R, Fulton A. Comparison of ERGs recorded with skin and corneal-contact electrodes in normal children and adults. *Doc Ophthalmol*. 2004;109(1):43-55. doi:10.1007/s10633-004-1751-3

129. Mcculloch DL, Van Boemel GB, Borchert MS. Comparisons of contact lens, foil, fiber and skin electrodes for patterns electroretinograms. *Doc Ophthalmol*. 1997;94(4):327-340. doi:10.1007/BF02580858

130. Wali N, Leguire LE. Dark-adapted luminance-response functions with skin and corneal electrodes. *Doc Ophthalmol*. 1991;76(4):367-375. doi:10.1007/BF00142675

131. Fernandes AG, Salomão SR, Pereira JM, Berezovsky A. Full-field electroretinogram recorded with skin electrodes in normal adults. *Arq Bras Oftalmol*. 2016;79(6):390-394. doi:10.5935/0004-2749.20160110

132. Rossi EA, Roorda A. The relationship between visual resolution and cone spacing in the human fovea. *Nat Neurosci*. 2010;13(2):156-157. doi:10.1038/nn.2465

133. Baseler HA, Brewer AA, Sharpe LT, Morland AB, Jaägle H, Wandell BA. Reorganization of human cortical maps caused by inherited photoreceptor abnormalities. *Nat Neurosci*. 2002;5(4):364-370. doi:10.1038/nn817

134. Neveu MM, Von Dem Hagen E, Morland AB, Jeffery G. The fovea regulates symmetrical development of the visual cortex. *J Comp Neurol*. 2008;506(5):791-800. doi:10.1002/cne.21574

135. Ctori I, Huntjens B. Repeatability of foveal measurements using spectralis optical coherence tomography segmentation software. *PLoS One*. 2015;10(6):e0129005. doi:10.1371/journal.pone.0129005

136. Samarawickrama C, Wang JJ, Huynh SC, et al. Macular thickness, retinal thickness, and optic disk parameters in dominant compared with nondominant eyes. *J AAPOS*. 2009;13(2):147-7. doi:10.1016/j.jaapos.2008.11.004

137. Turan KE, Sekeroglu HT, Baytaroglu A, Bezci F, Karahan S. Normative values for optical coherence tomography parameters in healthy children and interexaminer agreement for choroidal thickness measurements. *Arq Bras Oftalmol*. 2018;81(1):3-6. doi:10.5935/0004-2749.20180003

138. Barrio-Barrio J, Noval S, Galdõs M, et al. Multicenter Spanish study of spectral-domain optical coherence tomography in normal children. *Acta Ophthalmol*. 2013;91(1):e56-63. doi:10.1111/j.1755-3768.2012.02562.x

139. Invernizzi A, Pellegrini M, Acquistapace A, et al. Normative data for retinal-layer thickness maps generated by spectral-domain OCT in a white population. *Ophthalmol Retin*. 2018;2(8):808-815.e1. doi:10.1016/j.oret.2017.12.012

140. Delori FC, Goger DG, Dorey CK. Age-related accumulation and spatial distribution of lipofuscin in RPE of normal subjects. *Invest Ophthalmol Vis Sci*. 2001;42(8):1855-1866.

141. Fernandez-Godino R, Pierce EA, Garland DL. Extracellular matrix alterations and deposit formation in AMD. In: *Advances in Experimental Medicine and Biology*. ; 2016:53-58. doi:10.1007/978-3-319-17121-0_8

142. Rodriguez S, Otero C, Moreno M, Relova. Electroretinographic changes during childhood and adolescence. *Eur J Ophthalmol*. 1993;3(1):6-12.

143. Tariq YM, Samarawickrama C, Pai A, Burlutsky G, Mitchell P. Impact of ethnicity on the correlation of retinal parameters with axial length. *Investig Ophthalmol Vis Sci*. 2010;51(10):4977-4982. doi:10.1167/iovs.10-5226